GSA Data Repository Item 2018199

Mosolf, J.G., Gans, P.B., Wyss, A.R., Cottle, J.M., and Flynn, J.J., 2018, Late Cretaceous to Miocene volcanism, sedimentation, and upper-crustal faulting and folding in the Principal Cordillera, central Chile: Field and geochronological evidence for protracted arc volcanism and transpressive deformation: GSA Bulletin, https://doi.org/10.1130/B31998.1.

Data Repository

Supplemental File 1. Geologic map of the upper Tinguiririca River Valley in the Principal Cordillera, Central Chile

Supplemental File 2. Ar^{40}/Ar^{39} Geochronology

Supplemental File 3. U-Pb Zircon Geochronology

Supplemental File 4. Common Lithofacies Observed in the Tinguiririca Area

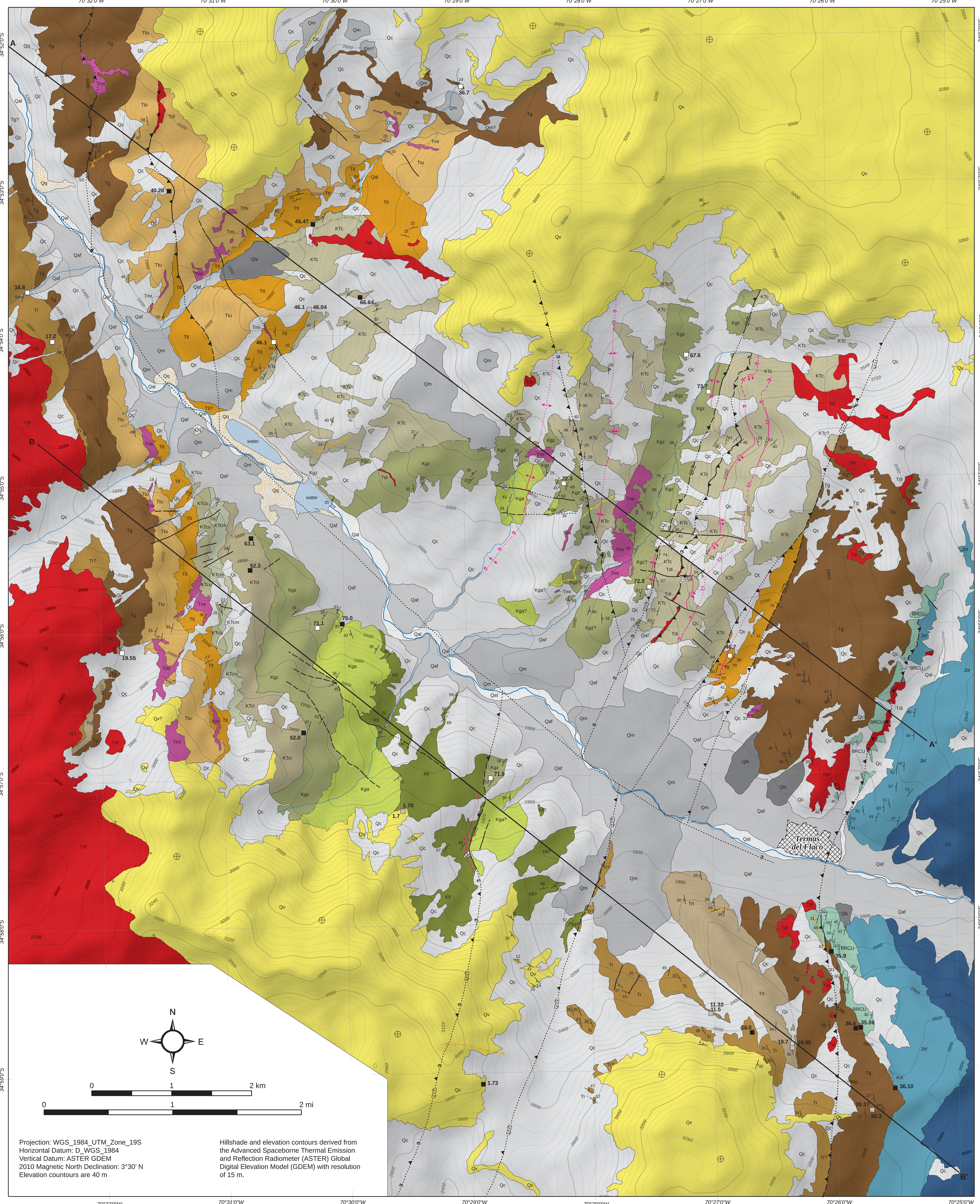

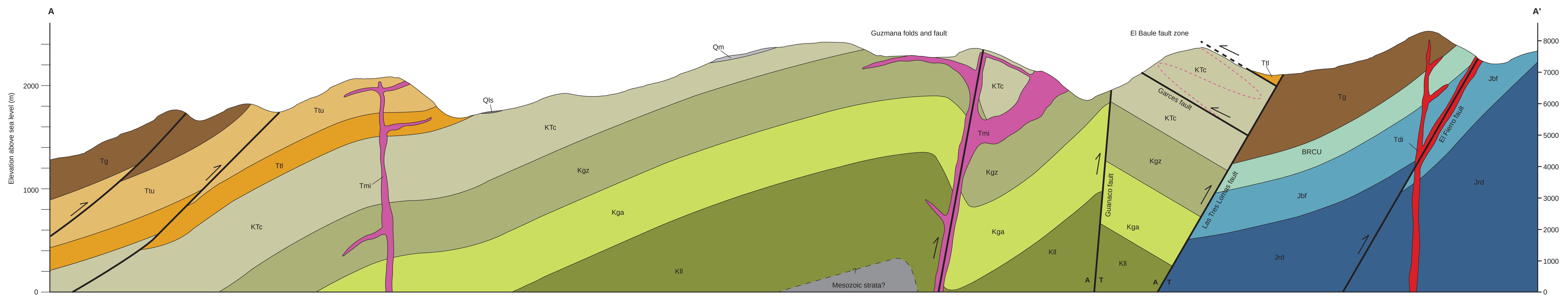

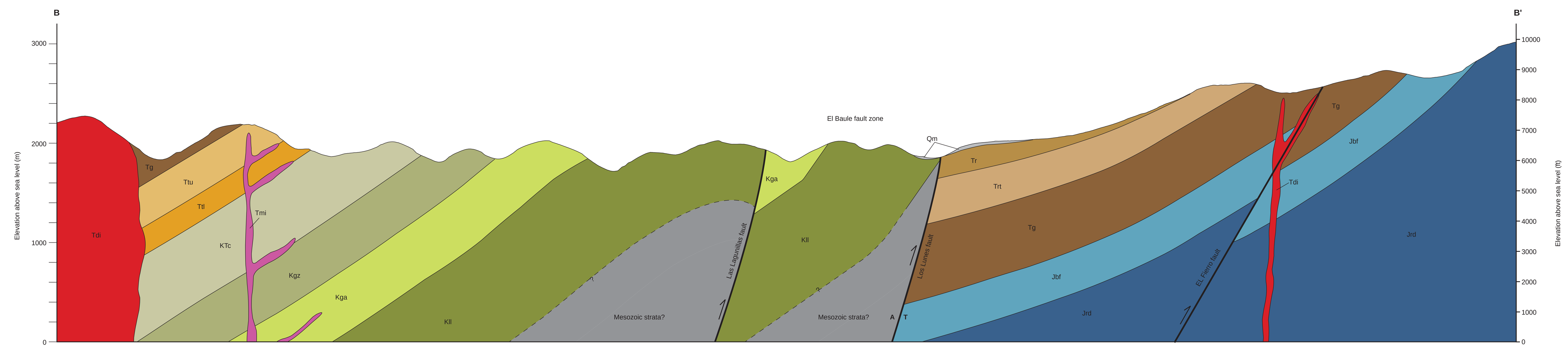

CORRELATION DIAGRAM

Quaternary
- Qal — Active alluvium
- Qc — Colluvium
- Qaf — Alluvial fan deposits
- Qls — Landslide deposits
- Qm — Glacial deposits
- Qv — Volcanic deposits

Intrusions
- Tdi — Diorite intrusions
- Tmi — Mafic intrusions

Abanico Fm. — Cenozoic
- Tr — Los Rios member
- Trt — Los Rios tuff
- Tg — La Gloria member
- Ttu — Upper Tapado member
- Ttl — Lower Tapado member

Mesozoic - early Cenozoic
- KTc — Circuelo member undivided
- KTcu — Upper Circuelo member
- KTcm — Middle Circuelo member
- KTcl — Lower Circuelo member
- Kgz — Guzmana member
- Kga — Guanaco member
- Kll — Los Lunes member
- BRCU — Brownish red clastic unit
- Kvt — 104 Ma tuff
- Jbf — Banos del Flaco Formation
- Jrd — Rio Damas Formation

MAP SYMBOLS

- Certain, inferred, concealed, and queried contact
- Certain, inferred, concealed, and queried fault
- Certain, approximate, concealed anticline
- Certain, approximate, concealed syncline
- Certain, approximate, concealed overturned anticline
- Certain, approximate, concealed overturned syncline
- Diabase dike/sill
- Diorite dike/sill
- Marker bed
- Horizontal bedding
- 76 Inclined bedding
- 41 Inclined volcanic foliation
- 65.82 $^{40}Ar/^{39}Ar$ age (Ma)
- 46.3 U-Pb age (Ma)
- 1.7 / 1.71 U-Pb + $^{40}Ar/^{39}Ar$ age (Ma)
- water — Reservoir
- Qq — Quarry/construction

INTRODUCTION

The upper Tinguiririca River Valley is located in the Principal Cordillera, near the town Termas del Flaco (Fig. 1). The map area is generally characterized by high relief and excellent bedrock exposure. The northwest striking Tinguiririca River Valley is the most prominent physiographic feature in the map area and has long served as a natural transportation corridor to Termas del Flaco.

The geologic setting of the upper Tinguiririca River Valley is a composite of prolonged volcanism and upper crustal deformation inboard of central Chile's long-lived subduction zone, forming the core of the Andean fold-thrust belt (Fig. 1). Back-arc volcanism associated with South America's subduction zone was initiated in the Principal Cordillera no later than the Jurassic (Rossel et al., 2013). Data presented herein suggest the volcanic arc axis had migrated to the Principal Cordillera by the Late Cretaceous, and has remained confined to an arc platform approximately 50 km wide to the present. Volcanic strata are locally deformed by transpressive faults and folds plausibly linked to oblique subduction of the Farallon Plate during the Cenozoic. The Principal Cordillera may have experienced multiple episodes of crustal shortening and extension (Charrier et al., 2007); however, tectonic structures delimiting multiple orogenic events are difficult to reconcile in the map area.

STRATIGRAPHY

Jurassic - Late Cretaceous strata

Jurassic through Late Cretaceous sedimentary and volcanic strata are the oldest rocks exposed in the map area and are divided into three map units including, from oldest to youngest, the Río Damas and Baños del Flaco formations, and a local informal unit designated the Brownish Red Clastic Unit (BRCU) known only from the Tinguiririca region (Charrier et al., 1996). These units generally record transgressive/regressive sedimentation and intermittent volcanism, presumably in a back-arc setting east of a contemporaneous volcanic arc front located in the modern-day Coastal Cordillera (Charrier et al., 2007; Rossel et al., 2013).

Abanico Formation

Well-stratified volcanic and volcaniclastic deposits composing the Abanico Formation are the oldest volcanogenic units in the map area (Fig. 2). Lithofacies are dominantly extrusive volcanic lavas and tuffs of intermediate to felsic composition intercalated with volcaniclastic intervals, mainly lahar-type deposits. These sequences are interpreted to be intra-arc accumulations formed in a volcano bounded, intermontane setting. While younger levels of the Abanico Formation rest directly on the older Mesozoic stratigraphy, the unit's chronostratigraphic base is not observed at the surface, leaving its maximum thickness uncertain. New radiometric age data reported herein show the age of the Abanico Formation to span 75.0 ± 0.5 to 11.32 ± 0.10 Ma (Tables 1 and 2; Fig. 3), indicating the volcanic arc front had migrated to what is now the Principal Cordillera by the Late Cretaceous.

Quaternary volcanic deposits

Pliocene to Quaternary volcanic deposits unconformably overlie the older Mesozoic-Cenozoic stratigraphy in the Principal Cordillera, consisting mainly of basaltic to rhyolitic lavas and domes, dacitic to rhyolitic ignimbrites, and volcanic breccia. These accumulations represent the Tinguiririca Volcanic Group that have yielded radiometric ages spanning 1.70 ± 0.08 to 0.95 ± 0.24 Ma (Charrier et al., 1996; this study). Strata are generally flat lying or gently dipping (less than 10°), resting on a prominent unconformity truncating underlying units which are tilted and deformed.

STRUCTURE

The most prominent structural feature in the Termas del Flaco area is the El Baule Fault Zone (EBFZ), a system of major northeast-striking faults that span the Río Tinguiririca valley in the southeast part of the map area. West of the EBFZ, the Río Tinguiririca divides the map area into two structural domains. Folding and faulting characterizes the northern structural domain, whereas the southern domain is characterized by a homocline of strata generally tilted to the northwest (Fig. 4). Major faults of the EBFZ achive up to 2.5 km of vertical separation, and an undetermined amount of strike-slip separation. Fault kinematic data collected throughout the map area (Fig. 5), however, indicate an ENE-WSW shortening direction, compatible with dextral shear across the EBFZ. Growth strata observed in the La Gloria and Los Rios members of the Abanico Formation suggest that transpressive shortening had commenced by 37 Ma and was mostly complete by ~11 Ma, by which time the locus of deformation had shifted eastward towards the Marlargue fold-thrust belt (Giambiagi et al., 2008).

PREVIOUS MAPPING

The first geological observations in the Principal Cordillera were made by Darwin in 1835 during his crossing of the Andes from Santiago to Mendoza via the Piuguenes Pass and Cordon del Portillo (Giambiagi et al., 2009). Parts of the map area were included in small-scale mapping by Klohn (1960, scale 1:100,000), and in a large-scale map by Arcos (1995, scale 1:25,000).

MAP UNITS

Qal **Alluvium (Quaternary: Holocene)**—Gravel, sand, silt, and clay along streams and their tributaries. Clasts are generally cobble size and smaller, and are rounded to subrounded. Thickness is generally less than 8 m (20 ft).

Qc **Colluvium (Quaternary: Holocene)**—Unconsolidated, poorly sorted debris deposited on steep slopes. Thickness is generally less than 8 m (20 ft).

Qaf **Alluvial-fan deposit (Quaternary: Holocene)**—Gravel, sand, silt, and clay in fan-shaped deposits where rivers and streams on steeper slopes met a gentler slope and dispersed their sediment load. Degree of sorting and rounding of clasts and geomorphic form varies widely depending on size and discharge of drainage above fan. Larger clasts, both matrix- and clast-supported, are derived from upstream sources. Coarse clast size dominantly cobbles, but also includes boulders and pebbles. Thickness generally less than 15 m (50 ft).

Qls **Landslide deposit (Quaternary: Holocene or Pleistocene)**—Mass-wasting deposits of rotated or chaotic strata and angular rock fragments that slid downslope.

Qm **Glacial deposit (Quaternary: Pleistocene)**—Unconsolidated, locally derived remnants of mountain glacial till and outwash deposits. Till is poorly sorted to unsorted fine-grained sediment to boulders as much as several meters in diameter. Thickness generally less than 45 m (150 ft).

Quaternary volcanic deposits

Qv **Volcanic deposit (Quaternary: Pleistocene)**—Undivided basaltic to andesitic lava flows, dacitic to rhyolitic ignimbrites, and pyroclastic breccia (Arcos, 1987; Charrier et al., 1996) that generally form broad, high elevation mesas with prominent, dark weathering cliff faces. Strata are generally flat lying or gently dipping (less than 10°), resting on a prominent unconformity truncating underlying units which are tilted and deformed. A rhyolitic ignimbrite sampled near the base of Tinguiririca Volcanic Group yielded a U-Pb zircon age of 1.7 ± 0.1 Ma, and an $^{40}Ar/^{39}Ar$ age of 1.70 ± 0.08 Ma. Cumulative thickness exceeds 800 m (2,625 ft).

Intrusions

Tdi **Diorite intrusion (Cenozoic)**—White to grey weathering dioritic intrusions exhibiting a wide range of sizes and geometries, forming 1-3 m (3–10 ft) wide dikes and sills or irregular bodies several hundred meters across, commonly with quenched margins. Typically porphyritic, containing phenocrysts of plagioclase ± hornblende ± pyroxene in a groundmass of interlocking plagioclase laths with occasional interstitial glass. Occurs throughout the map area, with larger bodies forming a conspicuous a north–northeast trending belt intruding the La Gloria member and older Mesozoic units east of the EBFZ. A large intrusion occurs in the extreme western part of the map area. A fresh plagioclase + pyroxene + hornblende sill intruding the Los Lunes member just below the contact with the overlying Quaternary Tinguiririca Group yielded $^{40}Ar/^{39}Ar$ age of 1.73 ± 0.12.

Tmi **Mafic intrusion (Tertiary: Eocene)**— Brown weathering mafic intrusions occur as 1-3 meters thick dikes and sills or irregular bodies hundreds of meters wide. Intrusions are phaneritic or porphyritic, containing phenocrysts of plagioclase + pyroxene + olivine. Groundmass commonly consists of plagioclase + pyroxene + Fe-oxides. No reliable age data were obtained for mafic intrusions.

Abanico Formation

Tr **Los Rios Member (Tertiary: Miocene)**—Light colored sequence of volcanic and volcaniclastic rocks up to 800 m (2625 ft) thick. Volcaniclastic intervals consist of channelized, cross-bedded sandstone and conglomerate accumulations interbedded with lahar and debris flow deposits. Porphyritic to sereriate basalt and basaltic andesite lava flows are up to 10 m (32 ft) thick and contain phenocrysts of plagioclase + pyroxene + olivine in a groundmass of plagioclase + Fe-oxides + interstitial glass. A plagioclase separate from a basaltic andesite lava flow east of the EBFZ yielded a $^{40}Ar/^{39}Ar$ age of 16.0 ± 0.6 Ma. Rhyolitic tuff deposits are generally less than 10 m (32 ft) thick and contain quartz + plagioclase + biotite phenocrysts in a groundmass (commonly devitrified) of ash and cuspate glass shards with abundant pumice lapilli/fiamme and angular lithic clasts. Quartz and plagioclase phenocrysts are commonly embayed or skeletal. Radiometric ages for tuffs span 17.2 ± 0.1 to 11.32 ± 0.10 Ma.

Trt **Los Rios tuff (Tertiary: Miocene)**— White weathering, cliff forming rhyolite tuff that is locally reworked. Contains quartz + plagioclase + biotite phenocrysts in a groundmass (commonly devitrified) of ash and cuspate glass shards with abundant pumice lapilli/fiamme and angular lithic clasts. Quartz and plagioclase phenocrysts are embayed or skeletal. $^{40}Ar/^{39}Ar$ and U-Pb zircon ages span 19.95 ± 0.13 to 19.6 ± 0.1 Ma. Laterally discontinuous and up to 300 m (984 ft) thick.

Tg **La Gloria Member (Cenozoic: late Eocene–early Miocene)**—Dominated by thick intervals of bulbous, purple and red weathering lahar and debris flow deposits that locally contain terrestrial mammal fossils, including those first discovered in this region (the Tinguiririca Fauna). Lahar deposits are up to 30 m (98 ft) thick, consisting of massive, medium to very coarse muddy sand with abundant free crystals of prismatic feldspar, angular lithic clasts, and occasional pumice lapilli. Intercalated basalt and basaltic-andesite flows are up to 10 m (32 ft) thick and contain phenocrysts of plagioclase ± pyroxene ± olivine. Olivine basalt flows and rhyolitic tuff near the stratigraphic base of the La Gloria member yielded radiometric ages ranging from 36.7 ± 0.2 to 35.06 ± 0.12 Ma. A rhyolitic tuff deposit near the top of the unit yielded ages spanning 20.37 ± 0.18 to 20.3 ± 0.2 Ma). Up to 500 m (1,640 ft) thick.

Ttu / Ttl **Tapado member (Tertiary: Eocene)**— The Tapado member is composed of dominantly purple-weathering volcaniclastic debris with subordinate primary volcanic intercalations. This unit was mapped as two lithologically similar submembers (Ttu and Ttl) divided by a conspicuous cliff-forming volcanic horizon of laterally discontinuous lavas and tuff deposits dated at 40.28 ± 0.30 Ma. Numerous sandstone dikes and brown weathering diabase cross-cut and intrude the Tapado member locally. Massive, purple-weathering lahar deposits are the dominant lithology. These beds are generally 2–4 m (7–13 ft) thick, but locally exceed 150 m (492 ft) in thickness, and consist of massive- to crudely-bedded tabular bedforms of poorly-sorted, medium to very coarse muddy sand with abundant free crystals of prismatic feldspar, pebble-sized lithic clasts, and pumice lapilli. Lahar deposits locally contain Cenozoic mammalian fossils distinctly older than those from the Tinguiririca Fauna. Lahar deposits are interbedded with thin intervals of poorly-sorted volcaniclastic conglomerate, laminated mudstone, siltstone, and fine-grained sandstone. Subordinate basalt and andesite lava flows are up to 6 m (20 ft) thick and contain phenocrysts of plagioclase ± pyroxene ± olivine in a groundmass of microcrystalline plagioclase + Fe-oxides with minor amounts of devitrified glass. Blocky andesite flows often contain coarse phenocrysts of glomeroporphyritic plagioclase with "turkey track" morphologies. Infrequent, weakly- to moderately-welded tuff deposits are usually 1–10 m (3–33 ft) thick, but are up to 100 m (328 ft) thick in the upper part of the unit. They are commonly porphyritic, consisting of fragmental phenocrysts of plagioclase ± quartz ± biotite ± pyroxene in an ash matrix containing abundant cuspate glass shards (commonly devitrified), small angular lithic clasts, and pumice lapilli. Plagioclase and quartz phenocrysts are frequently embayed or skeletal. Tuff intervals near the base of the Tapado member yielded $^{40}Ar/^{39}Ar$ and U-Pb zircon ages spanning 46.7 ± 0.2 to 45.47 ± 0.22 Ma. Up to 600 m (1,969 ft) thick.

KTc **Ciruelo member, undivided (Late Cretaceous to Eocene)**—Distinctive sequence of red/maroon weathering volcanic and volcaniclastic deposits 500–650 m (1,640–2,133 ft) thick. Mapped as three submembers where discernable. Red weathering, dominantly clastic strata north of the Río Tinguiririca and within the EBFZ are provisionally assigned to the Circuelo member. These deposits consist of rhythmically-bedded, volcaniclastic conglomerate and channelized sandstone that laterally grade northward to finer-grained intervals of sandstone, mudstone, and siltstone.

KTcu **Upper Circuelo member:** 16+ olivine basalt flows that eventually pinch out 2-3 km (6562-9843 ft) north and south of the river. These lavas form a marker bed that can be traced across the Río Tinguiririca. Basaltic lavas are generally porphyritic, consisting of plagioclase and olivine phenocrysts in a trachytic groundmass of plagioclase with interstitial pyroxene ± olivine. Up to 180 m (591 ft) thick.

KTcm **Middle Circuelo member:** Tabular beds up to 2 m (7 ft) thick of massive, red/maroon weathering volcaniclastic sandstone with occasional angular, pebble-sized clasts of volcanic debris. Forms distinct horizon south of the river. Up to 150 m (492 ft) thick.

KTcl **Lower Circuelo member:** Basalt and andesite lava flows intercalated with volcaniclastic debris. Lava flows are generally porphyritic and contain phenocrysts of plagioclase ± pyroxene ± olivine in a groundmass of microcrystalline plagioclase ± pyroxene + Fe-oxides. Intercalated volcaniclastic intervals consist of crudely bedded volcanic breccia and massive pebbly-sandstone intervals that contain abundant feldspar, occasional pumice lapilli, and angular volcanic clasts. Flows near the base yielded three $^{40}Ar/^{39}Ar$ ages spanning 66.64 ± 0.34 to 52.0 ± 0.5 Ma. Up to 340 m (1,116 ft) thick.

Kgz **Guzmana member (Late Cretaceous)**— Repeating intervals of basalt-to-andesitic lavas, lithic tuff deposits, and volcaniclastic debris that give the unit a distinctively pink, grey, and white candy-striped appearance in the field. Lava flows are most common in the lower 350 m (1148 ft) and are generally porphyritic, containing phenocrysts of plagioclase ± amphibole ± pyroxene ± olivine in a trachytic groundmass of plagioclase ± pyroxene and minor interstitial glass. Individual flows are 1–10 m (3–33 ft) thick and are commonly brecciated or have rubbly bases. Intercalated lithic tuff deposits are generally unwelded to weakly-welded and commonly contain accidental fragments of volcanic rock, pumice, and fragmental phenocrysts of plagioclase ± sanadine ± embayed quartz ± amphibole ± biotite in an ash matrix ± cuspate glass shards. Tuffs show evidence of minor fluvial reworking locally, but most appear to be primary ash deposits. Intercalated volcaniclastic breccias are massive, consisting of volcanic rock fragments and bombs exceeding 40 cm (16 in) in diameter and supported by a matrix of sandy-ash with abundant pumice fragments and free crystals of feldspar ± quartz ± biotite. The Guzmana member contains subordinate intervals of red and purple weathering mudstone, poorly sorted conglomerate, and massive or well-laminated sandstone. U-Pb zircon ages span 73.7 ± 0.36 to 67.6 ± 0.5 Ma. Thickness is up to 500–550 m (1640–1804 ft).

Kga **Guanaco member (Late Cretaceous)**—Stack of 40+ andesite, basaltic-andesite, and basalt lava flows with minor intercalations of volcanic tuff and volcaniclastic debris. Individual lava flows are 2–20 m (7–66 ft) thick and generally porphyritic, containing phenocrysts of plagioclase ± pyroxene ± amphibole ± olivine set in a trachytic groundmass of microcrystalline plagioclase + Fe-oxides with minor interstitial glass. Andesite flows are commonly blocky in appearance due to thick autobrecciated carapaces, whereas basalt and basaltic-andesite flows generally appear more coherent, consisting of rubbly bases overlain by dark weathering massive interiors. Rare intercalated tuffaceous intervals are 6-8 m (20-26 ft) thick and contain pumice lapilli and phenocrysts of feldspar ± quartz ± biotite. Thin interbeds of volcaniclastic debris consist of maroon to purple weathering, massive and laminated sandstone deposits that are commonly interbedded with volcaniclastic conglomerates and breccia deposits. A basaltic-andesite lava sampled near the stratigraphic top of the Guanaco member yielded a $^{40}Ar/^{39}Ar$ age of 75.0 ± 0.5 Ma. Up to 500 m (1,640 ft) thick.

Kll **Los Lunes member (Late Cretaceous)**— The upper 250 m (820 ft) consists mainly of alternating lavas and volcanic breccias. Volcanic breccias are grey to light-green weathering and massive, forming crude bedforms, 1–2 m (3–7 ft) thick. These deposits consist mainly of coarse angular andesitic to dacitic clasts, sometimes with abundant pumice lapilli and bombs. Interbedded volcaniclastic sandstones and conglomerates are massive, forming crude, 1–2 m (3–7 ft) thick bedforms. Intercalated basaltic-andesite flows, 6–8 m (20–26 ft) thick, consist of plagioclase + pyroxene ± olivine phenocrysts in a trachytic groundmass of plagioclase and Fe-oxides. The lower 700 m (2,297 ft) of the Los Lunes member are poorly exposed in limited outcrops to the southeast. These scattered exposures are strikingly similar to those higher in the section, and could potentially be intervals repeated by unidentified faults. Diabase and microdiorite intrusions, complex fracturing, and low-grade metamorphism and/or hydrothermal alteration of the Los Lunes member progressively increase to the southeast, near the Las Lagunillas and Los Lunes faults. The total thickness of this interval is uncertain due to its unexposed base and complex internal faulting, but is estimated to exceed 1,000 m (3,280 ft). Best observed west of the Los Lunes fault south of the Río Tinguiririca.

Jurassic – Late Cretecous stratigraphy

BRCU **Brownish Red Clastic Unit (Late Cretaceous)**—Distinct red-brown, fining-upward package of subaerial volcaniclastic sandstone and conglomerate, with subordinate intervals of fine-grained sandstone and mudstone. The lower 40 m (131 ft) of the BRCU consists of coarse, matrix-supported, heterolithologic breccia, whereas the upper 200 m (656 ft) are dominated by channelized, coarse-grained sandstone and conglomerate lenses interbedded with subordinate intervals of fine-grained sandstone and mudstone (Arcos, 1987; Charrier et al., 1996). Rests unconformably on the Baños del Flaco Formation. Up to 300 m (985 ft) thick and laterally discontinuous, pinching out 3–4 km (9,843–13,123 ft) north and south of Termas del Flaco.

Kvt **104 Ma tuff (Cretaceous)**—Fine-grained, massive, vitric tuff layer exposed north of El Fierro pass. 3-4 m (10–13 ft) thick. Isotopically dated at 104 Ma (sample 9OCS-BWA; Wyss et al., 1994).

Jbf **Baños del Flaco Formation (Jurassic)**—White-to-buff weathering, generally well-bedded fossiliferous calcarenites, calcilutites, and sandstone intervals (Arcos, 1987). Fossiliferous beds contain numerous Tithonian-Neocomian ammonite species (Covacevich et al., 1976; Biro-Bagoczky, 1984); its lower stratigraphic levels include dinosaur trace fossils (Casamiquela and Fasola, 1968). 400 m (1,312 ft) thick.

Jrd **Río Damas Formation (Jurassic)**— Dark weathering, coarse volcanic breccia and fine-grained sedimentary deposits intercalated with abundant mafic lavas in the upper thousand meters of the section (Charrier, 1981; Charrier et al., 1996). A sandstone collected near Termas del Flaco yielded a unimodal distribution of U-Pb zircon ages with a peak at 158 Ma; the youngest five grains yielded a mean age of 146.4 ± 4.4 Ma and are interpreted to be the maximum depositional age of the Río Damas Formation (Rossel et al., 2014). Up to 7,000 m (2,2965 ft) thick.

REFERENCES

Arcos, R., 1987, Geología del cuadrángulo Termas Del Flaco, provincia de Colchagua, VI Región, Chile: Universidad de Chile, 279 p.
Biro-Bagoczky, L., 1984, Nuevos antecedentes paleontologicos y estratigraficos de algunos afloramientos titono-neocomianos en la Cordillera Chilena, entre Los 33°45' y 35° lat. Sur: Dept. Geociencias, Universidad de Concepción, Chile. I.G.C.P. Project 117: Circumpacific Jurassic Report 2, Special paper 3.
Casamiquela, R.M., and Fasola, A., 1968, Sobre pisadas de dinosaurios del cretacico inferior de Colchagua (Chile): Publicacion - Departamento de Geologia, Facultad de Ciencias Fisicas y Matematicas, Universidad de Chile, v. 30, p. 1–24.
Charrier, R., 1981, Geologie der chilenischen hauptkordillere zwischen 34° und 34°30' suedliche Breite und ihre tektonische, magmatische und palaeogeographische Entwicklung. Geology of the Principal Cordillera of Chile between 34° and 34°30' south and its tectonic, magmatic and paleogeographic evolution. Berliner Geowissenschaftliche Abhandlungen (A) 36, 270 p.
Charrier, R., Wyss, A.R., Flynn, J.J., Swisher, C.C., Norell, M.A., Zapatta, F., McKenna, M.C., and Novacek, M.J., 1996, New evidence for late Mesozoic early Cenozoic evolution of the Chilean Andes in the Upper Tinguiririca Valley (35°S), Central Chile: Journal of South American Earth Sciences, v. 9, p. 393–422.
Charrier, R., Pinto, L., and Rodrguez, M., 2007, Tectonostratigraphic evolution of the Andean Orogen in Chile, in The geology of Chile, Geological Society, London, p. 21–114.
Covacevich, V., Varela, J., and Vergara, M., 1976, Estratigrafia y sedimentacion de la formacion Baños del Flaco al sur del Río Tinguiririca, Cordillera de los Andes, Provincia de Curico, Chile: Actas - Congreso Geologico Chileno, v. 1, p. A191–A211.
Giambiagi, L., Tunik, M., Ramos, V., and Godoy, E., 2009, The high Andean Cordillera of central Argentina and Chile along the Piuguenes Pass – Cordon del Portillo transect: Darwin's Pioneering observations compared with modern geology: Revista de la Asociacion Geologica Argentina, v. 31, p. 1443–1457.
Giambiagi, L., Bechis, F., Garcia, V., and Clark, A.H., 2008, Temporal and spatial relationships of thick- and thin-skinned deformation: A case study from the Malargue fold-and-thrust belt, southern Central Andes: Tectonophysics, v. 459, p. 123–139.
Klohn, C., 1960, Geologia de la Cordillera de los Andes de Chile Central (provincias de Santiago, O'Higgins, Colchagua y Curicó): Ins. Invest. Geológicas, v. 8, p. 95.
Rossel, P., Oliveros, V., Ducea, M., Charrier, R., Scaillet, S., Retamal, L., Figueroa, O., 2013, The Early Andean subduction system as an analog to island arcs: Evidence from across-arc geochemical variations in northern Chile: Lithos, v. 179, p. 211–230.
Rossel, P., Oliveros, V., Mescua, J., Tapia, F., Ducea, M., Calderón, S., Charrier, R., Hoffman, D., 2014, The Upper Jurassic volcanism of the Río Damas-Tordillo Formation (33°- 35.5°S): Insights on petrogenesis, chronology, provenance, and tectonic implications: Andean Geology, v. 41(3), p. 529–557.
Wyss, A.R., Norell, M.A., Flynn, J.J., Novacek, M.J., Charrier, R., McKenna, M.C., Frassinetti, D., Salinas, P., and Meng, J., 1994, A new early Tertiary mammal fauna from central Chile: Implications for Andean stratigraphy and tectonics: Tectonophysics, v. 229, p. 251–264.

TABLE 1. $^{40}Ar/^{39}Ar$ GEOCHRONOLOGY

Sample	Lithology	Unit	Latitude	Longitude	Material analyzed	TCR age (Ma)*	2σ	FCT age (Ma)⊠	2σ
CHJ-01	plag+hbl+px ignimbrite	Qv	-34.9537	-70.4923	Plag	1.68	0.08	1.70	0.08
J446	px-hbl sill	Tdi	-34.9846	-70.4818	Plag	1.70	0.16	1.72	0.16
					Plag	1.71§	0.12	1.73§	0.12
J378	qz+plag+bio tuff	Tr	-34.9770	-70.4505	Plag ρ1	11.17§	0.10	11.32§	0.10
					Plag	11.7	2.1	11.9	2.1
J402	plag+px+olv lava	Tr	-34.9792	-70.4449	Plag	15.8§	0.6	16.0	0.6
					WR	16.3	0.1	16.5	0.1
J473	plag+qz+bio tuff	Trt	-34.9810	-70.4394	Coarse grain plag	19.66	0.20	19.92	0.20
					Fine grain plag	19.72	0.16	19.98	0.16
					Weighted mean	19.69§	0.13	19.95§	0.13
J417	plag+qz+bio tuff	Tg	-34.9881	-70.4286	Plag	20.11§	0.18	20.37§	0.18
					6 plag grains	23.4	1.0	23.7	1.0
CH-98	plag+olv lava	Tg	-34.9788	-70.4300	Plag	36.3	0.9	36.8	0.9
					GM	34.61§	0.12	35.06§	0.12
J338	plag+olv lava	Tg	-34.9702	-70.4339	Plag	35.4§	0.5	35.9§	0.5
					Plag	35.5	3.5	36.0	3.5
J424	plag+olv lava	Tg	-34.9857	-70.4254	Plag	35.64§	0.34	36.10§	0.34
					WR	35.01	0.12	35.46	0.12
CH-95	plag+olv lava	Tg	-34.9789	-70.4307	Plag	35.9	0.8	36.4	0.8
CHJ-46	plag+qz+px tuff	Ttu	-34.8834	-70.5230	Plag	39.77	0.30	40.28	0.30
CHJ-18	plag+qz+hbl+bio tuff	Ttl	-34.8874	-70.5034	Plag	44.89	0.22	45.47	0.22
CH-89	plag+qz tuff	Ttl	-34.8970	-70.5041	Plag ρ1	45.72	0.26	46.31	0.26
					Plag ρ2	45.30	0.26	45.89	0.26
					Fine grain plag	45.34	0.26	45.93	0.26
					Weighted mean	45.45§	0.15	46.04§	0.15
CHJ-08	plag + px lava	KTc	-34.9447	-70.5057	GM	51.3	0.5	52.0	0.5
CH-57	olv lava	KTc	-34.9263	-70.5127	GM plag	51.5	0.5	52.2	0.5
CH-56	plag+px lava	KTc	-34.9227	-70.5125	Plag	62.3§	0.4	63.1§	0.4
					Plag	63.4	1.2	64.2	1.2
CH-88	plag+px+olv lava	KTc	-34.8957	-70.4971	Plag	65.79	0.34	66.64	0.34
CH-53	plag+px+olv lava	Kga	-34.9325	-70.5002	Plag	74.0	0.5	75.0	0.5

Note: Mineral abbreviations: plag, plagioclase; qz, quartz; bio, biotite; hbl, hornblende; px, pyroxene; olv, olivine; WR, whole rock; GM, groundmass.
*$^{40}Ar/^{39}Ar$ ages from incremental heating experiments relative to the Taylor Creek Rhyolite (TCR) sanidine
⊠$^{40}Ar/^{39}Ar$ age recalculated relative to the Fish Canyon Tuff (FCT) sanidine.
§Preferred age for samples with multiple splits.
Mineral separates were prepared and analyzed at the University of California, Santa Barbara.
Latitudes and longitudes are in the 1984 World Geodetic Survey (WGS84) datum.

TABLE 2. U-Pb ZIRCON GEOCHRONOLOGY

Sample	Lithology	Unit	Latitude	Longitude	# of analyses	Age (Ma)	2σ	MSWD
CHJ-01	plag+hbl+px ignimbrite	Qv	-34.9537	-70.4923	27	1.7	0.1	2.6
J378	qz+plag+bio tuff	Tr	-34.9770	-70.4505	24	11.5	0.2	3.5
CHJ-13	qz+plag+bio tuff	Tr	-34.8946	-70.5426	33	16.8	0.1	1.3
CHJ-15	qz+plag+bio tuff	Tr	-34.9002	-70.5393	37	17.2	0.1	0.8
CHJ-16.1	plag+qz+bio tuff	Trt	-34.9354	-70.5304	19	19.6	0.1	1.1
J473	plag+qz+bio tuff	Trt	-34.9810	-70.4394	33	19.7	0.1	1.4
J417	plag+qz+bio tuff	Tg	-34.9881	-70.4286	20	20.3	0.2	1.9
CHJ-24	reworked plag+qz tuff	Tg	-34.8721	-70.4829	22	36.7	0.2	0.9
CHJ-16	plag+qz+bio tuff	Ttl	-34.9006	-70.5090	22	46.1	0.3	0.5
CH-89	plag+qz dacite tuff	Ttl	-34.8970	-70.5041	23	46.1	0.3	0.6
CHJ-41	plag+qz+hbl(?) tuff	Ttl	-34.9367	-70.4472	31	46.7	0.2	0.9
CHJ-34	plag+qz+bio(?) tuff	Kgz	-34.9027	-70.4526	22	67.6	0.5	4.1
CHJ-04	plag+bio(?) tuff	Kgz	-34.9329	-70.5036	22	71.1	0.4	0.7
CHJ-02	altered plag+qz tuff	Kgz	-34.9501	-70.4802	24	71.9	0.3	1.0
CHJ-36	crystal poor plag + qz tuff	Kgz	-34.9170	-70.4696	31	72.3	0.3	1.0
CHJ-27	plag+qz+hbl dacite tuff	Kgz	-34.9288	-70.4581	32	72.3	0.3	1.2
CHJ-33	crystal poor plag + qz tuff	Kgz	-34.9069	-70.4496	40	73.7	0.3	1.1

Note: Mineral abbreviations: plag, plagioclase; qz, quartz; bio, biotite; hbl, hornblende; px, pyroxene.
U-Pb ages are weighted mean of $^{206}Pb/^{238}U$ ages. Uncertainties are ± 2s.
Zircon separates were prepared and analyzed at the University of California, Santa Barbara.
Latitudes and longitudes are in the 1984 World Geodetic Survey (WGS84) datum.

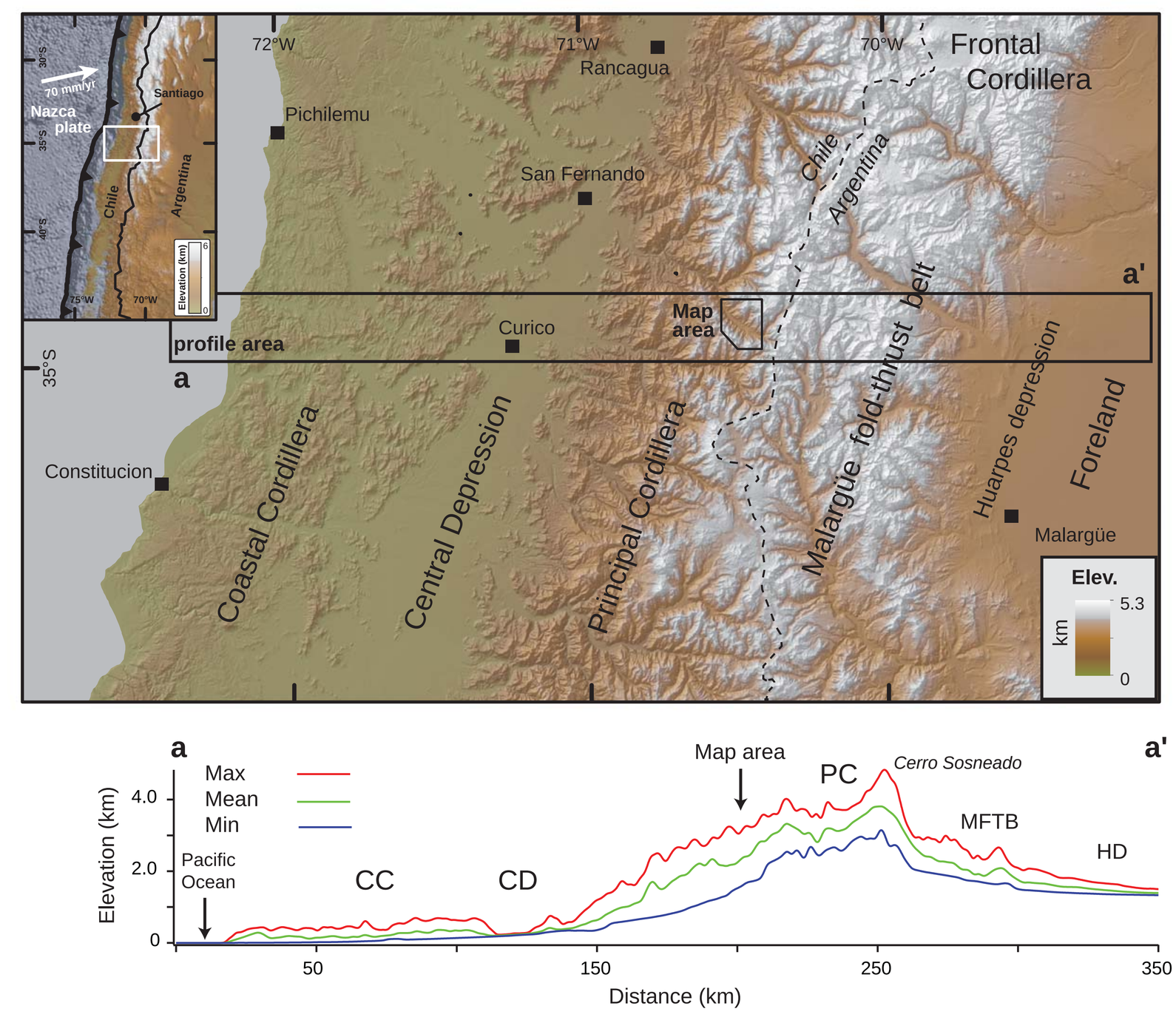

Figure 1. Map and elevation profiles showing the main morphostructural domains of western South America between 34° and 36°S. These domains include the Coastal Cordillera (CC), Central Depression (CD), Principal Cordillera (PC), and Foreland (F). The approximate location of the Malargüe fold-and-thrust belt (MFTB) and the Huarpes depression (HD) are also shown. Maximum, minimum, and mean elevation profiles are given for a 10 km wide swath (shown by larger rectangular box) across all the morphostructural domains at this latitude. In set shows modern tectonic setting.

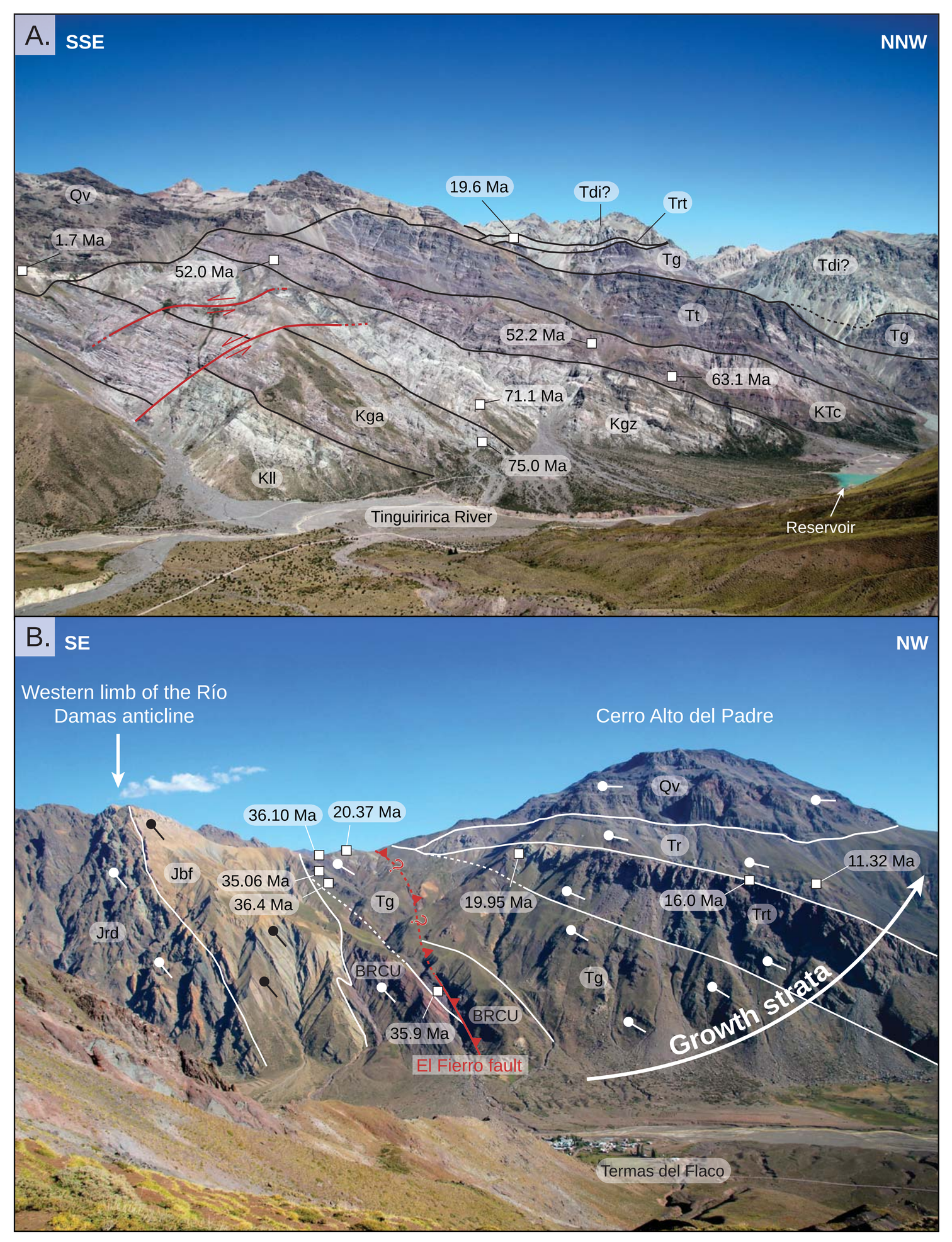

Figure 2. Overview of the map units. (A) View southwest of the Abanico Formation's lower stratigraphic members Kll, Kga, Kgz, KTc, Tt, and Tg. Radiometric ages obtained in this study shown by boxes, and apparent bedding by ball-and-sticks. (B) The upper stratigraphic levels of the Abanico Formation (Tg, Trt, & Tr) are seen overlying the older Mesozoic stratigraphy (BRCU, Jbf, & Jrd) in slight angular unconformity. Note the progressive decrease of dip of bedding up section and the southeastern thinning and truncation of the Abanico Formations younger members. Cerro Alto del Padre is the prominent peak photo right.

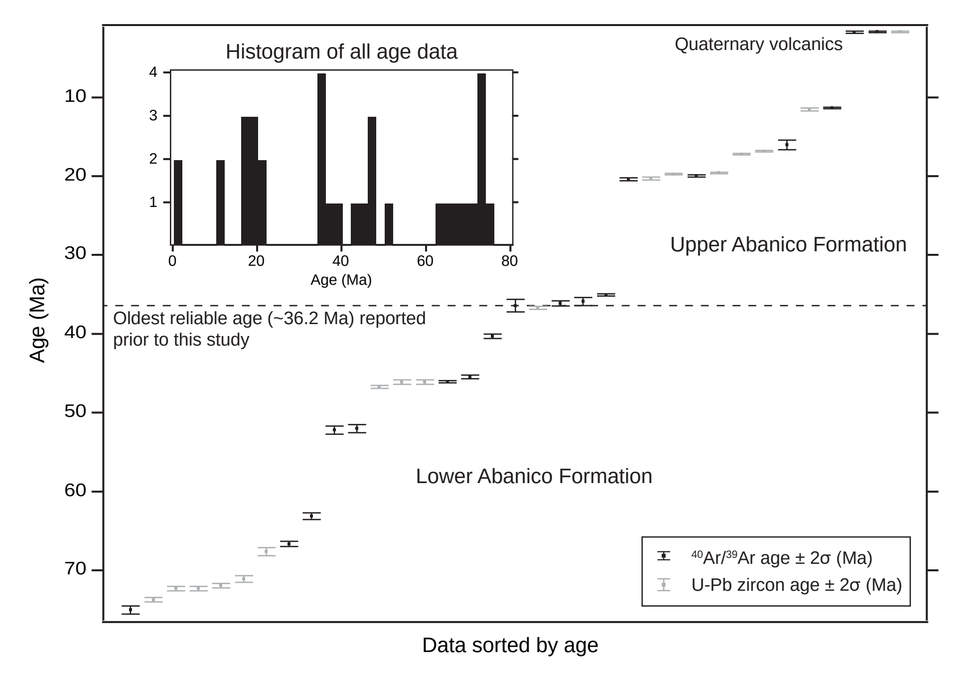

Figure 3. Plot of all unique geochronology data obtained in this study, sorted by age. $^{40}Ar/^{39}Ar$ ages are shown in black, and U-Pb zircon ages in gray. Inset plot is a histogram of the combined age data. The dashed line represents the oldest reliable age reported prior to this study (~36.2 Ma).

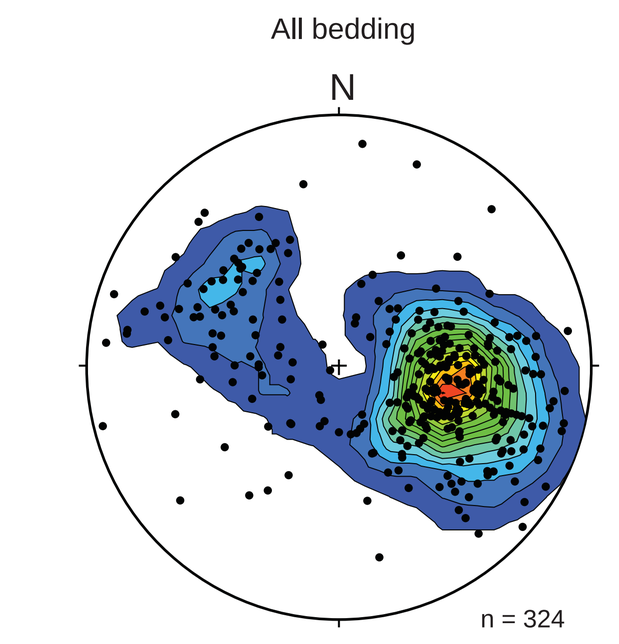

Figure 4. Lower hemisphere projection of poles to bedding measurements collected in the map area fit with a colored Kamb contour.

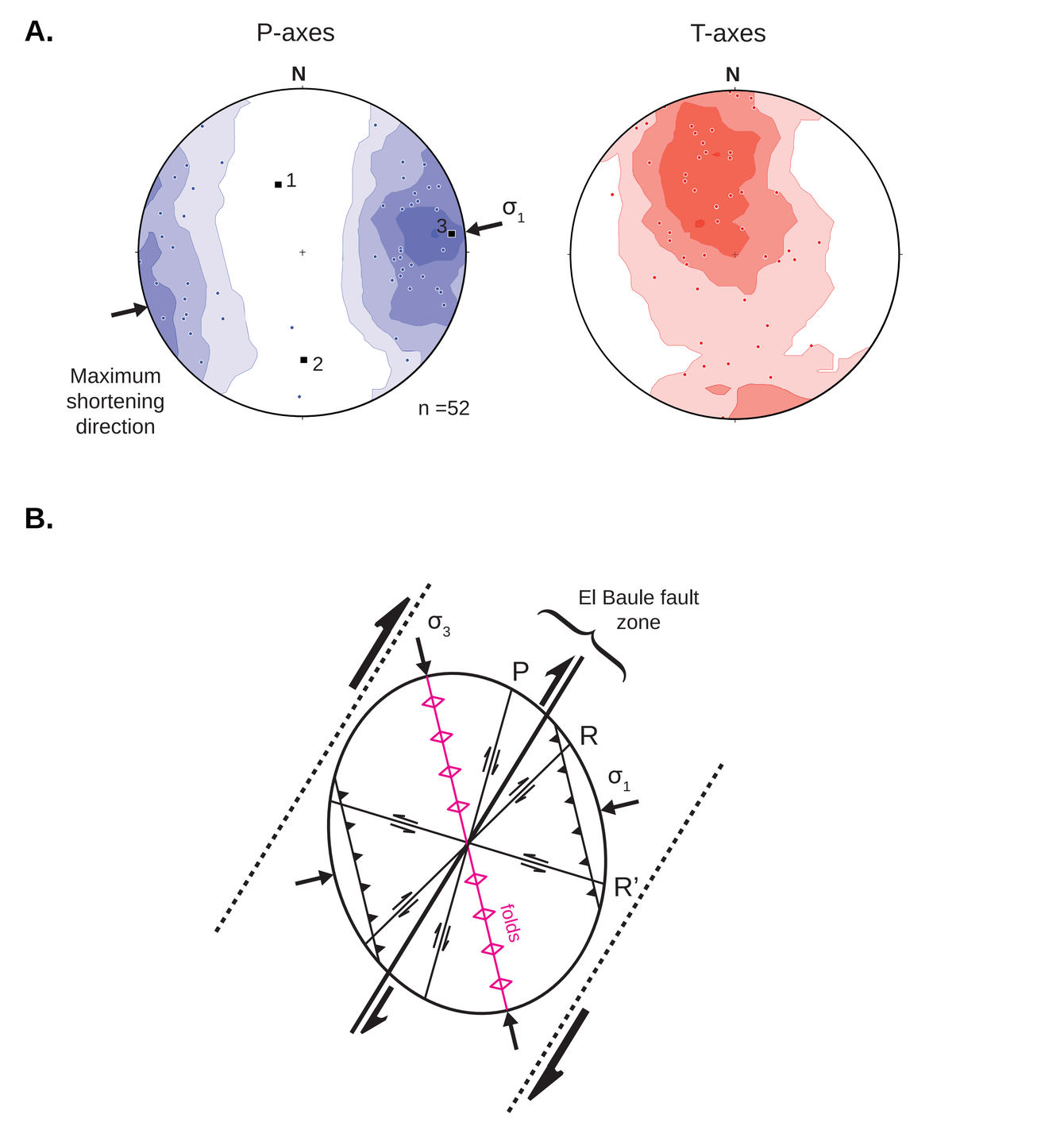

Figure 5. A) Lower hemisphere projection of P- and T-axes of inverted fault data; fit with Kamb contour. Bingham kinematic axes shown by small boxes (axis of maximum shortening is labeled "3" and axis of minimum shortening is labeled "1"). (B) Idealized pattern of deformation for an oblique dextral shear zone rotated into alignment with maximum shortening direction inferred from fault kinematic data.

Geologic map of the upper Tinguiririca River Valley in the Principal Cordillera, Central Chile

Mapped by Jesse G. Mosolf

2018

Ar^{40}/Ar^{39} GEOCHRONOLOGY

Samples were irradiated during multiple runs in a cadmium-lined tube at the TRIGA reactor at Oregon State University for durations spanning 8 to 20 hours depending on the estimated ages of the samples. Samples were then dated at the $^{40}Ar/^{39}Ar$ geochronology laboratory at the University of California, Santa Barbara. Each sample was step-heated in a Staudacher-type resistance furnace; isotopic analyses were undertaken in a MAP 216 mass spectrometer following the general procedures outlined by Gans (1997). Sanidine from the Taylor Creek rhyolite (27.92 Ma; Duffield and Dalrymple, 1988) was utilized as the flux monitor in all irradiations. Analysis of unknowns typically involved 4 to 13 step heating experiments, ramping up from 560°C to 1450°C. In some cases, replicate splits were analyzed to assess internal consistency and to improve precision. Data were reduced and spectra generated using in-house software written by Brad Hacker. Errors associated with age determinations are reported at the ± 2 σ (95% confidence) level. Ages were then recalculated relative to the Fish Canyon tuff with an assigned age of 28.1 Ma. Ages relative to the Taylor Creek Rhyolite and Fish Canyon Tuff sanidine are reported for each sample.

All data are readily interpretable. Plagioclase separates generally yielded simple age plateaus or slightly climbing age spectra suggesting minor loss of radiogenic Ar. In some instances, plagioclase separates yielded saddle shaped spectra or spectra that climb over low temperature steps, flatten, and then climb abruptly to anomalously old apparent ages at the highest temperature steps. The shapes of these types of spectra are interpreted to be caused by a combination of argon loss associated with weak alteration (evident in

the low T steps) and excess argon held in the most retentive reservoirs that is released at the highest temperature steps. The low temperature steps or central flat part of these spectra were used to approximate the age. Whole rock and groundmass separates commonly yielded down-stepping spectra or subtle saddle shaped spectra. The shapes of these types of spectra are interpreted to be the combined effects of ^{39}ArK recoil and excess ^{40}Ar. The central flats occurring at the mid-temperatures steps of these spectra were used to approximate the age of the sample.

REFERENCES CITED

Gans, P. B., 1997, Large-magnitude Oligo-Miocene extension in southern Sonora: Implications for the tectonic evolution of northwest Mexico: Tectonics, v. 16(3), p. 388-408.

Duffield W. A. and Dalrymple, G. B., 1990, The Taylor Creek Rhyolite of New Mexico: A Rapidly Emplaced Field of Lava Domes and Flows. Bulletin of Volcanology, v. 52(6), p. 475-487.

Supplemental File 2

TABLE S1. SB56-77; CH-53 Plag; J=0.0114267

Temp (°C)	t	^{40}Ar (mol)	^{40}Ar/^{39}Ar	^{38}Ar/^{39}Ar	^{37}Ar/^{39}Ar	^{36}Ar/^{39}Ar	K/Ca	∑ ^{39}Ar	^{40}Ar*	Age (Ma)
720	12	2.4e-14	3.4900	4.5e-4	12.6091	0.0025	0.039	0.10121	0.787	55.7 ± 0.4
780	12	3.5e-14	3.6292	0.0e+0	11.7754	0.0016	0.042	0.24207	0.866	63.7 ± 0.3
840	12	4.0e-14	3.8919	0.0e+0	11.2278	0.0015	0.044	0.38946	0.890	70.0 ± 0.3
900	12	3.8e-14	4.1558	0.0e+0	10.9193	0.0017	0.045	0.52044	0.878	73.7 ± 0.3
970	12	3.2e-14	4.5436	0.0e+0	10.6617	0.0029	0.046	0.62071	0.809	74.2 ± 0.4
1040	12	2.8e-14	5.4564	0.0e+0	10.4832	0.0061	0.047	0.69577	0.672	74.1 ± 0.6
1110	12	2.1e-14	6.8319	0.0e+0	10.4010	0.0104	0.047	0.74068	0.550	75.8 ± 0.8
1180	12	4.0e-14	8.9066	0.0e+0	10.1888	0.0159	0.048	0.80627	0.472	84.7 ± 0.7
1260	12	7.1e-14	11.8078	0.0e+0	11.7909	0.0218	0.042	0.89294	0.454	107.3 ± 0.6
1360	12	5.6e-14	7.5973	0.0e+0	11.0023	0.0103	0.045	1.00000	0.600	91.5 ± 0.5

Note: Total fusion age, TFA = 75.70 ± 0.17 Ma (including J).
Weighted mean plateau age, WMPA = 74.03 ± 0.23 Ma (including J).
Inverse isochron age =73.36 ± 0.42 Ma (MSWD =0.68; ^{40}Ar/^{36}Ar = 305.8 ± 3.9).
Steps used: 900, 970, 1040, 1110 (4–7/10 or 35% ∑ 39Ar).
t = dwell time in minutes.
^{40}Ar (mol) = moles corrected for blank and reactor-produced ^{40}Ar.
Ratios are corrected for blanks, decay, and interference.
$\sum^{39}$Ar is cumulative, ^{40}Ar* = rad fraction.

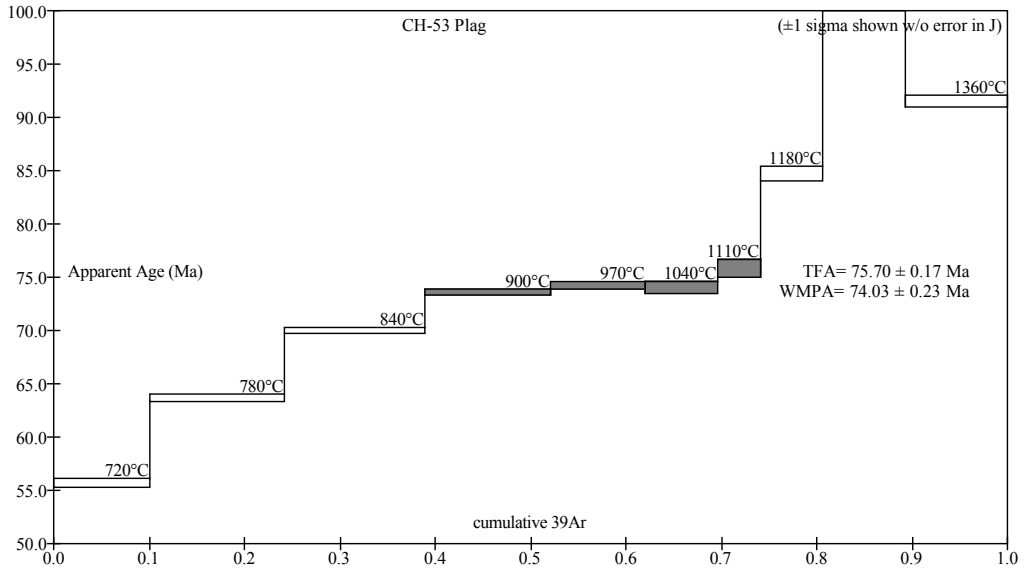

Decent plateau, but only using 35% of gas - evidence for low temperature argon loss and some excess argon in most retentive sites.

Supplemental File 2

TABLE S2. SB56-85; CH-56 Plag; J=0.0112108

Temp (°C)	t	^{40}Ar (mol)	^{40}Ar/^{39}Ar	^{38}Ar/^{39}Ar	^{37}Ar/^{39}Ar	^{36}Ar/^{39}Ar	K/Ca	∑ ^{39}Ar	^{40}Ar*	Age (Ma)
720	12	3.8e-14	3.1251	0.0e+0	14.8539	0.0012	0.033	0.12703	0.891	55.4 ± 0.3
780	12	5.5e-14	3.2775	0.0e+0	14.8608	0.0009	0.033	0.30029	0.923	60.2 ± 0.3
840	12	4.9e-14	3.3998	0.0e+0	14.6338	0.0009	0.033	0.45158	0.920	62.2 ± 0.3
900	12	4.0e-14	3.4632	0.0e+0	14.3051	0.0011	0.034	0.57162	0.908	62.5 ± 0.3
960	12	2.6e-14	3.4971	0.0e+0	13.8860	0.0012	0.035	0.64817	0.899	62.5 ± 0.4
1020	12	1.7e-14	3.6412	0.0e+0	13.3490	0.0018	0.037	0.69760	0.850	61.6 ± 0.6
1080	12	2.4e-14	4.5087	0.0e+0	13.3274	0.0039	0.037	0.75241	0.743	66.5 ± 0.6
1140	12	2.3e-14	6.1694	0.0e+0	13.7034	0.0070	0.036	0.79089	0.664	81.0 ± 0.8
1200	12	5.3e-14	8.2533	0.0e+0	14.1433	0.0113	0.035	0.85805	0.596	96.8 ± 0.6
1270	12	5.4e-14	8.0430	0.0e+0	14.3324	0.0119	0.034	0.92731	0.562	89.1 ± 0.6
1350	12	4.8e-14	6.8037	0.0e+0	14.5552	0.0097	0.034	1.00000	0.579	78.0 ± 0.6

Note: Total fusion age, TFA = 67.35 ± 0.15 Ma (including J).
Weighted mean plateau age, WMPA = 62.27 ± 0.20 Ma (including J).
Inverse isochron age = 62.89 ± 0.84 Ma (MSWD =0.69; ^{40}Ar/^{36}Ar = 267.3 ± 31.0).
Steps used: 840, 900, 960, 1020 (3–6/11 or 40% ∑ ^{39}Ar).
t = dwell time in minutes.
^{40}Ar (mol) = moles corrected for blank and reactor-produced ^{40}Ar.
Ratios are corrected for blanks, decay, and interference.
∑^{39}Ar is cumulative, ^{40}Ar* = rad fraction.

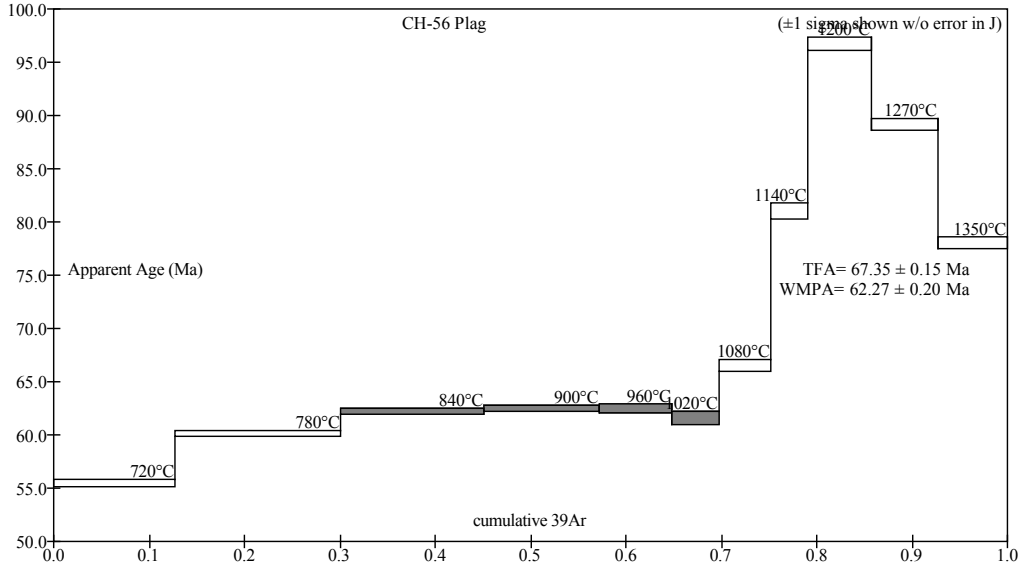

Decent plateau for 40% of gas - evidence for low temperature argon loss and some excess argon in most retentive sites.

Supplemental File 2

TABLE S3. SB56-87; CH-56 Plag h.p.'d; J=0.0111626

Temp (°C)	t	^{40}Ar (mol)	^{40}Ar/^{39}Ar	^{38}Ar/^{39}Ar	^{37}Ar/^{39}Ar	^{36}Ar/^{39}Ar	K/Ca	∑ ^{39}Ar	^{40}Ar*	Age (Ma)
800	12	1.8e-14	3.3737	0.0e+0	14.5420	0.0010	0.034	0.31570	0.908	60.7 ± 0.6
910	12	1.5e-14	3.5297	0.0e+0	14.1033	0.0011	0.035	0.56400	0.906	63.3 ± 0.7
1020	12	9.4e-15	3.7218	0.0e+0	13.3192	0.0017	0.037	0.71566	0.865	63.7 ± 1.1
1140	12	1.0e-14	5.7717	0.0e+0	13.1167	0.0060	0.037	0.82293	0.694	79.0 ± 1.5
1250	12	1.2e-14	7.2031	0.0e+0	13.8773	0.0105	0.035	0.92192	0.568	80.6 ± 1.7
1360	12	8.8e-15	6.7794	0.0e+0	13.8203	0.0100	0.035	1.00000	0.566	75.6 ± 2.0

Note: Total fusion age, TFA = 66.89 ± 0.43 Ma (including J).
Weighted mean plateau age, WMPA = 63.39 ± 0.61 Ma (including J).
Steps used: 910, 1020.
t = dwell time in minutes.
^{40}Ar (mol) = moles corrected for blank and reactor-produced ^{40}Ar.
Ratios are corrected for blanks, decay, and interference.
Σ^{39}Ar is cumulative, ^{40}Ar* = rad fraction.

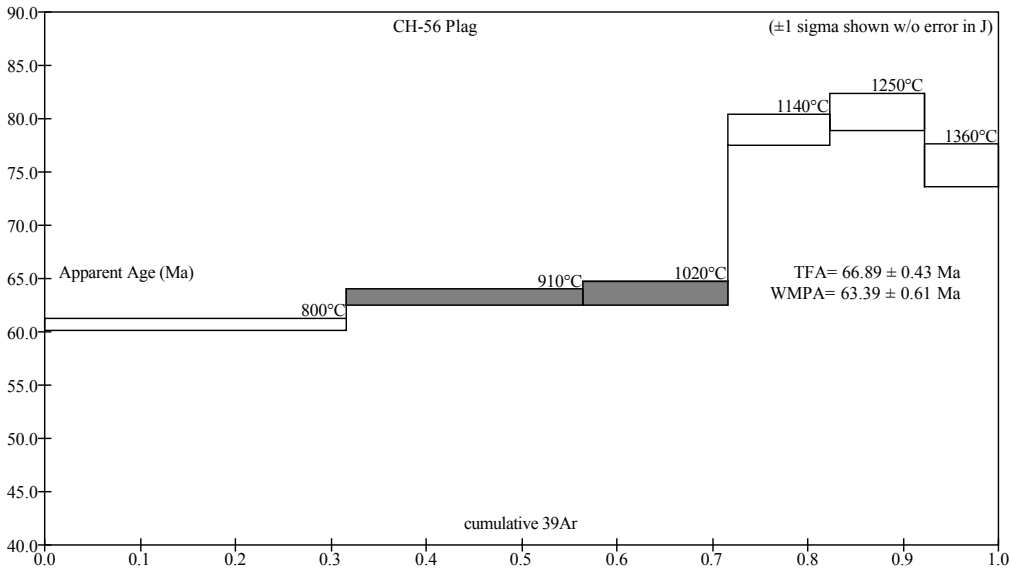

Decent plateau for 40% of gas - evidence for low temperature argon loss and some excess argon in most retentive sites.

Supplemental File 2

TABLE S4. SB56-89; CH-57 gm Plag; J=0.0111163

Temp (°C)	t	^{40}Ar (mol)	^{40}Ar/^{39}Ar	^{38}Ar/^{39}Ar	^{37}Ar/^{39}Ar	^{36}Ar/^{39}Ar	K/Ca	∑ ^{39}Ar	^{40}Ar*	Age (Ma)
720	12	4.7e-14	2.3989	0.0e+0	12.2203	0.0005	0.040	0.16030	0.934	44.4 ± 0.2
780	12	5.7e-14	2.6381	0.0e+0	10.6950	0.0005	0.046	0.33827	0.949	49.5 ± 0.2
840	12	4.9e-14	2.7624	0.0e+0	10.2198	0.0005	0.048	0.48419	0.948	51.8 ± 0.2
880	12	2.8e-14	2.7907	0.0e+0	10.2196	0.0006	0.048	0.56659	0.940	51.9 ± 0.3
920	12	1.9e-14	2.8021	0.0e+0	8.5236	0.0007	0.057	0.62166	0.922	51.1 ± 0.3
960	12	1.7e-14	2.8193	0.0e+0	7.0682	0.0007	0.069	0.67102	0.927	51.7 ± 0.4
1000	12	1.9e-14	2.8504	0.0e+0	7.1456	0.0008	0.069	0.72477	0.918	51.8 ± 0.3
1050	12	2.2e-14	2.8837	0.0e+0	7.9105	0.0010	0.062	0.78778	0.901	51.3 ± 0.3
1100	12	2.3e-14	2.9607	0.0e+0	8.7051	0.0014	0.056	0.85060	0.860	50.4 ± 0.3
1150	12	1.4e-14	3.2665	1.2e-4	12.3248	0.0023	0.040	0.88546	0.792	51.1 ± 0.5
1200	12	1.8e-14	3.5162	0.0e+0	15.4830	0.0030	0.032	0.92724	0.745	51.8 ± 0.5
1250	12	1.9e-14	3.5691	0.0e+0	17.6407	0.0032	0.028	0.97062	0.731	51.6 ± 0.5
1300	12	1.3e-14	3.7188	0.0e+0	18.5409	0.0037	0.026	1.00000	0.707	51.9 ± 0.7

Note: Total fusion age, TFA = 50.01 ± 0.10 Ma (including J).
Weighted mean plateau age, WMPA = 51.50 ± 0.12 Ma (including J).
Inverse isochron age =51.49 ± 0.25 Ma (MSWD =1.65; ^{40}Ar/^{36}Ar = 294.6 ± 9.0).
Steps used: 840, 880, 920, 960, 1000, 1050, 1100, 1150, 1200, 1250, 1300 (3–13/13 or 66% ∑ ^{39}Ar)
t = dwell time in minutes.
^{40}Ar (mol) = moles corrected for blank and reactor-produced ^{40}Ar.
Ratios are corrected for blanks, decay, and interference.
∑^{39}Ar is cumulative, ^{40}Ar* = rad fraction.

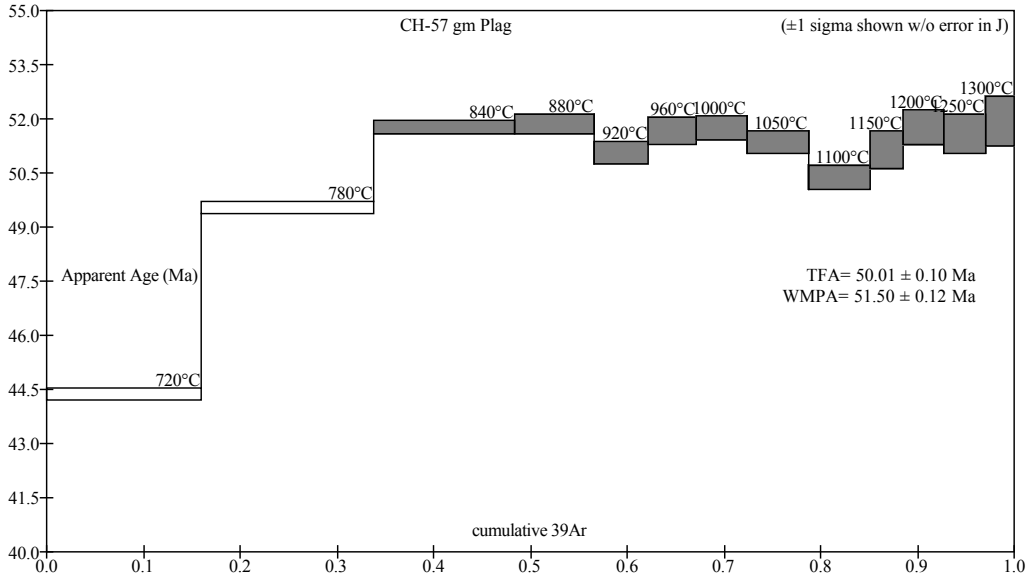

Bouncy spectrum, the isochron age of 51.49 ± 0.5 Ma is preferred.

Supplemental File 2

TABLE S5. SB61-32; CH-88 plag; J=0.0034042

Temp (°C)	t	^{40}Ar (mol)	^{40}Ar/^{39}Ar	^{38}Ar/^{39}Ar	^{37}Ar/^{39}Ar	^{36}Ar/^{39}Ar	K/Ca	∑ ^{39}Ar	^{40}Ar*	Age (Ma)
650	12	1.8e-14	11.2280	0.0e+0	8.8976	0.0015	0.055	0.02916	0.961	65.1 ± 0.5
730	12	5.0e-14	11.1537	0.0e+0	8.9368	0.0008	0.055	0.11083	0.978	65.8 ± 0.2
800	12	7.3e-14	11.0680	0.0e+0	8.1986	0.0007	0.060	0.23117	0.982	65.5 ± 0.2
860	12	7.9e-14	11.0264	0.0e+0	8.1120	0.0004	0.060	0.36243	0.989	65.8 ± 0.2
920	12	8.0e-14	11.0144	0.0e+0	8.0565	0.0004	0.061	0.49585	0.989	65.7 ± 0.2
980	12	7.2e-14	11.0437	0.0e+0	7.9134	0.0004	0.062	0.61493	0.990	65.9 ± 0.2
1040	12	5.7e-14	11.0845	0.0e+0	7.7366	0.0005	0.063	0.70866	0.985	65.9 ± 0.2
1100	12	3.7e-14	11.2021	0.0e+0	7.4322	0.0011	0.066	0.76936	0.971	65.6 ± 0.3
1160	12	3.0e-14	11.2887	3.7e-4	7.9207	0.0013	0.062	0.81770	0.966	65.8 ± 0.3
1220	12	3.9e-14	11.3869	0.0e+0	8.3799	0.0014	0.058	0.88015	0.964	66.2 ± 0.3
1290	12	4.0e-14	11.3087	0.0e+0	8.2136	0.0011	0.060	0.94509	0.970	66.2 ± 0.3
1400	12	3.4e-14	11.3536	0.0e+0	8.5935	0.0020	0.057	1.00000	0.948	64.9 ± 0.3

Note: Total fusion age, TFA= 65.72 ± 0.17 Ma (including J).
Weighted mean plateau age, WMPA = 65.79 ± 0.17 Ma (including J).
Inverse isochron age = 65.59 ± 0.21 Ma (MSWD =1.04; ^{40}Ar/^{36}Ar = 346.6 ± 32.5).
Steps used: 730, 800, 860, 920, 980, 1040, 1100, 1160, 1220, 1290 (2–11/12 or 92% ∑ ^{39}Ar).
t = dwell time in minutes.
^{40}Ar (mol) = moles corrected for blank and reactor-produced ^{40}Ar.
Ratios are corrected for blanks, decay, and interference.
∑^{39}Ar is cumulative, ^{40}Ar* = rad fraction.

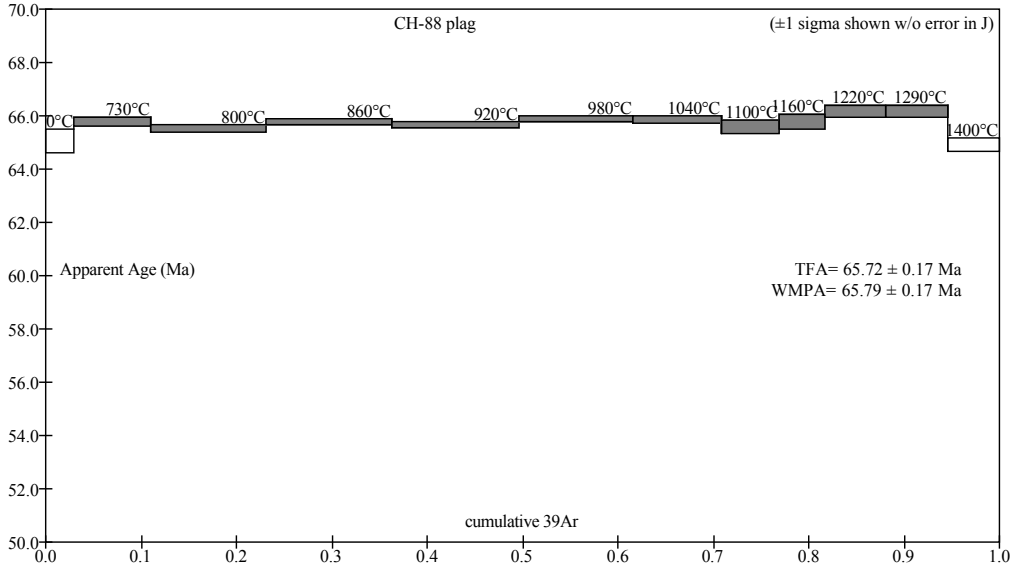

Excellent age plateau.

TABLE S6. SB61-21; CH-89 c.g. plag-e1; J=0.0034894

Temp (°C)	t	^{40}Ar (mol)	^{40}Ar/^{39}Ar	^{38}Ar/^{39}Ar	^{37}Ar/^{39}Ar	^{36}Ar/^{39}Ar	K/Ca	∑ ^{39}Ar	^{40}Ar*	Age (Ma)
600	14	3.9e-15	12.5259	1.1e-3	4.5930	0.0217	0.11	0.00790	0.488	38.0 ± 2.0
670	14	8.9e-15	9.1505	0.0e+0	6.4732	0.0073	0.076	0.03249	0.764	43.5 ± 0.6
740	14	1.9e-14	8.3638	0.0e+0	7.3489	0.0034	0.067	0.09047	0.879	45.7 ± 0.3
810	14	2.8e-14	7.9143	0.0e+0	7.1630	0.0019	0.068	0.18095	0.928	45.6 ± 0.2
880	14	3.7e-14	7.6984	0.0e+0	7.0092	0.0012	0.070	0.30115	0.953	45.6 ± 0.2
940	14	3.6e-14	7.5822	0.0e+0	6.8417	0.0007	0.072	0.41969	0.971	45.8 ± 0.2
1000	14	3.2e-14	7.5752	0.0e+0	6.6384	0.0007	0.074	0.52492	0.974	45.9 ± 0.2
1060	14	2.3e-14	7.6660	0.0e+0	6.4682	0.0011	0.076	0.60125	0.959	45.7 ± 0.2
1120	14	1.6e-14	8.2157	0.0e+0	6.5612	0.0020	0.075	0.65071	0.930	47.4 ± 0.4
1190	14	3.0e-14	8.7098	0.0e+0	6.5461	0.0029	0.075	0.73708	0.903	48.9 ± 0.2
1260	14	5.2e-14	8.2858	0.0e+0	6.3803	0.0022	0.077	0.89469	0.922	47.4 ± 0.2
1320	14	3.0e-14	8.2848	0.0e+0	6.9555	0.0022	0.070	0.98598	0.921	47.4 ± 0.2
1400	14	5.7e-15	10.2503	8.9e-4	9.9501	0.0075	0.049	1.00000	0.785	50.0 ± 1.1

Note: Total fusion age, TFA = 46.44 ± 0.13 Ma (including J).
Weighted mean plateau age, WMPA = 45.72 ± 0.13 Ma (including J).
Steps used: 740, 810, 880, 940, 1000, 1060.
t = dwell time in minutes.
^{40}Ar (mol) = moles corrected for blank and reactor-produced ^{40}Ar.
Ratios are corrected for blanks, decay, and interference.
∑^{39}Ar is cumulative, ^{40}Ar* = rad fraction.

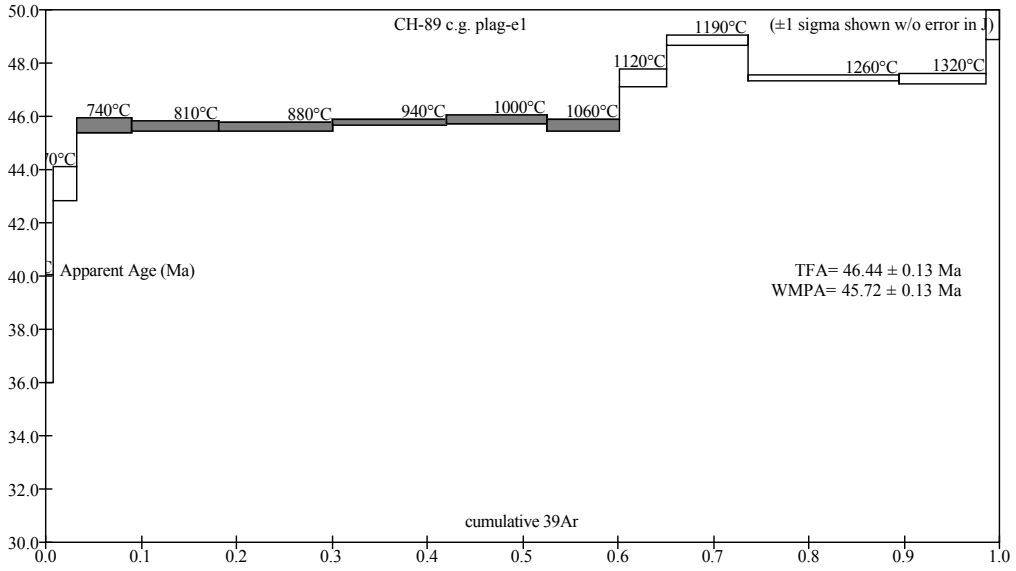

Good plateau for 55% of gas. Some excess argon in most retentive sites. Concordant with other splits.

Supplemental File 2

TABLE S7. SB61-25; CH-89 c.g. Plag-e2; J=0.0034660

Temp (°C)	t	^{40}Ar (mol)	^{40}Ar/^{39}Ar	^{38}Ar/^{39}Ar	^{37}Ar/^{39}Ar	^{36}Ar/^{39}Ar	K/Ca	∑ ^{39}Ar	^{40}Ar*	Age (Ma)
700	14	1.3e-14	8.6369	0.0e+0	6.5921	0.0056	0.074	0.04273	0.809	43.2 ± 0.4
780	14	2.4e-14	7.8838	0.0e+0	7.2475	0.0020	0.068	0.12528	0.925	45.0 ± 0.3
860	14	3.3e-14	7.7129	0.0e+0	7.1965	0.0013	0.068	0.24192	0.948	45.2 ± 0.2
930	14	3.5e-14	7.6132	0.0e+0	7.0839	0.0009	0.069	0.37068	0.963	45.3 ± 0.2
1000	14	3.5e-14	7.6049	0.0e+0	6.8385	0.0009	0.072	0.49702	0.966	45.3 ± 0.2
1080	14	2.8e-14	7.6908	0.0e+0	6.6005	0.0010	0.074	0.59611	0.960	45.6 ± 0.2
1150	14	1.8e-14	8.2082	0.0e+0	6.6514	0.0022	0.074	0.65637	0.922	46.7 ± 0.3
1210	14	3.1e-14	8.6722	0.0e+0	6.6481	0.0030	0.074	0.75518	0.897	48.0 ± 0.2
1260	14	3.7e-14	8.2638	0.0e+0	6.4380	0.0020	0.076	0.87969	0.929	47.3 ± 0.2
1320	14	3.0e-14	8.2470	0.0e+0	7.0124	0.0021	0.070	0.98110	0.926	47.1 ± 0.2
1400	14	6.2e-15	9.0782	1.7e-3	8.6908	0.0053	0.056	1.00000	0.826	46.3 ± 0.8

Note: Total fusion age, TFA = 46.01 ± 0.13 Ma (including J).
Weighted mean plateau age, WMPA = 45.30 ± 0.13 Ma (including J).
Steps used: 780, 860, 930, 1000,1080.
t = dwell time in minutes.
^{40}Ar (mol) = moles corrected for blank and reactor-produced ^{40}Ar.
Ratios are corrected for blanks, decay, and interference.
∑^{39}Ar is cumulative, ^{40}Ar* = rad fraction.

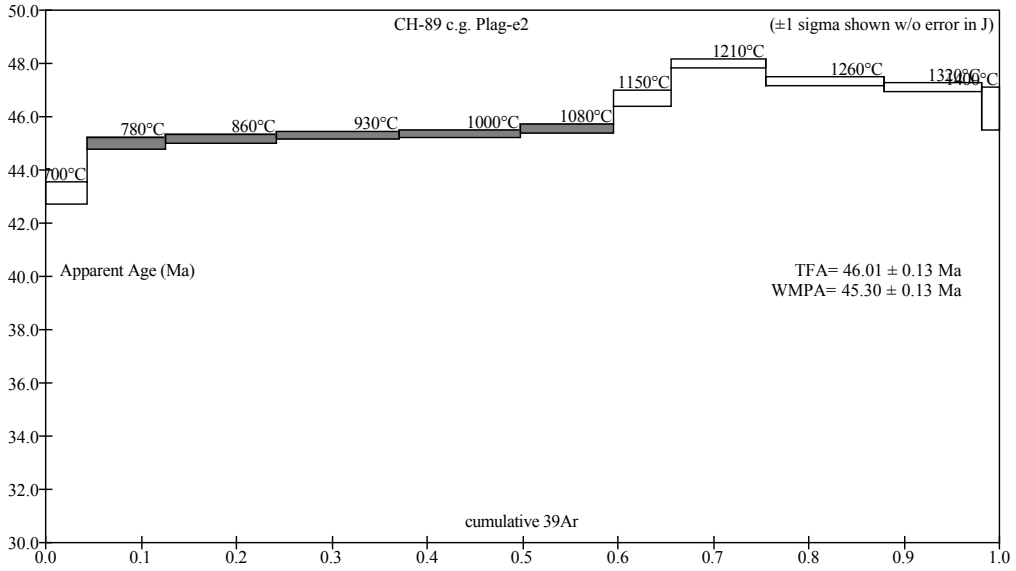

Good plateau for 55% of gas. Some excess argon released by retentive sites at high temperature. Concordant with other splits.

Supplemental File 2

TABLE S8. SB61-28; CH-89 f.g. plag-e1; J=0.0034418

Temp (°C)	t	^{40}Ar (mol)	^{40}Ar/^{39}Ar	^{38}Ar/^{39}Ar	^{37}Ar/^{39}Ar	^{36}Ar/^{39}Ar	K/Ca	∑ ^{39}Ar	^{40}Ar*	Age (Ma)
700	14	1.6e-14	8.3859	0.0e+0	5.2938	0.0049	0.093	0.04441	0.827	42.6 ± 0.3
780	14	3.1e-14	7.9420	0.0e+0	5.8079	0.0019	0.084	0.13256	0.931	45.3 ± 0.2
860	14	3.7e-14	7.7987	0.0e+0	5.9347	0.0014	0.083	0.24049	0.945	45.2 ± 0.2
930	14	4.8e-14	7.7405	0.0e+0	5.9185	0.0012	0.083	0.38184	0.955	45.3 ± 0.2
1000	14	4.5e-14	7.6958	0.0e+0	5.7738	0.0010	0.085	0.51540	0.962	45.4 ± 0.2
1080	14	3.5e-14	7.7537	0.0e+0	5.6152	0.0011	0.087	0.61658	0.957	45.5 ± 0.2
1150	14	1.9e-14	8.2956	0.0e+0	5.6239	0.0023	0.087	0.66805	0.919	46.7 ± 0.3
1210	14	3.0e-14	8.8348	0.0e+0	5.7354	0.0033	0.085	0.74486	0.890	48.2 ± 0.2
1260	14	4.6e-14	8.5071	0.0e+0	5.6010	0.0024	0.087	0.86644	0.916	47.7 ± 0.2
1330	14	4.3e-14	8.3759	0.0e+0	5.8668	0.0023	0.084	0.98269	0.919	47.2 ± 0.2
1410	14	6.3e-15	8.2797	0.0e+0	8.1178	0.0050	0.060	1.00000	0.821	41.7 ± 0.7

Note: Total fusion age, TFA = 45.95 ± 0.12 Ma (including J).
Weighted mean plateau age, WMPA = 45.34 ± 0.13 Ma (including J).
Inverse isochron age = 45.46 ± 0.30 Ma (MSWD = 0.64; ^{40}Ar/^{36}Ar = 279.5 ± 28.8).
Steps used: 780, 860, 930, 1000, 1080 (2–6/11 or 57% ∑ ^{39}Ar).
t = dwell time in minutes.
^{40}Ar (mol) = moles corrected for blank and reactor-produced ^{40}Ar.
Ratios are corrected for blanks, decay, and interference.
∑^{39}Ar is cumulative, ^{40}Ar* = rad fraction.

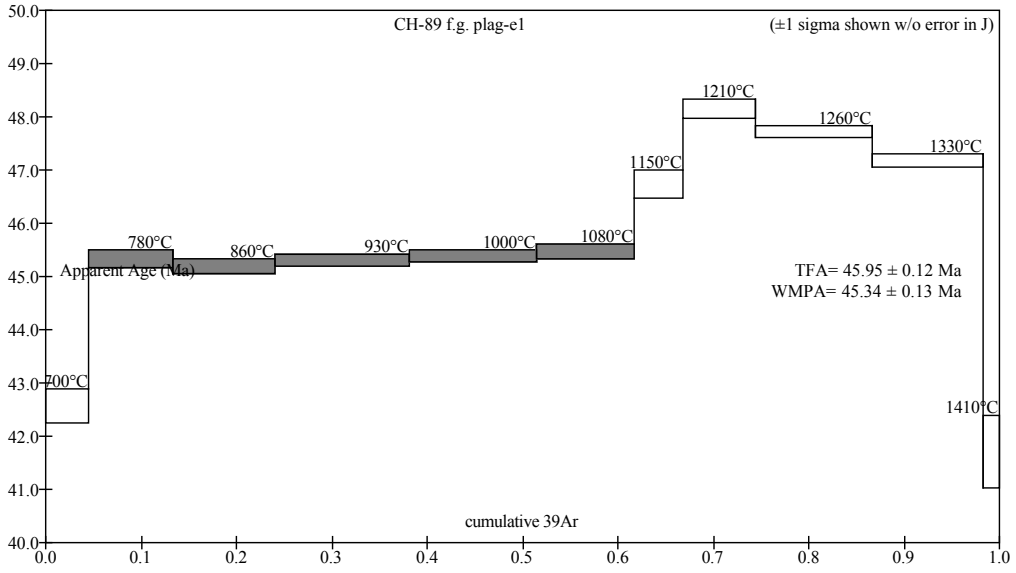

Good plateau for 55% of gas. Excess argon in retentive sites. Concordant with other splits.

Supplemental File 2

TABLE S9. SB61-46; CH-95 plag; J=0.0032705

Temp (°C)	t	^{40}Ar (mol)	^{40}Ar/^{39}Ar	^{38}Ar/^{39}Ar	^{37}Ar/^{39}Ar	^{36}Ar/^{39}Ar	K/Ca	∑ ^{39}Ar	^{40}Ar*	Age (Ma)
650	14	1.8e-14	5.6669	0.0e+0	16.8262	0.0018	0.029	0.12698	0.904	30.0 ± 0.3
730	14	4.6e-14	6.0720	0.0e+0	16.0735	0.0008	0.030	0.43783	0.960	34.1 ± 0.1
800	14	1.8e-14	6.8633	0.0e+0	14.8978	0.0023	0.033	0.54365	0.903	36.2 ± 0.3
860	14	9.2e-15	7.3355	0.0e+0	14.7908	0.0034	0.033	0.59503	0.861	36.9 ± 0.6
920	14	7.1e-15	7.6254	0.0e+0	14.6310	0.0045	0.033	0.63290	0.826	36.8 ± 0.8
980	14	6.9e-15	7.8269	0.0e+0	14.9826	0.0066	0.033	0.66891	0.750	34.3 ± 0.8
1040	14	8.7e-15	7.4374	0.0e+0	14.9585	0.0045	0.033	0.71644	0.822	35.7 ± 0.7
1100	14	9.3e-15	7.1738	0.0e+0	13.8059	0.0037	0.035	0.76941	0.848	35.5 ± 0.6
1160	14	7.0e-15	6.9017	4.1e-4	13.7290	0.0013	0.036	0.81061	0.945	38.1 ± 0.8
1220	14	8.0e-15	7.0050	0.0e+0	14.5246	0.0022	0.034	0.85718	0.908	37.1 ± 0.6
1290	14	9.7e-15	7.1884	0.0e+0	14.5420	0.0026	0.034	0.91242	0.895	37.5 ± 0.6
1400	14	1.6e-14	7.2571	0.0e+0	13.8949	0.0023	0.035	1.00000	0.905	38.3 ± 0.4

Note: Total fusion age, TFA = 35.06 ± 0.14 Ma (including J).
Weighted mean plateau age, WMPA = 36.87 ± 0.19 Ma (including J).
Inverse isochron age = 36.63 ± 0.76 Ma (MSWD =1.89; ^{40}Ar/^{36}Ar = 266.1 ± 39.0).
Steps used: 800, 860, 920, 980, 1040, 1100, 1160, 1220, 1290, 1400 (3–12/12 or 56% ∑ ^{39}Ar).
t = dwell time in minutes.
^{40}Ar (mol) = moles corrected for blank and reactor-produced ^{40}Ar.
Ratios are corrected for blanks, decay, and interference.
Σ^{39}Ar is cumulative, ^{40}Ar* = rad fraction.

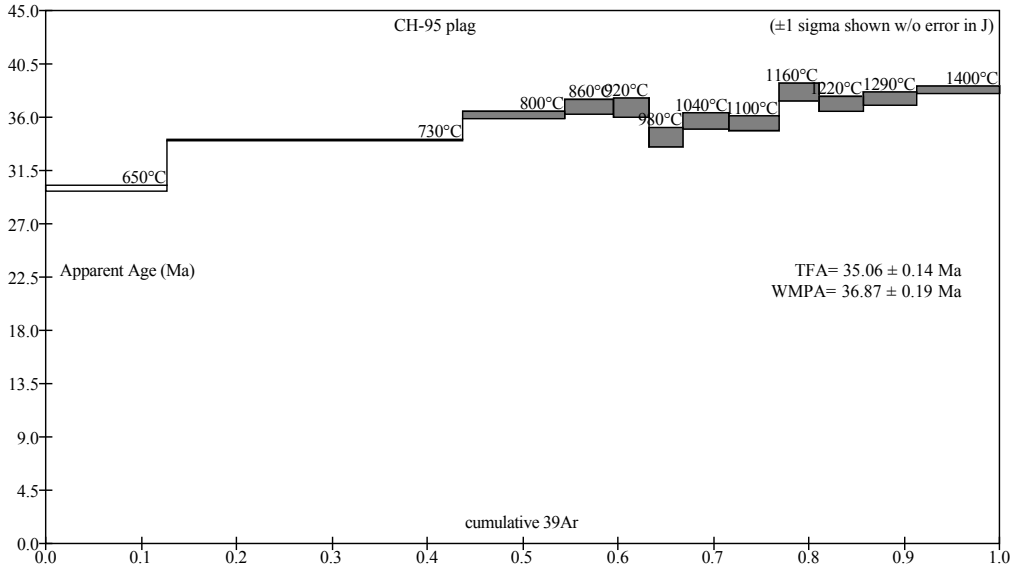

Bouncy spectrum with excess Ar. Evidence of Ar loss at low temperature steps. Preferred age of 35.9 ± 0.8 Ma recalculated using the 800°C -1100°C steps.

TABLE S10. SB61-139; CH-98 Plag; J=0.0035531

Temp (°C)	t	^{40}Ar (mol)	^{40}Ar/^{39}Ar	^{38}Ar/^{39}Ar	^{37}Ar/^{39}Ar	^{36}Ar/^{39}Ar	K/Ca	∑ ^{39}Ar	^{40}Ar*	Age (Ma)
720	14	8.1e-15	5.5003	0.0e+0	13.1619	0.0014	0.037	0.27224	0.926	32.3 ± 0.5
820	14	9.5e-15	5.9984	0.0e+0	11.4469	0.0010	0.043	0.56444	0.951	36.2 ± 0.5
950	14	3.8e-15	6.3735	3.2e-3	10.2828	0.0017	0.048	0.67430	0.920	37.2 ± 1.2
1100	14	4.2e-15	7.8310	3.8e-3	11.2357	0.0044	0.044	0.77222	0.836	41.5 ± 1.4
1250	14	4.5e-15	7.2287	0.0e+0	11.8408	0.0028	0.041	0.88724	0.887	40.6 ± 1.2
1400	14	4.8e-15	7.8402	4.3e-5	11.9703	0.0033	0.041	1.00000	0.877	43.5 ± 1.3

Note: Total fusion age, TFA = 37.11 ± 0.35 Ma (including J).
Weighted mean plateau age, WMPA = 36.31 ± 0.44 Ma (including J).
Inverse isochron age =33.73 ± 1.60 Ma (MSWD = 0.39; ^{40}Ar/^{36}Ar = 675.3 ± 83.1 Ma).
Steps used: 820, 950 (2–3/6 or 40% ∑ ^{39}Ar).
t = dwell time in minutes.
^{40}Ar (mol) = moles corrected for blank and reactor-produced ^{40}Ar.
Ratios are corrected for blanks, decay, and interference.
∑^{39}Ar is cumulative, ^{40}Ar* = rad fraction.

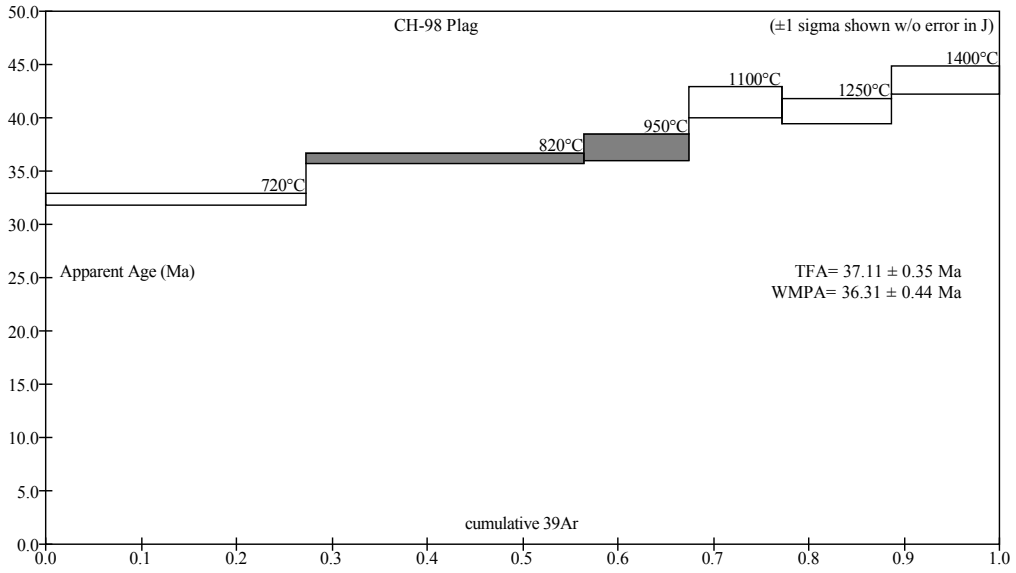

Small signal with larger errors; decent plateau for mid-temperature steps.

Supplemental File 2

TABLE S11. SB61-166; CH-98 gm; J=0.0033657

Temp (°C)	t	^{40}Ar (mol)	^{40}Ar/^{39}Ar	^{38}Ar/^{39}Ar	^{37}Ar/^{39}Ar	^{36}Ar/^{39}Ar	K/Ca	∑ ^{39}Ar	^{40}Ar*	Age (Ma)
620	15	3.5e-14	7.6180	0.0e+0	2.2868	0.0078	0.21	0.06003	0.699	32.0 ± 0.2
680	15	5.9e-14	7.3829	0.0e+0	2.6851	0.0057	0.18	0.16532	0.773	34.3 ± 0.1
740	15	7.3e-14	6.6822	0.0e+0	1.7402	0.0031	0.28	0.30912	0.864	34.7 ± 0.1
800	15	6.1e-14	6.6743	0.0e+0	1.1307	0.0030	0.43	0.42899	0.868	34.8 ± 0.1
860	15	3.3e-14	6.6146	0.0e+0	1.1921	0.0031	0.41	0.49435	0.864	34.4 ± 0.1
920	15	3.0e-14	6.5698	0.0e+0	1.2185	0.0032	0.40	0.55352	0.854	33.8 ± 0.1
980	15	4.1e-14	7.0412	0.0e+0	1.2264	0.0048	0.40	0.62949	0.799	33.8 ± 0.1
1040	15	5.9e-14	7.2285	0.0e+0	1.3693	0.0050	0.36	0.73541	0.796	34.6 ± 0.1
1100	15	6.2e-14	7.5883	0.0e+0	1.6128	0.0057	0.30	0.84267	0.776	35.4 ± 0.1
1170	15	5.5e-14	8.4043	0.0e+0	2.6275	0.0079	0.19	0.92896	0.721	36.4 ± 0.1
1250	15	5.2e-14	9.5252	0.0e+0	6.7010	0.0121	0.073	1.00000	0.626	35.8 ± 0.2

Note: Total fusion age, TFA = 34.67 ± 0.06 Ma (including J).
Weighted mean plateau age, WMPA = 34.61 ± 0.06 Ma (including J).
Inverse isochron age = 34.11 ± 0.68 Ma (MSWD = 25.18; ^{40}Ar/^{36}Ar = 315.8 ± 27.4).
Steps used: 680, 740, 800, 860, 920, 980, 1040, 1100 (2–9/11 or 78% ∑ ^{39}Ar).
t = dwell time in minutes.
^{40}Ar (mol) = moles corrected for blank and reactor-produced ^{40}Ar.
Ratios are corrected for blanks, decay, and interference.
∑^{39}Ar is cumulative, ^{40}Ar* = rad fraction.

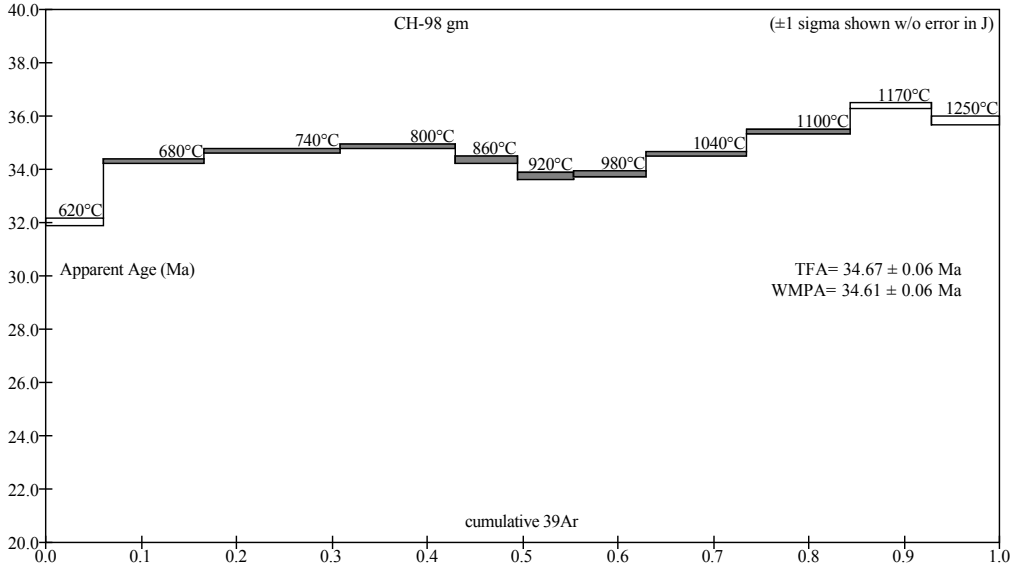

Slight saddle in spectrum with evidence of argon loss at low temperature step.

TABLE S12. SB61-162; J338 plag; J=0.0034037

Temp (°C)	t	^{40}Ar (mol)	^{40}Ar/^{39}Ar	^{38}Ar/^{39}Ar	^{37}Ar/^{39}Ar	^{36}Ar/^{39}Ar	K/Ca	∑ ^{39}Ar	^{40}Ar*	Age (Ma)
650	14	2.6e-14	7.1331	2.8e-3	16.5020	0.0107	0.030	0.16067	0.555	24.1 ± 0.3
730	14	3.1e-14	6.9254	1.4e-5	14.6445	0.0082	0.033	0.35780	0.650	27.4 ± 0.2
800	14	2.0e-14	9.4397	0.0e+0	13.4902	0.0134	0.036	0.44991	0.582	33.4 ± 0.5
870	14	1.5e-14	9.6141	0.0e+0	13.8520	0.0128	0.035	0.51778	0.608	35.5 ± 0.6
940	14	1.4e-14	8.6396	0.0e+0	14.5990	0.0094	0.034	0.58730	0.679	35.7 ± 0.6
1010	14	1.4e-14	8.0141	0.0e+0	15.1893	0.0075	0.032	0.66441	0.725	35.3 ± 0.5
1080	14	1.5e-14	7.8651	0.0e+0	15.4710	0.0070	0.032	0.74898	0.737	35.2 ± 0.5
1150	14	1.6e-14	10.8541	0.0e+0	15.1778	0.0153	0.032	0.81499	0.583	38.4 ± 0.7
1230	14	2.6e-14	13.1177	0.0e+0	14.8057	0.0238	0.033	0.90058	0.463	36.9 ± 0.5
1310	14	1.5e-14	10.8252	0.0e+0	14.4393	0.0152	0.034	0.96106	0.584	38.4 ± 0.7
1400	14	9.5e-15	10.6716	0.0e+0	14.0990	0.0148	0.035	1.00000	0.590	38.2 ± 1.0

Note: Total fusion age, TFA = 32.48 ± 0.15 Ma (including J).
Weighted mean plateau age, WMPA = 35.41 ± 0.27 Ma (including J).
Inverse isochron age = 34.91 ± 1.14 Ma (MSWD =0.09; ^{40}Ar/^{36}Ar = 305.0 ± 6.4).
Steps used: 870, 940, 1010, 1080 (4–7/11 or 30% ∑ ^{39}Ar).
t = dwell time in minutes.
^{40}Ar (mol) = moles corrected for blank and reactor-produced ^{40}Ar.
Ratios are corrected for blanks, decay, and interference.
∑^{39}Ar is cumulative, ^{40}Ar* = rad fraction.

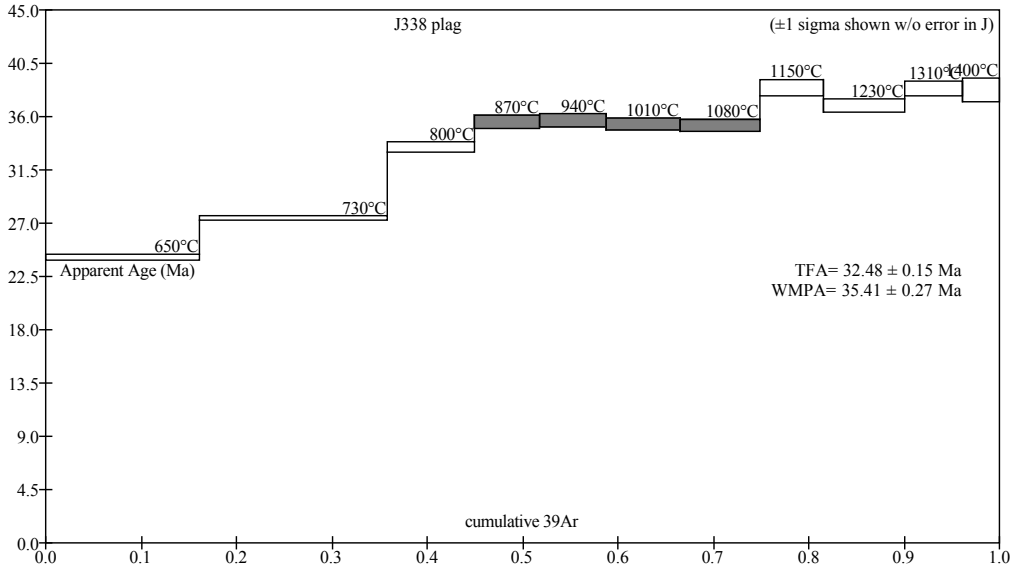

Good mini-plateau but it only represents only 30% of gas released, and there is evidence for both argon loss and excess argon.

Supplemental File 2

TABLE S13. SB61-161; J338 plag; J=0.0034108

Temp (°C)	t	^{40}Ar (mol)	^{40}Ar/^{39}Ar	^{38}Ar/^{39}Ar	^{37}Ar/^{39}Ar	^{36}Ar/^{39}Ar	K/Ca	∑ ^{39}Ar	^{40}Ar*	Age (Ma)
750	14	1.3e-14	41.6037	7.0e-3	14.6758	0.1234	0.033	0.28692	0.123	31.3 ± 3.4
900	14	9.4e-15	34.7021	1.2e-3	14.4301	0.0970	0.034	0.53395	0.174	36.7 ± 3.8
1150	14	3.5e-15	21.2745	0.0e+0	14.3869	0.0527	0.034	0.68585	0.268	34.8 ± 5.6
1380	14	3.7e-15	10.6073	5.2e-4	13.3971	0.0150	0.037	1.00000	0.583	37.6 ± 2.7

Note: Total fusion age, TFA = 35.15 ± 1.80 Ma (including J).
Weighted mean plateau age, WMPA = 35.48 ± 1.75 Ma (including J).
Inverse isochron age = 38.48 ± 2.90 Ma (MSWD = 0.45; ^{40}Ar/^{36}Ar = 287.8 ± 3.9).
Steps used: 750, 900, 1150, 1380 (1–4/4 or 100% ∑ ^{39}Ar).
t = dwell time in minutes.
^{40}Ar (mol) = moles corrected for blank and reactor-produced ^{40}Ar.
Ratios are corrected for blanks, decay, and interference.
∑^{39}Ar is cumulative, ^{40}Ar* = rad fraction.

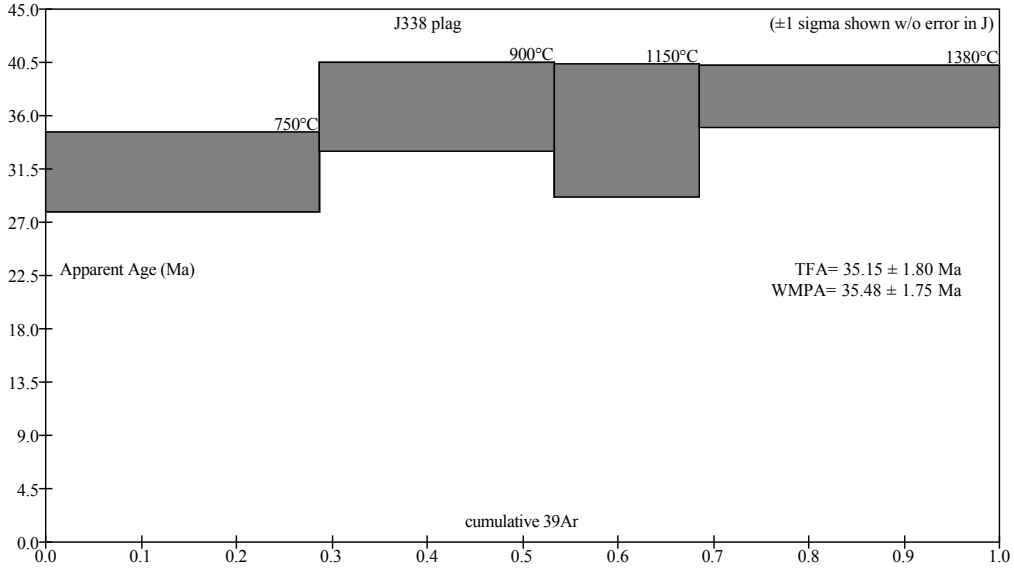

Small signal with large errors.

Supplemental File 2

TABLE S14. SB61-198; J378-e1 plag; J=0.0031182

Temp (°C)	t	^{40}Ar (mol)	^{40}Ar/^{39}Ar	^{38}Ar/^{39}Ar	^{37}Ar/^{39}Ar	^{36}Ar/^{39}Ar	K/Ca	∑ ^{39}Ar	^{40}Ar*	Age (Ma)
700	14	6.5e-15	3.2655	0.0e+0	3.8828	0.0046	0.13	0.04562	0.586	10.7 ± 0.4
800	14	1.2e-14	2.5242	0.0e+0	4.4128	0.0022	0.11	0.15108	0.740	10.5 ± 0.2
900	14	1.5e-14	2.3114	0.0e+0	4.2801	0.0013	0.11	0.29583	0.831	10.8 ± 0.1
970	14	1.2e-14	2.2479	0.0e+0	4.1700	0.0010	0.12	0.41786	0.867	10.9 ± 0.1
1040	14	9.8e-15	2.2820	0.0e+0	3.9888	0.0011	0.12	0.51607	0.863	11.0 ± 0.2
1110	14	8.0e-15	2.6974	0.0e+0	3.9757	0.0026	0.12	0.58371	0.717	10.8 ± 0.2
1200	14	2.1e-14	3.0568	0.0e+0	3.9184	0.0035	0.13	0.73873	0.658	11.3 ± 0.1
1300	14	2.7e-14	2.5811	0.0e+0	3.9853	0.0019	0.12	0.97506	0.778	11.3 ± 0.1
1400	14	4.0e-15	3.6649	0.0e+0	5.4921	0.0037	0.089	1.00000	0.704	14.5 ± 0.7

Note: Total fusion age, TFA = 11.08 ± 0.05 Ma (including J).
Weighted mean plateau age, WMPA = 11.17 ± 0.05 Ma (including J).
Inverse isochron age =1 0.94 ± 0.19 Ma (MSWD =1.58; ^{40}Ar/^{36}Ar = 315.2 ± 15.1).
Steps used: 970, 1040, 1110, 1200, 1300 (4–8/9 or 68% ∑ ^{39}Ar).
t = dwell time in minutes.
^{40}Ar (mol) = moles corrected for blank and reactor-produced ^{40}Ar.
Ratios are corrected for blanks, decay, and interference.
∑^{39}Ar is cumulative, ^{40}Ar* = rad fraction.

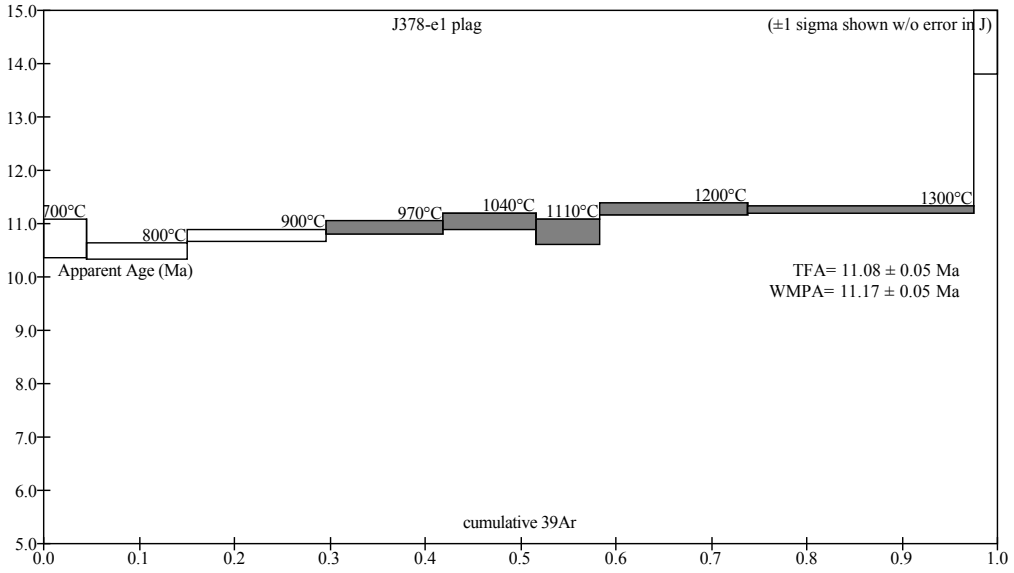

Decent plateau but slightly climbs and all steps are not within error of each other. Excess argon in most retentive sites.

Supplemental File 2

TABLE S15. SB61-201; 202 J378-e3 san?; Fusions of 10 grains each; J=0.0030705

Temp (°C)	t	^{40}Ar (mol)	^{40}Ar/^{39}Ar	^{38}Ar/^{39}Ar	^{37}Ar/^{39}Ar	^{36}Ar/^{39}Ar	K/Ca	∑ ^{39}Ar	^{40}Ar*	Age (Ma)
1350	20	1.5e-14	23.8266	0.0e+0	5.3142	0.0732	0.092	0.56603	0.092	12.1 ± 1.4
1350	20	1.4e-14	30.8245	1.7e-3	5.6883	0.0975	0.086	1.00000	0.065	11.0 ± 1.7

Note: Total fusion age, TFA = 11.61 ± 1.07 Ma (including J).
Weighted mean plateau age, WMPA = 11.68 ± 1.07 Ma (including J).
Inverse isochron age = 15.05 ± 6.73 Ma (MSWD = 0.00; ^{40}Ar/^{36}Ar = 288.0 ± 0.0).
Steps used: 1350, 1350 (1–2/2 or 100% ∑ ^{39}Ar).
t = dwell time in minutes.
^{40}Ar (mol) = moles corrected for blank and reactor-produced ^{40}Ar.
Ratios are corrected for blanks, decay, and interference.
∑^{39}Ar is cumulative, ^{40}Ar* = rad fraction.

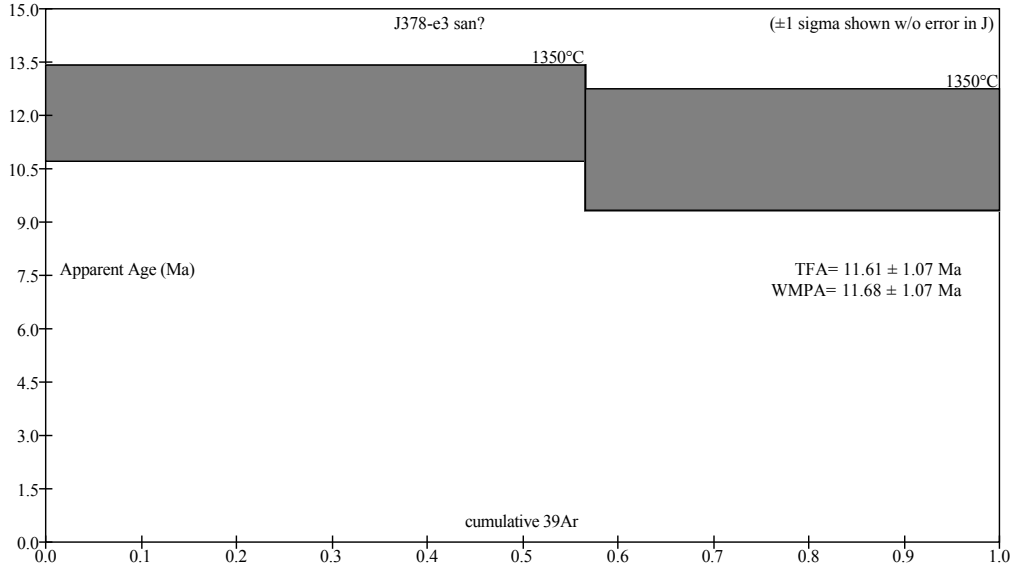

Small signals with big uncertainties.

Supplemental File 2

TABLE S16. SB61-190; J402 plag; J=0.0031997

Temp (°C)	t	^{40}Ar (mol)	^{40}Ar/^{39}Ar	^{38}Ar/^{39}Ar	^{37}Ar/^{39}Ar	^{36}Ar/^{39}Ar	K/Ca	∑ ^{39}Ar	^{40}Ar*	Age (Ma)
700	14	2.1e-14	17.1347	6.2e-2	106.2864	0.0482	0.005	0.10732	0.169	16.6 ± 0.7
800	14	2.8e-14	13.1798	7.0e-3	46.7776	0.0350	0.010	0.28235	0.215	16.3 ± 0.5
900	14	3.8e-14	16.1685	0.0e+0	17.3737	0.0459	0.028	0.47599	0.161	15.0 ± 0.5
970	14	3.4e-14	21.2420	0.0e+0	11.8335	0.0622	0.041	0.60738	0.135	16.5 ± 1.0
1040	14	5.6e-14	47.5360	0.0e+0	13.4143	0.1491	0.037	0.70374	0.073	19.9 ± 1.2
1150	14	2.3e-14	23.5739	4.3e-4	14.1324	0.0636	0.035	0.78209	0.203	27.4 ± 0.9
1280	14	1.0e-14	7.9624	8.6e-5	18.6957	0.0097	0.026	0.88546	0.639	29.1 ± 0.6
1400	14	6.6e-15	4.6699	0.0e+0	9.5890	0.0035	0.051	1.00000	0.776	20.8 ± 0.5

Note: Total fusion age, TFA = 19.16 ± 0.25 Ma (including J).
Weighted mean plateau age, WMPA = 15.84 ± 0.30 Ma (including J).
Inverse isochron age = 14.13 ± 0.85 Ma (MSWD = 2.14; ^{40}Ar/^{36}Ar = 302.0 ± 2.4).
Steps used: 700, 800, 900, 970 (1–4/8 or 61% ∑ ^{39}Ar).
t = dwell time in minutes.
^{40}Ar (mol) = moles corrected for blank and reactor-produced ^{40}Ar.
Ratios are corrected for blanks, decay, and interference.
∑^{39}Ar is cumulative, ^{40}Ar* = rad fraction.

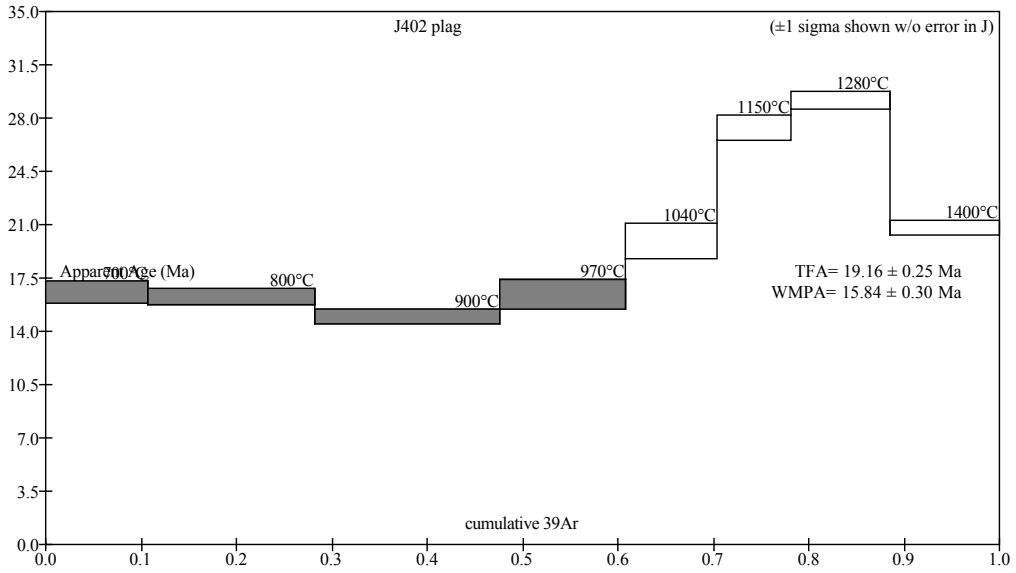

Exhibits decent flat before climbing at the higher temperature steps indicative of excess argon. More reliable than whole rock split.

Supplemental File 2

TABLE S17. SB61-191; J402 wr; J=0.0031871

Temp (°C)	t	^{40}Ar (mol)	^{40}Ar/^{39}Ar	^{38}Ar/^{39}Ar	^{37}Ar/^{39}Ar	^{36}Ar/^{39}Ar	K/Ca	∑ ^{39}Ar	^{40}Ar*	Age (Ma)
620	15	4.6e-14	7.6635	0.0e+0	3.0718	0.0155	0.16	0.07808	0.403	17.7 ± 0.1
680	15	4.6e-14	4.5820	0.0e+0	3.1101	0.0051	0.16	0.20904	0.672	17.6 ± 0.1
740	15	4.8e-14	3.6602	0.0e+0	2.1233	0.0024	0.23	0.37888	0.806	16.9 ± 0.1
800	15	4.2e-14	3.6081	0.0e+0	1.6354	0.0025	0.30	0.53070	0.794	16.4 ± 0.1
860	15	3.6e-14	4.1956	0.0e+0	1.4580	0.0048	0.34	0.64273	0.661	15.9 ± 0.1
920	15	2.6e-14	3.8594	0.0e+0	1.6203	0.0038	0.30	0.72985	0.707	15.6 ± 0.1
980	15	2.2e-14	3.6478	0.0e+0	1.6675	0.0033	0.29	0.80898	0.735	15.4 ± 0.1
1040	15	2.2e-14	4.1883	8.0e-4	1.8862	0.0053	0.26	0.87635	0.629	15.1 ± 0.1
1100	15	2.3e-14	3.7690	2.7e-3	4.5473	0.0046	0.11	0.95713	0.642	13.8 ± 0.1
1170	15	8.5e-15	4.4004	4.7e-3	16.3233	0.0073	0.030	0.98253	0.511	12.9 ± 0.3
1250	15	7.2e-15	5.4307	3.4e-3	13.8803	0.0100	0.035	1.00000	0.454	14.1 ± 0.4

Note: Total fusion age, TFA = 16.11 ± 0.04 Ma (including J).
Weighted mean plateau age, WMPA = 16.27 ± 0.04 Ma (including J).
Inverse isochron age = 15.86 ± 0.60 Ma (MSWD = 127.05; ^{40}Ar/^{36}Ar = 315.8 ± 22.3).
Steps used: 740, 800, 860, 920, 980, 1040 (3–8/11 or 67% ∑ ^{39}Ar).
t = dwell time in minutes.
^{40}Ar (mol) = moles corrected for blank and reactor-produced ^{40}Ar.
Ratios are corrected for blanks, decay, and interference.
∑^{39}Ar is cumulative, ^{40}Ar* = rad fraction.

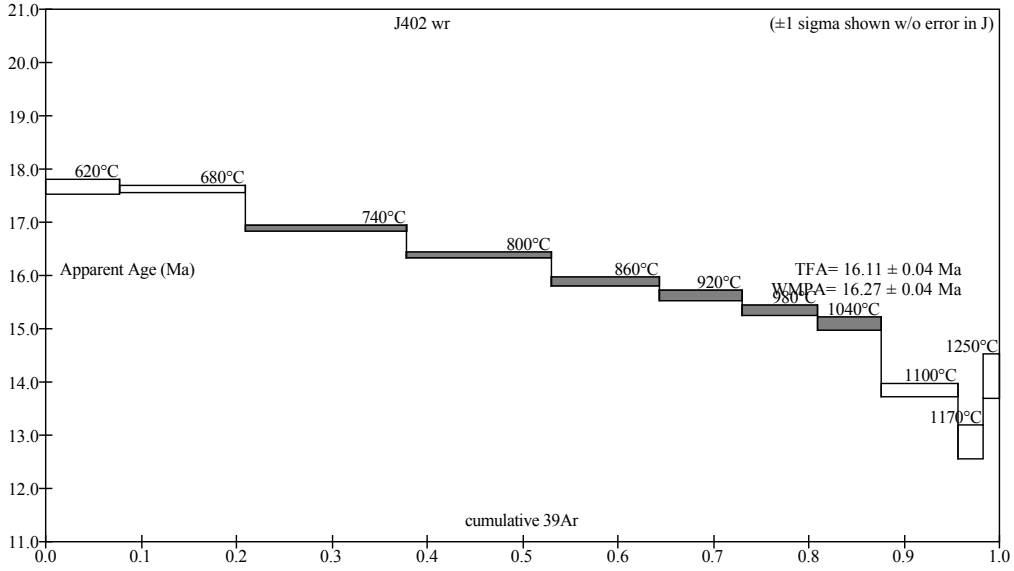

Down stepping spectrum indicative of excess Ar or K loss; no steps are within error. The plag split is more reliable.

Supplemental File 2

TABLE S18. SB61-174; J417 plag; J=0.0033163

Temp (°C)	t	^{40}Ar (mol)	^{40}Ar/^{39}Ar	^{38}Ar/^{39}Ar	^{37}Ar/^{39}Ar	^{36}Ar/^{39}Ar	K/Ca	∑ ^{39}Ar	^{40}Ar*	Age (Ma)
650	14	1.0e-14	13.7171	1.5e-2	2.4003	0.0347	0.20	0.01432	0.253	20.6 ± 1.0
730	14	1.6e-14	7.4469	4.5e-4	2.7502	0.0141	0.18	0.05580	0.441	19.6 ± 0.4
800	14	2.1e-14	5.2659	0.0e+0	2.7168	0.0062	0.18	0.12957	0.650	20.4 ± 0.2
880	14	2.5e-14	3.9942	0.0e+0	2.6544	0.0021	0.18	0.24676	0.848	20.1 ± 0.1
960	14	2.6e-14	3.6374	0.0e+0	2.5330	0.0009	0.19	0.38309	0.928	20.1 ± 0.1
1040	14	2.3e-14	3.5720	0.0e+0	2.4057	0.0006	0.20	0.50649	0.949	20.2 ± 0.1
1120	14	1.5e-14	3.7258	0.0e+0	2.3332	0.0011	0.21	0.58290	0.911	20.2 ± 0.2
1150	14	9.6e-15	3.9812	0.0e+0	2.3046	0.0018	0.21	0.62833	0.864	20.5 ± 0.3
1200	14	2.6e-14	4.2860	0.0e+0	2.1904	0.0027	0.22	0.74398	0.813	20.7 ± 0.1
1300	14	4.7e-14	4.0454	0.0e+0	2.3800	0.0019	0.21	0.96136	0.861	20.7 ± 0.1
1400	14	9.7e-15	4.7296	0.0e+0	3.2629	0.0039	0.15	1.00000	0.759	21.3 ± 0.3

Note: Total fusion age, TFA = 20.39 ± 0.05 Ma (including J).
Weighted mean plateau age, WMPA = 20.17 ± 0.06 Ma (including J).
Inverse isochron age = 20.11 ± 0.09 Ma (MSWD =0.41; ^{40}Ar/^{36}Ar = 302.5 ± 4.2).
Steps used: 800, 880, 960, 1040, 1120, 1150 (3–8/11 or 57% ∑ ^{39}Ar).
t = dwell time in minutes.
^{40}Ar (mol) = moles corrected for blank and reactor-produced ^{40}Ar.
Ratios are corrected for blanks, decay, and interference.
∑^{39}Ar is cumulative, ^{40}Ar* = rad fraction.

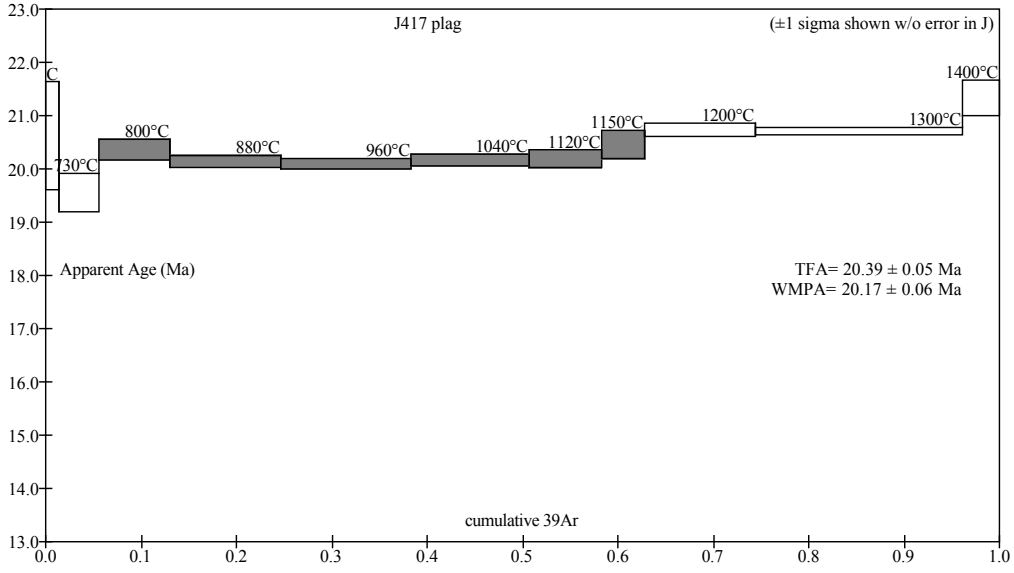

Good plateau for 50% of the gas. Evidence for excess argon at high and low temperature steps. An age of 20.11 ± 0.18 Ma was recalculated using the 880°C -1150°C steps.

TABLE S19. SB61-170. 172; J417 plag; fusions; J=0.0033332

Temp (°C)	t	^{40}Ar (mol)	^{40}Ar/^{39}Ar	^{38}Ar/^{39}Ar	^{37}Ar/^{39}Ar	^{36}Ar/^{39}Ar	K/Ca	∑ ^{39}Ar	^{40}Ar*	Age (Ma)
1350	15	5.4e-15	4.5021	3.5e-4	4.1697	0.0019	0.12	0.62554	0.876	23.6 ± 0.6
1350	15	3.4e-15	4.7037	5.4e-4	3.8301	0.0030	0.13	1.00000	0.813	22.8 ± 1.1

Note: Total fusion age, TFA = 23.29 ± 0.54 Ma (including J).
Weighted mean plateau age, WMPA = 23.43 ± 0.52 Ma (including J).
Inverse isochron age = 24.80 ± 1.54 Ma (MSWD =0.00; ^{40}Ar/^{36}Ar = 184.5 ± 0.0).
Steps used: 1350, 1350 (1–2/2 or 100% ∑ ^{39}Ar).
t = dwell time in minutes.
^{40}Ar (mol) = moles corrected for blank and reactor-produced ^{40}Ar.
Ratios are corrected for blanks, decay, and interference.
∑^{39}Ar is cumulative, ^{40}Ar* = rad fraction.

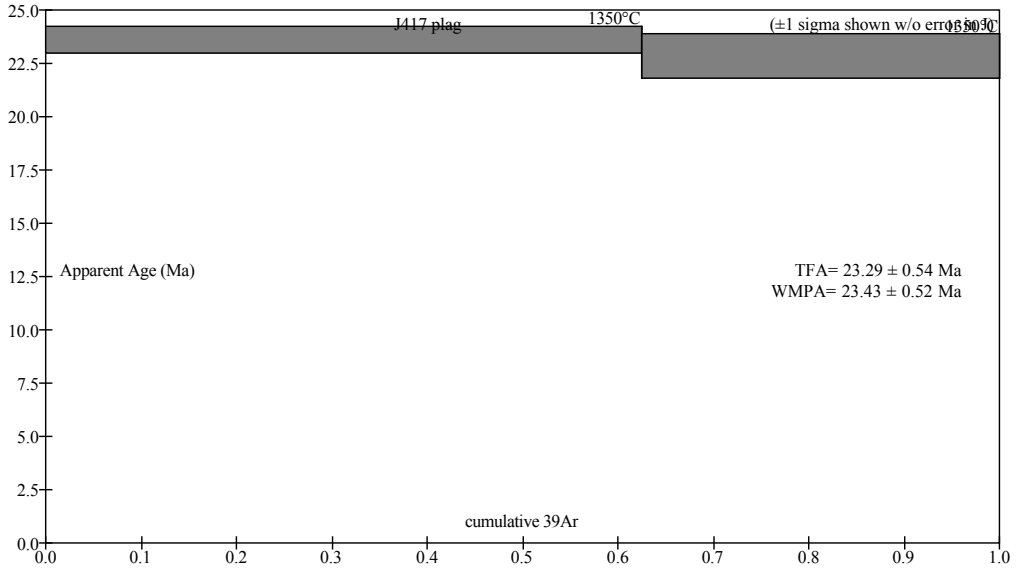

Low signals with large errors.

Supplemental File 2

TABLE S20. SB61-163; J424 plag; J=0.0033888

Temp (°C)	t	^{40}Ar (mol)	^{40}Ar/^{39}Ar	^{38}Ar/^{39}Ar	^{37}Ar/^{39}Ar	^{36}Ar/^{39}Ar	K/Ca	∑ ^{39}Ar	^{40}Ar*	Age (Ma)
650	14	1.7e-14	9.6290	1.1e-3	13.6126	0.0156	0.036	0.06736	0.522	30.4 ± 0.6
730	14	5.0e-14	7.2169	0.0e+0	13.6741	0.0056	0.036	0.33785	0.772	33.8 ± 0.2
800	14	3.8e-14	7.4954	0.0e+0	13.3673	0.0056	0.037	0.53522	0.781	35.4 ± 0.2
880	14	1.8e-14	8.0194	0.0e+0	11.7892	0.0074	0.042	0.62231	0.728	35.3 ± 0.4
960	14	8.2e-15	9.6749	3.6e-4	11.5294	0.0132	0.043	0.65502	0.598	35.0 ± 1.0
1040	14	1.1e-14	8.3025	0.0e+0	9.9763	0.0074	0.049	0.70653	0.738	37.1 ± 0.7
1120	14	1.2e-14	6.8105	0.0e+0	9.1657	0.0025	0.053	0.77415	0.893	36.8 ± 0.5
1200	14	1.6e-14	7.1306	0.0e+0	9.6486	0.0022	0.051	0.86147	0.908	39.1 ± 0.4
1300	14	2.0e-14	7.8535	0.0e+0	9.8553	0.0020	0.050	0.95813	0.926	43.9 ± 0.4
1400	14	9.9e-15	9.0961	8.8e-5	10.6816	0.0027	0.046	1.00000	0.912	50.0 ± 0.8

Note: Total fusion age, TFA = 36.56 ± 0.13 Ma (including J).
Weighted mean plateau age, WMPA = 35.64 ± 0.17 Ma (including J).
Inverse isochron age = 35.17 ± 1.30 Ma (MSWD =2.60; ^{40}Ar/^{36}Ar = 304.8 ± 34.7).
Steps used: 800, 880, 960, 1040, 1120 (3–7/10 or 44% ∑ ^{39}Ar).
t = dwell time in minutes.
^{40}Ar (mol) = moles corrected for blank and reactor-produced ^{40}Ar.
Ratios are corrected for blanks, decay, and interference.
∑^{39}Ar is cumulative, ^{40}Ar* = rad fraction.

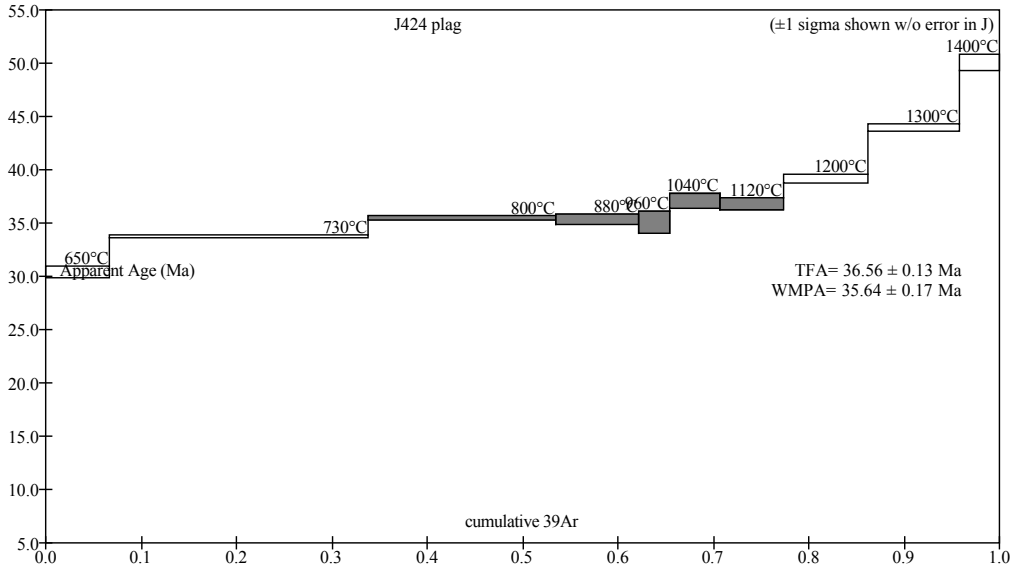

Decent plateau using only ~40% of gas - evidence for excess argon at high temperature steps.

Supplemental File 2

TABLE S21. SB61-165; J424 wr; J=0.0033735

Temp (°C)	t	^{40}Ar (mol)	^{40}Ar/^{39}Ar	^{38}Ar/^{39}Ar	^{37}Ar/^{39}Ar	^{36}Ar/^{39}Ar	K/Ca	∑ ^{39}Ar	^{40}Ar*	Age (Ma)
620	15	4.1e-14	12.4924	0.0e+0	4.6398	0.0243	0.11	0.04702	0.426	32.1 ± 0.3
680	15	7.8e-14	11.2858	0.0e+0	5.6505	0.0190	0.087	0.14648	0.502	34.2 ± 0.2
740	15	8.6e-14	7.9168	0.0e+0	2.7603	0.0071	0.18	0.30292	0.734	35.0 ± 0.1
800	15	6.3e-14	6.4150	0.0e+0	1.0639	0.0019	0.46	0.44480	0.913	35.3 ± 0.1
860	15	3.6e-14	6.5901	0.0e+0	1.3664	0.0028	0.36	0.52313	0.876	34.8 ± 0.1
920	15	3.1e-14	6.7663	0.0e+0	1.7904	0.0035	0.27	0.58848	0.848	34.6 ± 0.1
990	15	3.6e-14	6.9785	0.0e+0	1.7574	0.0043	0.28	0.66271	0.817	34.4 ± 0.1
1060	15	5.7e-14	7.0477	2.6e-5	1.4774	0.0042	0.33	0.77867	0.824	35.0 ± 0.1
1130	15	5.8e-14	7.1776	3.0e-5	2.0306	0.0045	0.24	0.89456	0.814	35.2 ± 0.1
1200	15	3.7e-14	7.6502	1.2e-4	4.1650	0.0062	0.12	0.96449	0.762	35.1 ± 0.1
1270	15	1.6e-14	8.0042	0.0e+0	8.7673	0.0076	0.056	0.99321	0.719	34.7 ± 0.3
1340	15	4.0e-15	8.5144	3.2e-3	19.9834	0.0105	0.025	1.00000	0.637	32.7 ± 1.1

Note: Total fusion age, TFA = 34.74 ± 0.06 Ma (including J).
Weighted mean plateau age, WMPA = 35.01 ± 0.06 Ma (including J).
Inverse isochron age = 35.08 ± 0.25 Ma (MSWD = 8.09; ^{40}Ar/^{36}Ar = 292.6 ± 9.1).
Steps used: 740, 800, 860, 920, 990, 1060, 1130, 1200, 1270 (3–11/12 or 85% ∑ ^{39}Ar).
t = dwell time in minutes.
^{40}Ar (mol) = moles corrected for blank and reactor-produced ^{40}Ar.
Ratios are corrected for blanks, decay, and interference.
∑^{39}Ar is cumulative, ^{40}Ar* = rad fraction.

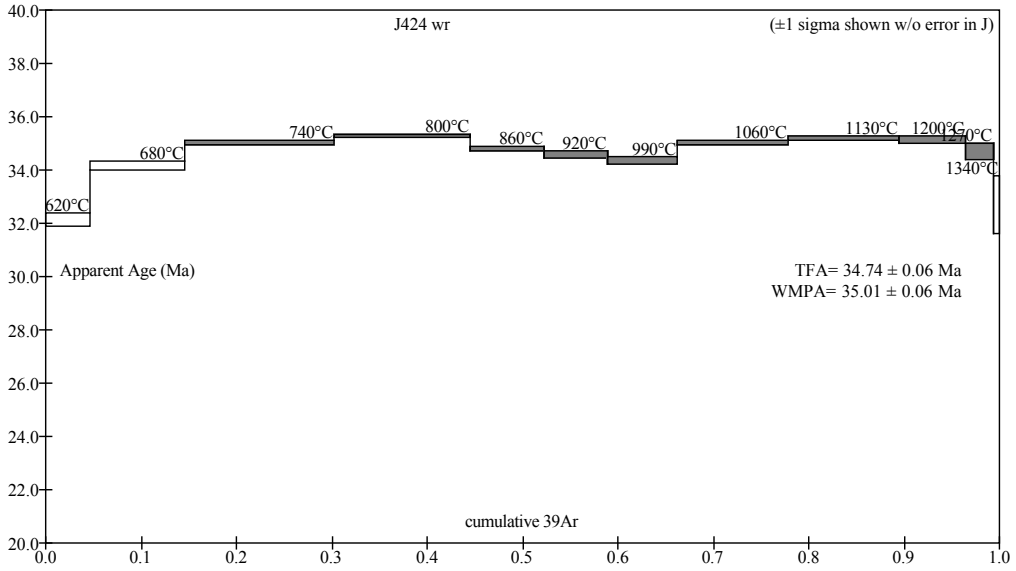

Bouncy spectrum indicative of recoil or argon loss at low temperature steps. Plag split yielded more reliable age.

TABLE S22. SB61-210; J446 plag; J=0.0029498

Temp (°C)	t	^{40}Ar (mol)	^{40}Ar/^{39}Ar	^{38}Ar/^{39}Ar	^{37}Ar/^{39}Ar	^{36}Ar/^{39}Ar	K/Ca	∑ ^{39}Ar	^{40}Ar*	Age (Ma)
700	14	2.7e-15	1.7238	0.0e+0	10.4097	0.0041	0.047	0.06626	0.302	2.8 ± 0.4
800	14	3.2e-15	0.9622	0.0e+0	13.2260	0.0022	0.037	0.20877	0.310	1.6 ± 0.2
880	14	2.7e-15	0.6841	0.0e+0	13.7832	0.0014	0.036	0.38031	0.389	1.4 ± 0.2
960	14	3.1e-15	0.6489	0.0e+0	13.6094	0.0011	0.036	0.58143	0.513	1.8 ± 0.1
1040	14	2.8e-15	0.6368	0.0e+0	13.1438	0.0010	0.037	0.76627	0.523	1.8 ± 0.2
1120	14	1.7e-15	0.6995	0.0e+0	12.4638	0.0009	0.039	0.86883	0.611	2.3 ± 0.3
1200	14	1.3e-15	1.0203	0.0e+0	12.0717	0.0024	0.041	0.92181	0.300	1.6 ± 0.5
1290	14	1.3e-15	1.4066	0.0e+0	11.5890	0.0029	0.042	0.96263	0.395	3.0 ± 0.6
1450	25	3.4e-15	3.9320	5.3e-4	11.4352	0.0047	0.043	1.00000	0.644	13.4 ± 0.7

Note: Total fusion age, TFA = 2.28 ± 0.08 Ma (including J).
Weighted mean plateau age, WMPA = 1.70 ± 0.08 Ma (including J).
Inverse isochron age = 1.87 ± 0.27 Ma (MSWD = 1.81; ^{40}Ar/^{36}Ar = 272.8 ± 42.4).
Steps used: 800, 880, 960, 1040, 1120, 1200 (2–7/9 or 86% ∑ ^{39}Ar).
t = dwell time in minutes.
^{40}Ar (mol) = moles corrected for blank and reactor-produced ^{40}Ar.
Ratios are corrected for blanks, decay, and interference.
∑^{39}Ar is cumulative, ^{40}Ar* = rad fraction.

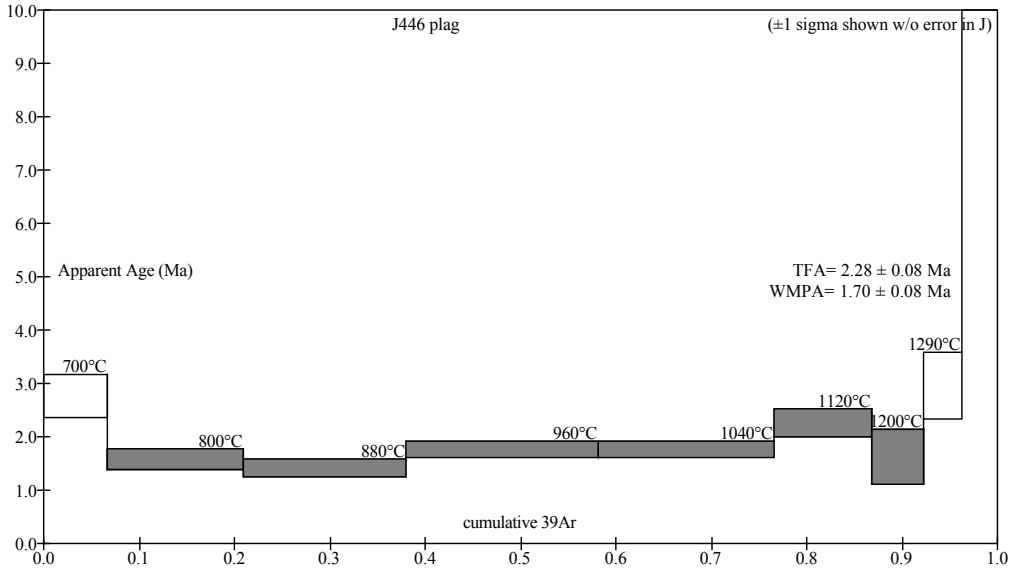

Decent age plateau that is slightly discordant between steps. Excess argon at low and high temperature steps.

Supplemental File 2

TABLE S23. SB61-211; J446 plag; J=0.0029306

Temp (°C)	t	^{40}Ar (mol)	^{40}Ar/^{39}Ar	^{38}Ar/^{39}Ar	^{37}Ar/^{39}Ar	^{36}Ar/^{39}Ar	K/Ca	∑ ^{39}Ar	^{40}Ar*	Age (Ma)
700	14	1.3e-14	8.4981	0.0e+0	9.9515	0.0278	0.049	0.06723	0.034	1.5 ± 0.4
820	14	7.6e-15	2.0236	0.0e+0	13.4099	0.0057	0.037	0.23398	0.172	1.8 ± 0.2
950	14	7.2e-15	1.1303	0.0e+0	13.7564	0.0028	0.036	0.51709	0.262	1.6 ± 0.1
1100	14	7.6e-15	1.1474	0.0e+0	13.1278	0.0027	0.037	0.80966	0.298	1.8 ± 0.1
1250	14	2.3e-15	0.8639	0.0e+0	12.2744	0.0015	0.040	0.92919	0.477	2.2 ± 0.2
1400	14	4.3e-15	2.6556	1.6e-3	9.8921	0.0041	0.050	1.00000	0.545	7.6 ± 0.3

Note: Total fusion age, TFA = 2.18 ± 0.06 Ma (including J).
Weighted mean plateau age, WMPA = 1.71 ± 0.06 Ma (including J).
Inverse isochron age = 1.72 ± 0.12 Ma. (MSWD = 1.65; ^{40}Ar/^{36}Ar = 294.9 ± 4.1).
Steps used: 700, 820, 950, 1100 (1–4/6 or 81% ∑ ^{39}Ar).
t = dwell time in minutes.
^{40}Ar (mol) = moles corrected for blank and reactor-produced ^{40}Ar.
Ratios are corrected for blanks, decay, and interference.
∑^{39}Ar is cumulative, ^{40}Ar* = rad fraction.

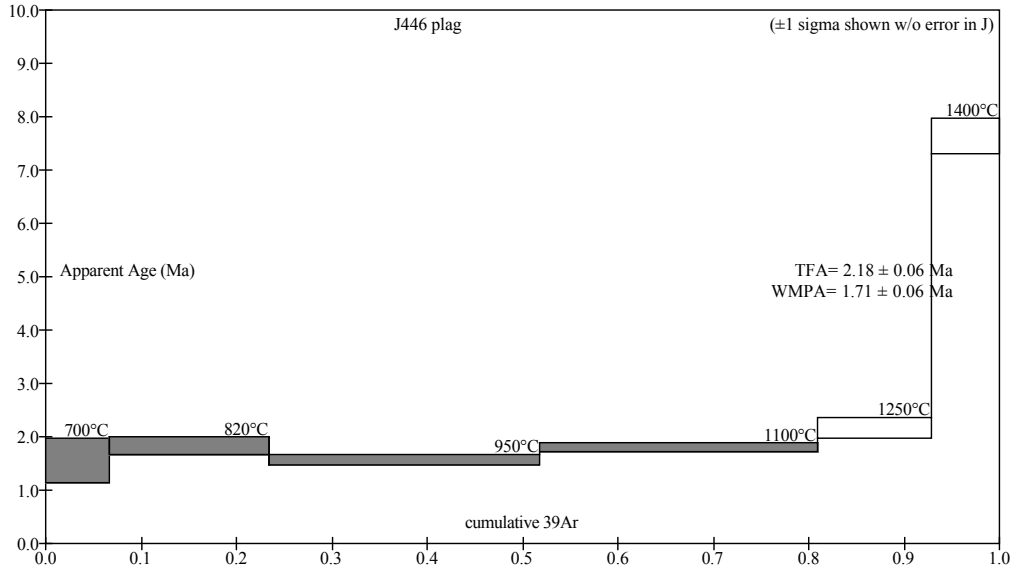

Decent flat in the spectrum. Excess argon at the higher temperature steps.

Supplemental File 2

TABLE S24. SB61-184; J473 plag-c.g; bulk separate; J=0.0032438

Temp (°C)	t	^{40}Ar (mol)	^{40}Ar/^{39}Ar	^{38}Ar/^{39}Ar	^{37}Ar/^{39}Ar	^{36}Ar/^{39}Ar	K/Ca	∑ ^{39}Ar	^{40}Ar*	Age (Ma)
700	14	2.6e-15	5.7420	1.2e-4	2.4750	0.0091	0.20	0.01976	0.531	17.8 ± 1.4
800	14	6.1e-15	4.0134	0.0e+0	2.9886	0.0028	0.16	0.08645	0.795	18.6 ± 0.4
900	14	1.1e-14	3.6844	0.0e+0	2.9762	0.0015	0.16	0.21737	0.883	18.9 ± 0.2
970	14	9.1e-15	3.4488	0.0e+0	2.9472	0.0005	0.17	0.33349	0.958	19.2 ± 0.3
1040	14	7.7e-15	3.4859	0.0e+0	2.8197	0.0008	0.17	0.43157	0.934	19.0 ± 0.3
1110	14	5.1e-15	3.6090	0.0e+0	2.7557	0.0008	0.18	0.49342	0.936	19.7 ± 0.5
1200	14	1.1e-14	4.1010	0.0e+0	2.6010	0.0025	0.19	0.61387	0.823	19.6 ± 0.3
1300	14	2.2e-14	3.8753	0.0e+0	2.7435	0.0017	0.18	0.86491	0.868	19.6 ± 0.1
1400	14	1.2e-14	3.9102	0.0e+0	2.8630	0.0017	0.17	1.00000	0.874	19.9 ± 0.2

Total fusion age, TFA = 19.35 ± 0.09 Ma (including J).
Weighted mean plateau age, WMPA = 19.36 ± 0.09 Ma (including J).
Inverse isochron age = 18.96 ± 0.39 Ma (MSWD = 2.07; ^{40}Ar/^{36}Ar = 340.2 ± 42.1).
Steps used: 800, 900, 970, 1040, 1110, 1200, 1300 (2–8/9 or 85% ∑ ^{39}Ar).
t = dwell time in minutes.
^{40}Ar (mol) = moles corrected for blank and reactor-produced ^{40}Ar.
Ratios are corrected for blanks, decay, and interference.
∑^{39}Ar is cumulative, ^{40}Ar* = rad fraction.

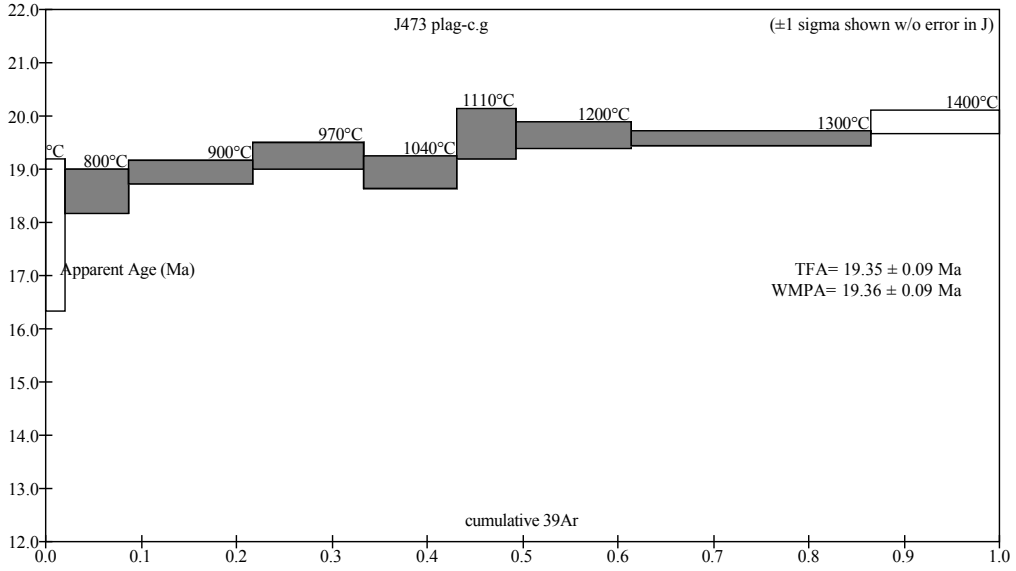

Decent plateau for 80% of the gas. An age of 19.66 ± 0.20 Ma was recalculated for the 1100°C -1300°C steps.

Supplemental File 2

TABLE S25. SB61-185; J473 plag-f.g.; J=0.0032342

Temp (°C)	t	^{40}Ar (mol)	^{40}Ar/^{39}Ar	^{38}Ar/^{39}Ar	^{37}Ar/^{39}Ar	^{36}Ar/^{39}Ar	K/Ca	∑ ^{39}Ar	^{40}Ar*	Age (Ma)
700	14	3.7e-15	5.5783	0.0e+0	3.1198	0.0071	0.16	0.02862	0.624	20.2 ± 0.9
800	14	7.6e-15	3.9745	0.0e+0	3.3117	0.0020	0.15	0.11232	0.852	19.7 ± 0.3
900	14	1.1e-14	3.6585	0.0e+0	3.1344	0.0009	0.16	0.24551	0.925	19.6 ± 0.2
980	14	1.0e-14	3.5740	0.0e+0	2.9867	0.0009	0.16	0.37135	0.928	19.2 ± 0.2
1060	14	8.3e-15	3.5837	0.0e+0	2.8459	0.0009	0.17	0.47265	0.925	19.2 ± 0.2
1140	14	6.1e-15	4.0521	0.0e+0	2.8372	0.0021	0.17	0.53783	0.847	19.9 ± 0.3
1220	14	1.5e-14	4.2410	0.0e+0	2.8003	0.0027	0.17	0.69554	0.812	20.0 ± 0.2
1300	14	1.6e-14	4.0293	0.0e+0	3.0291	0.0020	0.16	0.86881	0.856	20.0 ± 0.1
1380	14	6.2e-15	4.2026	0.0e+0	3.2214	0.0022	0.15	0.93261	0.846	20.6 ± 0.3
1440	14	6.7e-15	4.3417	0.0e+0	3.4006	0.0027	0.14	1.00000	0.817	20.6 ± 0.3

Total fusion age, TFA = 19.83 ± 0.08 Ma (including J).
Weighted mean plateau age, WMPA = 19.73 ± 0.08 Ma (including J).
Steps used: 800, 900, 980, 1060, 1140, 1220, 1300, 1380, 1440.
t = dwell time in minutes.
^{40}Ar (mol) = moles corrected for blank and reactor-produced ^{40}Ar.
Ratios are corrected for blanks, decay, and interference.
∑^{39}Ar is cumulative, ^{40}Ar* = rad fraction.

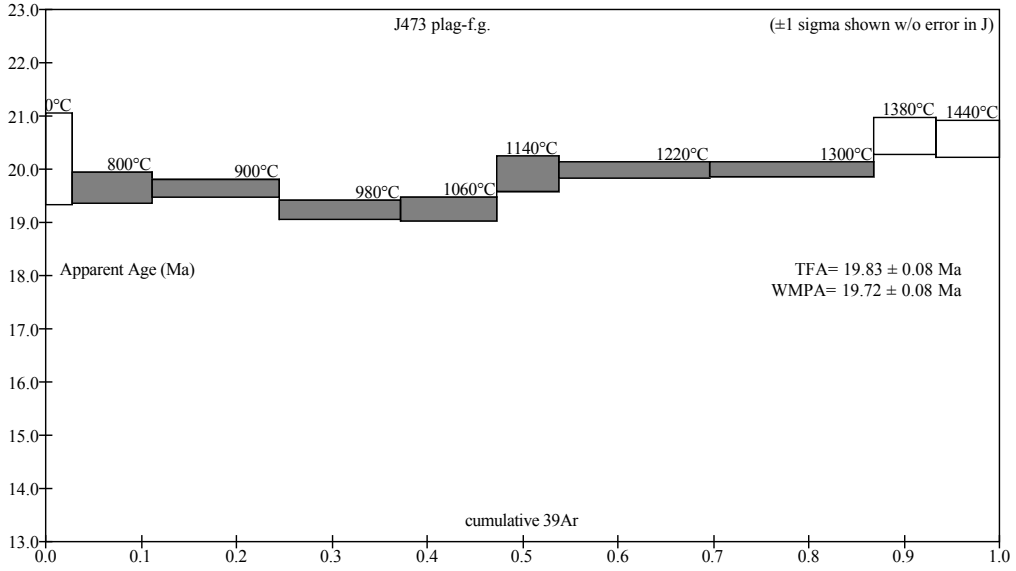

Decent plateau for over 70% of the gas.

Supplemental File 2

TABLE S26. SB64-182; CHJ-01 Plag; J=0.0035336

Temp (°C)	t	^{40}Ar (mol)	^{40}Ar/^{39}Ar	^{38}Ar/^{39}Ar	^{37}Ar/^{39}Ar	^{36}Ar/^{39}Ar	K/Ca	∑ ^{39}Ar	^{40}Ar*	Age (Ma)
700	20	1.4e-14	3.2672	1.2e-3	0.8794	0.0103	0.56	0.03045	0.066	1.4 ± 0.1
900	20	1.8e-14	1.0797	0.0e+0	7.3451	0.0028	0.067	0.15480	0.229	1.6 ± 0.1
980	20	1.4e-14	0.6781	0.0e+0	9.4763	0.0014	0.052	0.30264	0.370	1.6 ± 0.1
1060	20	1.6e-14	0.5474	0.0e+0	9.5943	0.0010	0.051	0.51408	0.477	1.7 ± 0.1
1140	20	1.4e-14	0.4924	0.0e+0	9.3284	0.0008	0.053	0.72343	0.541	1.7 ± 0.1
1220	20	8.4e-15	0.5890	0.0e+0	9.0137	0.0011	0.054	0.82750	0.456	1.7 ± 0.1
1300	20	5.9e-15	0.6787	0.0e+0	8.5177	0.0013	0.058	0.89055	0.417	1.8 ± 0.1
1380	20	7.3e-15	0.7357	0.0e+0	7.7301	0.0015	0.063	0.96286	0.411	1.9 ± 0.1
1460	20	4.6e-15	0.9048	0.0e+0	7.2747	0.0017	0.067	1.00000	0.436	2.5 ± 0.2

Note: Total fusion age, TFA = 1.71 ± 0.04 Ma (including J).
Weighted mean plateau age, WMPA = 1.68 ± 0.04 Ma (including J).
Inverse isochron age = 1.75 ± 0.10 Ma. (MSWD =0.40; ^{40}Ar/^{36}Ar = 287.0 ± 7.2).
Steps used: 900, 980, 1060, 1140, 1220, 1300 (2–7/9 or 86% ∑ ^{39}Ar).
t = dwell time in minutes.
^{40}Ar (mol) = moles corrected for blank and reactor-produced ^{40}Ar.
Ratios are corrected for blanks, decay, and interference.
∑^{39}Ar is cumulative, ^{40}Ar* = rad fraction.

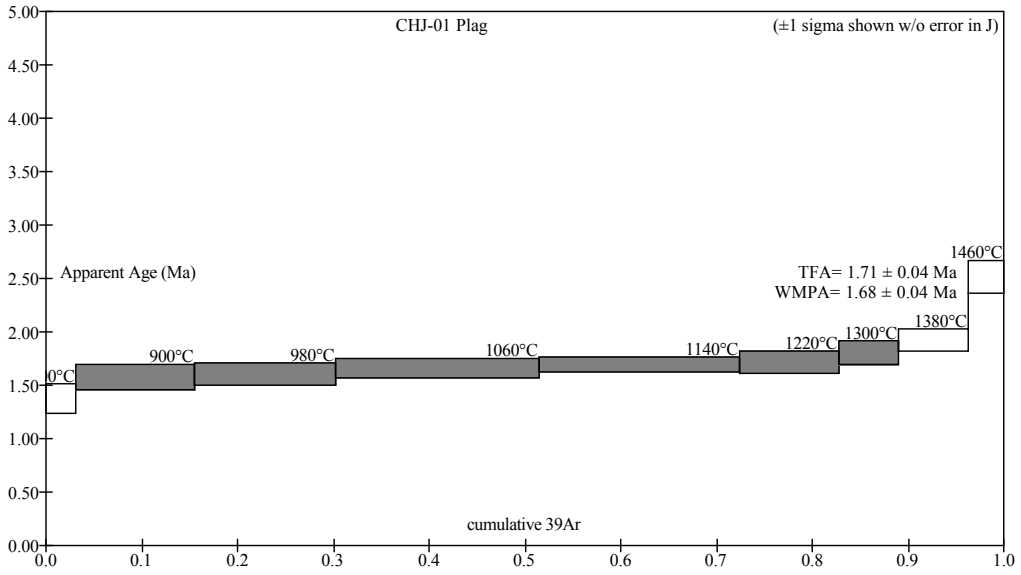

Excellent age plateau.

Supplemental File 2

TABLE S27. SB64-197; CHJ-08 GM; J=0.0039741

Temp (°C)	t	^{40}Ar (mol)	^{40}Ar/^{39}Ar	^{38}Ar/^{39}Ar	^{37}Ar/^{39}Ar	^{36}Ar/^{39}Ar	K/Ca	∑ ^{39}Ar	^{40}Ar*	Age (Ma)
600	14	4.3e-15	21.3599	2.5e-3	1.1517	0.0673	0.43	0.00412	0.069	10.5 ± 1.9
650	14	4.0e-15	8.3637	6.6e-4	0.8321	0.0220	0.59	0.01388	0.221	13.2 ± 0.8
700	14	6.1e-15	4.1480	0.0e+0	0.7220	0.0064	0.68	0.04369	0.545	16.1 ± 0.3
750	14	1.3e-14	4.1461	0.0e+0	1.1583	0.0037	0.42	0.10852	0.734	21.7 ± 0.1
800	14	2.5e-14	5.5462	0.0e+0	0.6548	0.0019	0.75	0.20082	0.901	35.5 ± 0.1
850	14	3.6e-14	7.0970	0.0e+0	0.8449	0.0012	0.58	0.30553	0.950	47.7 ± 0.1
900	14	4.1e-14	7.9876	0.0e+0	1.0156	0.0013	0.48	0.40925	0.953	53.8 ± 0.1
950	14	3.6e-14	8.6218	0.0e+0	0.8000	0.0016	0.61	0.49366	0.945	57.5 ± 0.1
1000	14	3.2e-14	8.4315	0.0e+0	0.6218	0.0016	0.79	0.57128	0.944	56.2 ± 0.1
1060	14	5.0e-14	8.1497	0.0e+0	0.5499	0.0023	0.89	0.69584	0.918	52.8 ± 0.1
1120	14	7.8e-14	8.2408	0.0e+0	0.5546	0.0032	0.88	0.88977	0.884	51.5 ± 0.1
1250	14	1.8e-14	8.5078	3.5e-4	3.9188	0.0046	0.13	0.93428	0.842	50.6 ± 0.2
1350	14	2.8e-14	8.6326	5.7e-4	4.8672	0.0048	0.10	1.00000	0.834	50.9 ± 0.2

Note: Total fusion age, TFA = 47.32 ± 0.08 Ma (including J).
Weighted mean plateau age, WMPA = 51.32 ± 0.10 Ma (including J).
Inverse isochron age = 52.91 ± 0.62 Ma (MSWD = 3.00; ^{40}Ar/^{36}Ar = 230.8 ± 24.0).
Steps used: 1120, 1250, 1350 (11–13/13 or 30% ∑ ^{39}Ar).
t = dwell time in minutes.
^{40}Ar (mol) = moles corrected for blank and reactor-produced ^{40}Ar.
Ratios are corrected for blanks, decay, and interference.
∑^{39}Ar is cumulative, ^{40}Ar* = rad fraction.

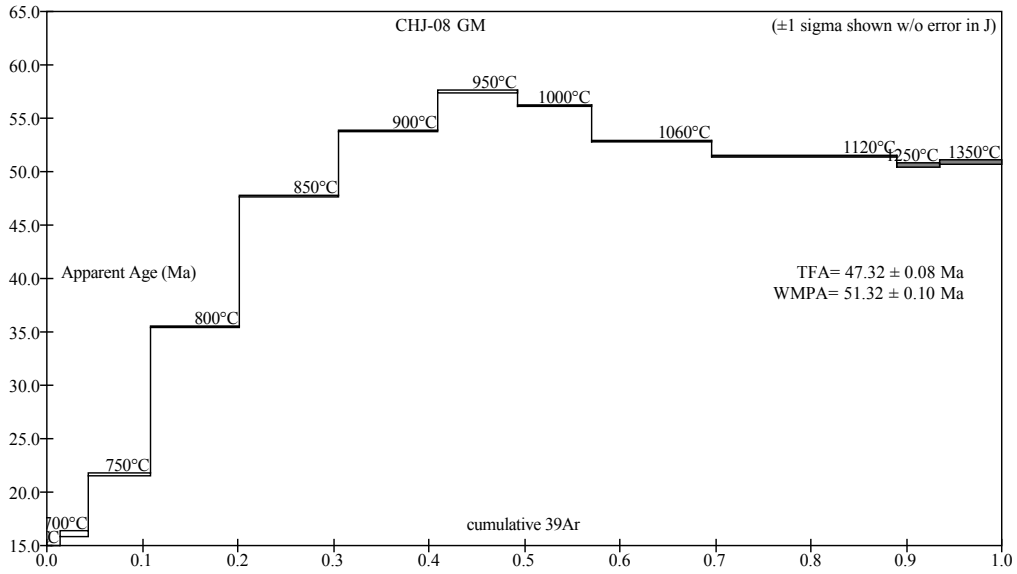

The spectrum is indicative of extensive argon loss plus some recoil, but has decent high temperature mini-plateau of 51.3 Ma. Preferred age is 51.3 ± 0.5 Ma.

Supplemental File 2

TABLE S28. SB64-198; CHJ-18 Plag; J=0.0039678

Temp (°C)	t	^{40}Ar (mol)	^{40}Ar/^{39}Ar	^{38}Ar/^{39}Ar	^{37}Ar/^{39}Ar	^{36}Ar/^{39}Ar	K/Ca	∑ ^{39}Ar	^{40}Ar*	Age (Ma)
800	15	5.0e-15	8.3088	1.5e-3	4.1179	0.0116	0.12	0.02590	0.588	34.6 ± 0.7
900	15	1.3e-14	6.8462	0.0e+0	6.3995	0.0027	0.077	0.11094	0.885	42.9 ± 0.3
960	15	1.6e-14	6.7402	0.0e+0	6.5762	0.0015	0.075	0.21530	0.934	44.5 ± 0.3
1020	15	1.9e-14	6.6521	0.0e+0	6.5769	0.0012	0.075	0.34163	0.948	44.6 ± 0.3
1080	15	2.0e-14	6.6112	0.0e+0	6.4160	0.0010	0.076	0.46996	0.956	44.7 ± 0.2
1140	15	1.5e-14	6.6391	0.0e+0	6.2537	0.0012	0.078	0.56926	0.948	44.5 ± 0.2
1200	15	8.2e-15	6.8805	0.0e+0	6.2368	0.0023	0.079	0.62042	0.901	43.8 ± 0.4
1260	15	7.0e-15	7.0313	1.3e-4	6.4391	0.0028	0.076	0.66325	0.884	43.9 ± 0.5
1330	15	2.2e-14	7.1735	0.0e+0	6.3005	0.0023	0.078	0.79352	0.906	45.9 ± 0.2
1400	15	2.5e-14	6.9247	0.0e+0	6.2576	0.0016	0.078	0.95141	0.931	45.6 ± 0.2
1500	15	5.7e-15	5.0356	0.0e+0	7.5125	0.0028	0.065	1.00000	0.839	30.0 ± 0.4

Note: Total fusion age, TFA = 43.73 ± 0.11 Ma (including J).
Weighted mean plateau age, WMPA = 44.89 ± 0.11 Ma (including J).
Inverse isochron age = 45.13 ± 0.26 Ma (MSWD = 0.25; ^{40}Ar/^{36}Ar = 227.2 ± 12.0)
Steps used: 960, 1020, 1080, 1140, 1200, 1260, 1330, 1400 (3–10/11 or 84% ∑ ^{39}Ar).
t = dwell time in minutes.
^{40}Ar (mol) = moles corrected for blank and reactor-produced ^{40}Ar.
Ratios are corrected for blanks, decay, and interference.
∑^{39}Ar is cumulative, ^{40}Ar* = rad fraction.

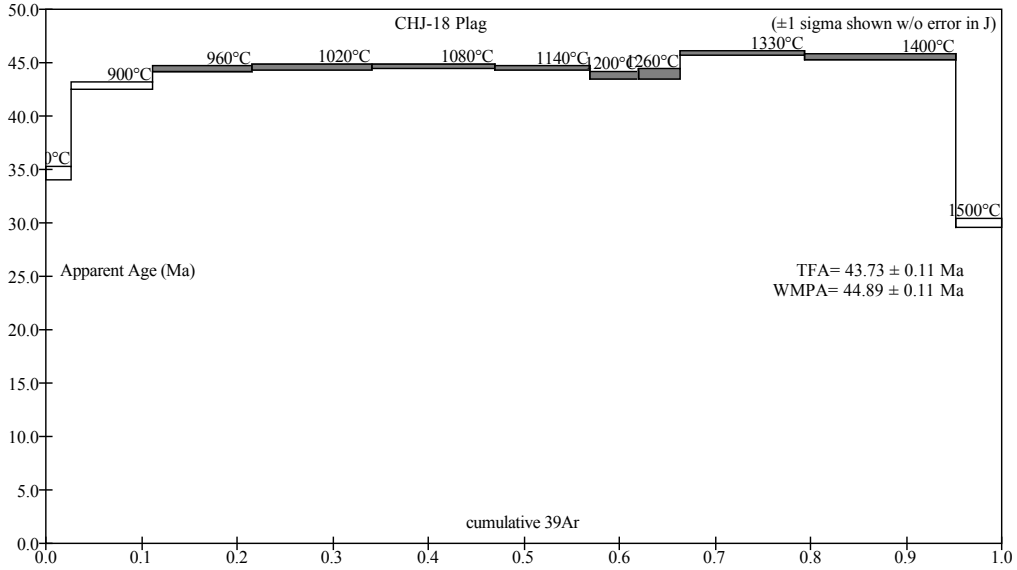

Excellent age plateau.

Supplemental File 2

TABLE S29. SB64-201; CHJ-46 Plag; J=0.0039443

Temp (°C)	t	^{40}Ar (mol)	^{40}Ar/^{39}Ar	^{38}Ar/^{39}Ar	^{37}Ar/^{39}Ar	^{36}Ar/^{39}Ar	K/Ca	∑ ^{39}Ar	^{40}Ar*	Age (Ma)
800	14	4.8e-15	7.4942	0.0e+0	7.9118	0.0095	0.062	0.03904	0.625	33.0 ± 0.7
900	14	1.2e-14	6.4477	0.0e+0	9.7516	0.0033	0.050	0.15635	0.850	38.6 ± 0.4
960	14	1.3e-14	6.2520	0.0e+0	9.7752	0.0022	0.050	0.27786	0.898	39.5 ± 0.3
1020	14	1.4e-14	6.0998	0.0e+0	9.8055	0.0016	0.050	0.41245	0.925	39.7 ± 0.3
1080	14	1.3e-14	6.0188	0.0e+0	9.7197	0.0014	0.050	0.54030	0.931	39.4 ± 0.3
1140	14	8.7e-15	6.1546	0.0e+0	9.4596	0.0019	0.052	0.62622	0.907	39.3 ± 0.4
1210	14	4.8e-15	6.7748	0.0e+0	9.2190	0.0039	0.053	0.66948	0.831	39.6 ± 0.7
1280	14	9.5e-15	7.3158	0.0e+0	9.2165	0.0053	0.053	0.74815	0.785	40.4 ± 0.5
1350	14	1.6e-14	7.1844	0.0e+0	9.2718	0.0049	0.053	0.88401	0.799	40.4 ± 0.4
1420	14	1.1e-14	7.2227	0.0e+0	9.7594	0.0052	0.050	0.97275	0.789	40.1 ± 0.4
1500	14	3.4e-15	7.5108	0.0e+0	11.1068	0.0111	0.044	1.00000	0.563	29.8 ± 1.0

Note: Total fusion age, TFA = 39.13 ± 0.14 Ma (including J).
Weighted mean plateau age, WMPA = 39.77 ± 0.15 Ma (including J).
Inverse isochron age = 39.09 ± 0.31 Ma (MSWD = 0.28; ^{40}Ar/^{36}Ar = 328.9 ± 7.0).
Steps used: 960, 1020, 1080, 1140, 1210, 1280, 1350, 1420 (3–10/11 or 82% ∑ ^{39}Ar).
t = dwell time in minutes.
^{40}Ar (mol) = moles corrected for blank and reactor-produced ^{40}Ar.
Ratios are corrected for blanks, decay, and interference.
∑^{39}Ar is cumulative, ^{40}Ar* = rad fraction.

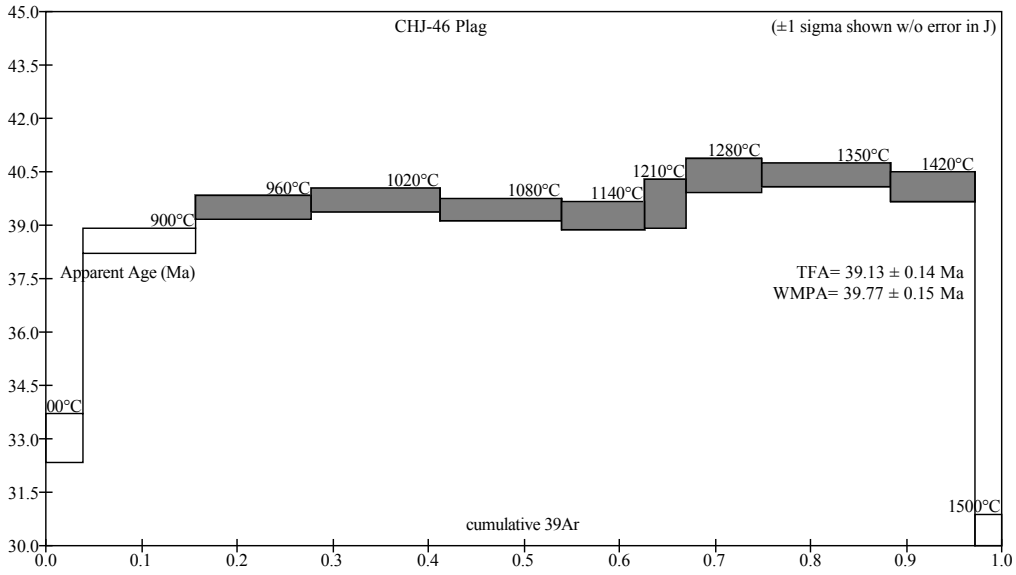

Decent age plateau. Argon loss at the low and high temperature steps.

U-Pb ZIRCON GEOCHRONOLOGY

Zircons were separated from 1-2 kg of sample using standard density and magnetic separation techniques. Approximately 100 to 200 zircon grains were hand selected per sample and set in a 2.5 cm epoxy grain mount. The mount was polished until grain cores were exposed. Cathodoluminescence (CL) imaging was used to map the internal structure of zircon grains, assisting in the selection of grains suitable for U-Pb dating. CL images were obtained on UCSB's FEI Quanta 400 F scanning electron microscope equipped with a CL detector. U-Pb zircon geochronology was performed on selected grains at UCSB using a Nu Plasma HR MC-ICPMS equipped with four low-mass side electron multipliers (for simultaneous measurement of ^{208}Pb, ^{207}Pb, ^{206}Pb and, ^{204}Pb) and an Analyte 193 excimer ArF laser-ablation system equipped with a HeLex sample cell (Photon Machines, Bozeman, MT, USA). Data from 22 samples were collected over four analytical sessions; at least 28 analyses, including on rims and cores, were conducted on each sample. Due to the high sensitivity of the electron multipliers, 24.1 μm spots were ablated during a 25 second analysis run at 4 Hz, yielding a pit depth of ~10 μm. Sample analyses were preceded by a 10 second baseline measurement and unknown analyses were corrected with the 91500 reference standard (1065.4 ± 0.3 Ma ^{207}Pb/^{206}Pb ID-TIMS age and 1062.4 ± 0.4 Ma ^{206}Pb/^{238}U ID-TIMS age; Wiedenbeck et al., 1995) every 5-7 measurements. For quality control, the reference standards GJ1 (608.5 ± 0.4 Ma ^{207}Pb/^{206}Pb and 601.7 ± 1.3 Ma ^{206}Pb/^{238}U ID-TIMS ages, Horswtood et al., 2016), and Plešovice (^{206}Pb/^{238}U ID-TIMS age 337 ± 0.3 Ma; Sláma et al., 2008) were run after each 91500 analysis. All age uncertainties reported are 2σ, unless otherwise stated and include contributions from the external reproducibility of the

primary reference material for the $^{207}Pb/^{206}Pb$ and $^{206}Pb/^{238}U$ ratios. Data reduction, including corrections for baseline, instrumental drift, mass bias, down-hole fractionation and age calculations were carried out using Iolite v. 2.1.2 (Paton et al., 2010) and data were further visualized using Isoplot (Ludwig, 2000).

CL imaging revealed zircon grains to be mostly euhedral with oscillatory zoning indicative of a magmatic origin with no metamorphic recrystallization. Zircon spot analyses generally yielded tight U-Pb age distributions with little intra-sample variance. Plotting the (uncorrected for common Pb) data on concordia diagrams, however, highlighted a number analyses slightly above theoretical concordia. This discordance is interpreted to be caused by common Pb. Therefore, individual $^{206}Pb/^{238}U$ age calculations were corrected for common Pb using the "^{207}Pb method" of Andersen (2002) and an assumed common lead $^{207}Pb/^{206}Pb$ ratio of 0.836 (Stacey and Kramers, 1975) as well as an 2% uncertainty on the assumed common lead composition. Ages reported in Table 2 of the manuscript are the weighted mean of ^{207}Pb-corrected $^{206}Pb/^{238}U$ ages obtained for each sample. Tabulated data of all analyses are provided in this appendix. Tera-Wasserburg diagrams and weighted mean plots are also included for each sample.

REFERENCES CITED

Anderson T., 2002. Correction of common lead in U-Pb analyses that do not report ^{204}Pb: Chemical Geology v. 192, p. 59–79.

Horstwood, M. S. A., Košler, J., Gehrels, G., Jackson, S. E., McLean, N. M., Paton, C., Pearson, N. J., Sircombe, K., Sylvester, P., Vermeesch, P., Bowring, J. F., Condon, D. J. and Schoene, B., 2016, Community-Derived Standards for LA-ICP-MS U-(Th-)Pb Geochronology – Uncertainty Propagation, Age Interpretation and Data Reporting: Geostandards and Geoanalytical Research, v. 40, p. 311–332.

Ludwig, K.R., 2000, User's manual for Isoplot/Ex version 2.4: a geochronological toolkit for Microsoft Excel: Berkeley Geo-chronological Center, Special Publication No. 1a.

Paton, C., Hellstrom, J., Paul, B., and Woodhead, J., 2011, Iolite: Freeware for the visualization and processing of mass spectrometric data: Atomic Spectrometry, v. 26, p. 2508-2518.

Sláma, J., Košler, J., Condon, D.J., Crowley, J.L., Gerdes, A., Hanchar, J.M., Horstwood, M.S.A., Morris, G.A., Nasdala, L., Norberg, N., Schaltegger, U., Schoene, B., Tubrett, M.N., and Whitehouse, M.J., 2008, Plešovice zircon — A new natural reference material for U–Pb and Hf isotopic microanalysis: Chemical Geology, v. 249, p. 1–35.

Stacey, J., and Kramers, J.D., 1975, Approximation of terrestrial lead isotope evolution by a two- stage model: Earth and Planetary Science Letters, v. 26, p. 207-211.

Wiedenbeck, M., Alle, P., Corfu, F., Griffin, W., Meier, M., Oberli, F., Vonquadt, A., Roddick, J.C., and Speigel, W., 1995, 3 Natural zircon standards for U-Th-Pb, Lu-Hf, trace-element and Ree Analyses: Geostandards Newsletter, v. 19, p. 1–23.

Supplemental File 3

TABLE S30. LA-ICP-MS RESULTS

Sample ID[a]	U ppm	Th ppm	$^{207}Pb/^{206}Pb$	± 2σ	$^{207}Pb/^{235}U$	± 2σ	$^{238}U/^{206}Pb$	± 2σ	$^{206}Pb/^{238}U$ age (Ma)*	± 2σ (Ma)
CH89_1	296	222	0.05002	0.00189	0.0537	0.0137	128.944	3.588	49.6	1.4
CH89_2	1564	1881	0.04810	0.00114	0.0476	0.0066	139.720	3.639	45.9	1.2
CH89_3	434	280	0.04984	0.00178	0.0497	0.0123	138.977	3.705	46.0	1.2
CH89_4	511	1052	0.05077	0.00182	0.0506	0.0128	139.309	3.768	45.9	1.2
CH89_5	210	111	0.05232	0.00228	0.0517	0.0155	139.936	3.849	45.6	1.3
CH89_6	592	483	0.04780	0.00125	0.0483	0.0079	136.851	3.711	46.9	1.3
CH89_7	589	332	0.04760	0.00136	0.0475	0.0090	138.858	3.753	46.2	1.2
CH89_8	198	104	0.05090	0.00223	0.0509	0.0161	138.511	3.721	46.1	1.2
CH89_9	525	334	0.04835	0.00148	0.0484	0.0089	137.705	3.704	46.6	1.3
CH89_10	484	231	0.04768	0.00134	0.0472	0.0082	139.203	3.554	46.1	1.2
CH89_11	916	665	0.04693	0.00119	0.0454	0.0065	141.920	3.835	45.3	1.2
CH89_12	593	347	0.04794	0.00136	0.0468	0.0076	141.281	3.695	45.4	1.2
CH89_13	399	216	0.04804	0.00152	0.0481	0.0107	138.764	3.813	46.2	1.3
CH89_14	588	432	0.04853	0.00144	0.0492	0.0099	136.399	3.828	47.0	1.3
CH89_15	642	464	0.04733	0.00128	0.0465	0.0078	140.789	3.767	45.6	1.2
CH89_16	441	224	0.04858	0.00154	0.0483	0.0099	139.006	3.908	46.1	1.3
CH89_17	542	713	0.04832	0.00144	0.0474	0.0088	140.195	3.824	45.7	1.2
CH89_18	487	258	0.05280	0.00188	0.0517	0.0128	141.022	3.857	45.2	1.2
CH89_19	357	170	0.05114	0.00171	0.0508	0.0117	139.299	4.090	45.9	1.3
CH89_20	460	332	0.05077	0.00177	0.0521	0.0127	134.041	3.823	47.7	1.4
CH89_21	1099	1277	0.04782	0.00119	0.0467	0.0070	141.394	3.818	45.4	1.2
CH89_22	852	593	0.04789	0.00121	0.0495	0.0078	133.335	3.542	48.1	1.3
CH89_23	976	760	0.07407	0.00198	0.0770	0.0207	132.482	3.717	46.8	1.3
CH89_24	2582	3710	0.04747	0.00106	0.0497	0.0070	131.333	3.739	48.9	1.4
CH89_25	536	292	0.04960	0.00142	0.0514	0.0115	133.674	3.823	47.9	1.4
CH89_26	1696	1823	0.04677	0.00109	0.0466	0.0068	138.679	3.809	46.3	1.3
CH89_27	322	223	0.05007	0.00169	0.0521	0.0142	133.320	3.835	48.0	1.4
CH89_28	629	446	0.04812	0.00145	0.0482	0.0088	137.896	3.718	46.5	1.3
CH89_29	587	406	0.04920	0.00141	0.0500	0.0102	136.750	3.966	46.8	1.4
CH89_30	912	832	0.04780	0.00126	0.0478	0.0080	138.678	3.757	46.3	1.3
CH89_31	482	277	0.04955	0.00164	0.0482	0.0110	141.615	3.857	45.2	1.2
CH89_32	461	254	0.04816	0.00149	0.0481	0.0116	138.550	4.469	46.3	1.5
CH89_33	353	165	0.04784	0.00153	0.0478	0.0105	138.982	4.163	46.2	1.4
CH89_34	870	621	0.04845	0.00128	0.0485	0.0092	138.015	3.980	46.5	1.3
CH89_35	399	153	0.05029	0.00163	0.0503	0.0101	137.033	4.072	46.7	1.4
CH89_36	3031	6639	0.04798	0.00107	0.0477	0.0065	138.857	3.973	46.2	1.3
CH89_37	467	252	0.04960	0.00222	0.0475	0.0148	143.088	5.746	44.7	1.8
CH89_38	597	468	0.04770	0.00129	0.0476	0.0095	138.875	4.176	46.2	1.4
CH89_39	918	647	0.04862	0.00129	0.0485	0.0090	138.896	3.968	46.1	1.3
CH89_40	413	204	0.04959	0.00173	0.0496	0.0101	137.856	4.034	46.4	1.4
CH89_41	764	72	0.05314	0.00111	0.4023	0.0597	18.240	0.507	344.2	9.4
CH89_42	709	66	0.05308	0.00111	0.4022	0.0698	18.267	0.541	343.7	10.0
CH89_43	871	88	0.05303	0.00110	0.4030	0.0763	18.251	0.570	344.0	10.6
CH89_44	328	12	0.05976	0.00126	0.8114	0.1601	10.154	0.309	605.8	18.0
CH89_45	324	13	0.06097	0.00129	0.8375	0.1684	10.064	0.304	610.1	18.0
CH89_46	319	12	0.06023	0.00127	0.8472	0.1752	9.807	0.307	626.3	19.1
CHJ01_1	1058	1197	0.12925	0.01422	0.0055	0.0122	3339.343	102.159	1.7	0.1

Supplemental File 3

CHJ01_2	497	387	0.07431	0.00538	0.0027	0.0019	3819.994	103.819	1.6	0.0
CHJ01_3	274	152	0.08263	0.00825	0.0030	0.0033	3787.751	109.279	1.6	0.1
CHJ01_4	292	214	0.07529	0.00808	0.0027	0.0030	3801.073	108.987	1.6	0.1
CHJ01_5	372	245	0.07416	0.00680	0.0028	0.0025	3730.706	98.650	1.7	0.0
CHJ01_6	196	96	0.25007	0.01761	0.0117	0.0328	2982.424	116.109	1.6	0.1
CHJ01_7	952	1318	0.06814	0.00434	0.0025	0.0014	3796.819	98.078	1.7	0.0
CHJ01_8	393	227	0.09905	0.00771	0.0038	0.0039	3640.897	99.556	1.7	0.0
CHJ01_9	488	293	0.07013	0.00546	0.0026	0.0018	3809.427	104.993	1.6	0.0
CHJ01_10	317	136	0.07874	0.00721	0.0030	0.0029	3632.584	103.198	1.7	0.1
CHJ01_11	264	131	0.08959	0.00856	0.0033	0.0039	3823.114	111.980	1.6	0.1
CHJ01_12	144	70	0.05908	0.00342	0.0133	0.0060	619.918	15.686	10.2	0.3
CHJ01_13	243	126	0.09307	0.01033	0.0034	0.0045	3781.661	110.020	1.6	0.1
CHJ01_14	381	253	0.07681	0.00633	0.0027	0.0022	3835.756	107.211	1.6	0.0
CHJ01_15	84	35	0.15466	0.02342	0.0055	0.0161	3853.112	187.773	1.4	0.1
CHJ01_16	360	225	0.07514	0.00746	0.0027	0.0027	3739.637	126.170	1.7	0.1
CHJ01_17	253	139	0.08386	0.00807	0.0031	0.0032	3696.758	110.755	1.7	0.1
CHJ01_18	368	225	0.06967	0.00657	0.0026	0.0022	3712.977	115.136	1.7	0.1
CHJ01_19	443	218	0.06453	0.00501	0.0025	0.0016	3510.420	104.792	1.8	0.1
CHJ01_20	231	118	0.09058	0.00886	0.0034	0.0041	3702.423	121.451	1.6	0.1
CHJ01_21	698	766	0.07142	0.00405	0.0026	0.0015	3734.737	112.683	1.7	0.1
CHJ01_22	377	180	0.07902	0.00620	0.0031	0.0026	3525.219	109.876	1.8	0.1
CHJ01_23	365	233	0.06798	0.00538	0.0025	0.0019	3741.546	106.790	1.7	0.0
CHJ01_24	310	176	0.07337	0.00690	0.0028	0.0025	3654.595	112.292	1.7	0.1
CHJ01_25	963	544	0.04760	0.00125	0.0198	0.0031	330.160	8.444	19.5	0.5
CHJ01_26	224	112	0.08280	0.00831	0.0031	0.0034	3654.085	116.117	1.7	0.1
CHJ01_27	334	192	0.06146	0.00604	0.0023	0.0017	3611.938	111.196	1.7	0.1
CHJ01_28	240	124	0.09543	0.01034	0.0038	0.0055	3507.942	114.077	1.7	0.1
CHJ01_29	293	175	0.07838	0.00715	0.0030	0.0026	3679.005	108.027	1.7	0.1
CHJ01_30	1391	3353	0.13957	0.01443	0.0059	0.0138	3377.009	101.733	1.7	0.1
CHJ01_31	205	129	0.09266	0.00924	0.0035	0.0041	3577.931	115.406	1.7	0.1
CHJ01_32	353	185	0.08186	0.00660	0.0032	0.0028	3555.504	104.312	1.7	0.1
CHJ01_33	582	507	0.06587	0.00454	0.0024	0.0014	3738.040	105.561	1.7	0.0
CHJ01_34	501	356	0.06549	0.00511	0.0025	0.0018	3723.596	105.263	1.7	0.0
CHJ01_35	271	161	0.33416	0.01306	0.0190	0.0334	2427.770	73.495	1.7	0.1
CHJ01_36	166	200	0.09228	0.01105	0.0035	0.0052	3623.439	121.154	1.7	0.1
CHJ01_37	330	211	0.10813	0.00912	0.0040	0.0048	3614.828	113.814	1.6	0.1
CHJ01_38	513	383	0.06676	0.00494	0.0025	0.0016	3610.791	97.116	1.7	0.0
CHJ01_39	146	83	0.79056	0.01927	0.4581	1.4727	239.508	8.857	1.5	1.7
CHJ01_40	444	335	0.07553	0.00502	0.0029	0.0019	3620.341	105.528	1.7	0.1
CHJ01_41	366	275	0.08197	0.00745	0.0029	0.0027	3751.000	112.845	1.6	0.1
CHJ02_1	1637	1918	0.04794	0.00105	0.0739	0.0071	88.467	1.953	72.4	1.6
CHJ02_2	1401	1520	0.04779	0.00105	0.0744	0.0067	88.618	2.012	72.3	1.6
CHJ02_3	1713	2113	0.04759	0.00103	0.0747	0.0081	87.015	2.042	73.7	1.7
CHJ02_4	403	276	0.04817	0.00125	0.0765	0.0104	86.559	2.027	74.0	1.7
CHJ02_5	477	321	0.04780	0.00125	0.0791	0.0106	82.689	1.934	77.5	1.8
CHJ02_6	501	367	0.04860	0.00121	0.0743	0.0083	89.823	1.997	71.3	1.6
CHJ02_7	345	203	0.04931	0.00137	0.0750	0.0105	89.497	2.006	71.5	1.6
CHJ02_8	328	246	0.04929	0.00144	0.0755	0.0129	89.402	2.049	71.5	1.6
CHJ02_9	361	249	0.04904	0.00122	0.0774	0.0099	87.592	2.029	73.0	1.7
CHJ02_10	338	446	0.06266	0.00310	0.0911	0.0318	93.549	2.385	67.2	1.7
CHJ02_11	143	91	0.05368	0.00188	0.0835	0.0197	88.117	2.118	72.2	1.7
CHJ02_12	988	824	0.04747	0.00110	0.0734	0.0083	88.434	2.087	72.5	1.7
CHJ02_13	269	156	0.04899	0.00145	0.0755	0.0121	89.401	2.065	71.6	1.7

Supplemental File 3

CHJ02_14	116	60	0.05018	0.00200	0.0776	0.0181	89.771	2.283	71.2	1.8
CHJ02_15	764	998	0.04707	0.00113	0.0723	0.0083	90.428	2.172	70.9	1.7
CHJ02_16	201	129	0.05222	0.00182	0.0814	0.0187	88.667	2.074	71.9	1.7
CHJ02_17	286	197	0.05451	0.00170	0.0852	0.0190	88.812	2.147	71.5	1.7
CHJ02_18	585	435	0.04753	0.00118	0.0725	0.0096	90.949	2.188	70.5	1.7
CHJ02_19	493	344	0.04834	0.00118	0.0743	0.0096	90.137	2.073	71.0	1.6
CHJ02_20	309	145	0.04808	0.00141	0.0759	0.0116	87.721	2.112	73.0	1.8
CHJ02_21	343	223	0.04921	0.00149	0.0761	0.0142	88.802	2.160	72.0	1.8
CHJ02_22	380	247	0.04804	0.00133	0.0749	0.0110	88.975	2.272	72.0	1.8
CHJ02_23	397	253	0.04880	0.00130	0.0757	0.0107	89.843	2.141	71.2	1.7
CHJ02_24	240	163	0.04842	0.00140	0.0756	0.0135	89.511	2.255	71.5	1.8
CHJ02_25	313	143	0.04959	0.00137	0.0762	0.0131	89.810	2.105	71.2	1.7
CHJ02_26	224	150	0.04902	0.00158	0.0759	0.0153	89.776	2.163	71.3	1.7
CHJ02_27	272	203	0.04880	0.00144	0.0766	0.0140	88.666	2.220	72.2	1.8
CHJ02_28	214	137	0.05033	0.00152	0.0796	0.0160	87.948	2.246	72.6	1.9
CHJ02_29	529	301	0.04774	0.00125	0.0741	0.0086	88.938	2.117	72.1	1.7
CHJ02_30	288	216	0.05024	0.00152	0.0787	0.0143	88.291	2.176	72.3	1.8
CHJ02_31	223	112	0.05089	0.00174	0.0776	0.0152	89.954	2.236	71.0	1.8
CHJ02_32	261	197	0.04948	0.00166	0.0771	0.0159	88.572	2.206	72.2	1.8
CHJ02_33	557	910	0.05060	0.00124	0.0781	0.0111	90.114	2.230	70.9	1.8
CHJ02_34	312	248	0.04967	0.00152	0.0767	0.0132	88.445	2.243	72.3	1.8
CHJ02_35	204	178	0.05064	0.00172	0.0818	0.0172	85.715	2.180	74.5	1.9
CHJ04_1	178	91	0.07386	0.00516	0.1194	0.0927	85.858	3.113	72.2	2.7
CHJ04_2	255	135	0.04841	0.00147	0.0745	0.0017	89.920	2.042	71.2	1.6
CHJ04_3	283	216	0.04871	0.00158	0.0744	0.0019	89.331	2.174	71.6	1.7
CHJ04_4	290	176	0.04888	0.00136	0.0747	0.0017	90.028	2.034	71.1	1.6
CHJ04_5	213	111	0.05066	0.00167	0.0770	0.0023	89.781	2.185	71.1	1.7
CHJ04_6	221	102	0.04979	0.00175	0.0749	0.0023	89.649	2.324	71.3	1.8
CHJ04_7	62	46	0.05477	0.00294	0.0850	0.0043	88.948	2.193	71.4	1.8
CHJ04_8	319	192	0.04855	0.00135	0.0739	0.0018	90.409	2.342	70.8	1.8
CHJ04_9	369	286	0.04844	0.00133	0.0731	0.0019	91.352	2.340	70.1	1.8
CHJ04_10	410	407	0.04851	0.00131	0.0741	0.0017	90.539	2.154	70.7	1.7
CHJ04_11	312	211	0.04845	0.00136	0.0744	0.0017	89.798	2.174	71.3	1.7
CHJ04_12	364	257	0.04876	0.00137	0.0738	0.0017	91.547	2.114	69.9	1.6
CHJ04_13	338	224	0.04882	0.00151	0.0755	0.0018	90.219	2.219	70.9	1.7
CHJ04_14	315	211	0.04990	0.00149	0.0755	0.0020	90.332	2.228	70.7	1.7
CHJ04_15	708	1055	0.04833	0.00121	0.0732	0.0015	91.237	2.300	70.2	1.8
CHJ04_16	319	256	0.04819	0.00136	0.0739	0.0018	89.742	2.293	71.4	1.8
CHJ04_17	159	102	0.05106	0.00180	0.0791	0.0025	88.993	2.205	71.7	1.8
CHJ04_18	86	48	0.05289	0.00206	0.0815	0.0030	90.225	2.422	70.6	1.9
CHJ04_19	148	114	0.04972	0.00200	0.0771	0.0028	88.849	2.181	71.9	1.8
CHJ04_20	331	190	0.04834	0.00144	0.0755	0.0021	88.887	2.255	72.0	1.8
CHJ04_21	120	66	0.05256	0.00197	0.0797	0.0026	89.524	2.241	71.1	1.8
CHJ04_22	99	65	0.05986	0.00303	0.0931	0.0043	88.100	2.335	71.6	1.9
CHJ04_23	168	67	0.04909	0.00180	0.0761	0.0025	88.735	2.313	72.1	1.9
CHJ04_24	254	157	0.05024	0.00147	0.0770	0.0020	90.049	2.347	70.9	1.8
CHJ04_25	166	64	0.05043	0.00173	0.0786	0.0022	89.248	2.280	71.6	1.8
CHJ04_26	131	70	0.05072	0.00214	0.0775	0.0029	89.595	2.266	71.3	1.8
CHJ04_27	167	144	0.05118	0.00156	0.0806	0.0024	87.441	2.341	73.0	2.0
CHJ04_28	222	115	0.05010	0.00169	0.0765	0.0025	89.832	2.398	71.1	1.9
CHJ04_29	266	168	0.04944	0.00148	0.0768	0.0020	88.503	2.240	72.2	1.8
CHJ04_30	264	143	0.04980	0.00154	0.0783	0.0020	88.554	2.164	72.2	1.8
CHJ04_31	238	87	0.04959	0.00165	0.0764	0.0023	89.666	2.321	71.3	1.8

Supplemental File 3

CHJ04_32	227	129	0.04944	0.00145	0.0770	0.0023	88.230	2.343	72.5	1.9
CHJ04_33	336	187	0.04923	0.00142	0.0751	0.0019	90.942	2.212	70.3	1.7
CHJ04_34	342	249	0.04798	0.00140	0.0729	0.0020	91.027	2.379	70.4	1.8
CHJ04_35	144	77	0.05100	0.00179	0.0821	0.0027	86.404	2.475	73.9	2.1
CHJ13_1	876	795	0.04796	0.00124	0.0174	0.0024	384.250	9.073	16.7	0.4
CHJ13_2	332	233	0.05029	0.00162	0.0183	0.0038	379.379	9.732	16.9	0.4
CHJ13_3	260	159	0.05445	0.00190	0.0198	0.0047	382.316	9.378	16.7	0.4
CHJ13_4	307	186	0.04818	0.00163	0.0178	0.0037	375.617	9.142	17.1	0.4
CHJ13_5	906	882	0.04768	0.00123	0.0173	0.0024	382.438	9.089	16.8	0.4
CHJ13_6	374	347	0.09487	0.00387	0.0376	0.0193	350.071	8.463	17.3	0.4
CHJ13_7	426	263	0.04787	0.00157	0.0173	0.0033	383.508	9.284	16.8	0.4
CHJ13_8	411	346	0.04800	0.00141	0.0183	0.0032	363.792	9.145	17.7	0.4
CHJ13_9	578	513	0.04753	0.00135	0.0175	0.0026	376.257	8.993	17.1	0.4
CHJ13_10	270	141	0.05074	0.00156	0.0188	0.0036	372.960	9.351	17.2	0.4
CHJ13_11	480	315	0.04848	0.00146	0.0179	0.0029	375.764	9.416	17.1	0.4
CHJ13_12	1049	1139	0.04673	0.00115	0.0168	0.0021	386.055	8.971	16.7	0.4
CHJ13_13	422	268	0.04813	0.00143	0.0174	0.0027	382.510	9.035	16.8	0.4
CHJ13_14	582	522	0.04782	0.00124	0.0174	0.0025	378.619	9.371	17.0	0.4
CHJ13_15	765	515	0.04748	0.00122	0.0170	0.0025	385.329	9.544	16.7	0.4
CHJ13_16	536	408	0.04701	0.00130	0.0171	0.0026	378.683	8.980	17.0	0.4
CHJ13_17	377	234	0.04835	0.00155	0.0176	0.0034	380.719	9.204	16.9	0.4
CHJ13_18	339	239	0.04958	0.00147	0.0182	0.0031	375.387	9.321	17.1	0.4
CHJ13_19	690	771	0.04759	0.00129	0.0172	0.0027	381.366	9.407	16.9	0.4
CHJ13_20	492	446	0.04823	0.00136	0.0174	0.0025	381.661	9.102	16.8	0.4
CHJ13_21	719	716	0.04769	0.00122	0.0170	0.0024	384.969	9.341	16.7	0.4
CHJ13_22	506	390	0.04727	0.00134	0.0173	0.0026	376.386	9.150	17.1	0.4
CHJ13_23	777	823	0.04702	0.00121	0.0167	0.0023	384.505	9.252	16.7	0.4
CHJ13_24	518	285	0.04734	0.00134	0.0171	0.0026	380.587	9.479	16.9	0.4
CHJ13_25	385	267	0.04884	0.00157	0.0178	0.0033	378.129	8.968	17.0	0.4
CHJ13_26	215	118	0.04894	0.00177	0.0182	0.0037	371.105	8.880	17.3	0.4
CHJ13_27	492	314	0.04819	0.00141	0.0171	0.0029	383.086	9.760	16.8	0.4
CHJ13_28	495	328	0.04671	0.00145	0.0169	0.0031	382.153	9.185	16.8	0.4
CHJ13_29	920	1180	0.04761	0.00117	0.0168	0.0021	390.321	9.321	16.5	0.4
CHJ13_30	939	1028	0.04673	0.00113	0.0165	0.0021	390.587	10.010	16.5	0.4
CHJ13_31	424	246	0.04897	0.00147	0.0174	0.0029	383.294	9.136	16.7	0.4
CHJ13_32	530	552	0.05021	0.00150	0.0181	0.0035	382.144	9.898	16.8	0.4
CHJ13_33	716	719	0.04740	0.00121	0.0173	0.0025	375.696	9.031	17.1	0.4
CHJ13_34	690	547	0.04660	0.00117	0.0165	0.0022	386.655	9.457	16.6	0.4
CHJ13_35	529	366	0.04805	0.00132	0.0170	0.0029	387.256	9.543	16.6	0.4
CHJ13_36	788	754	0.04675	0.00117	0.0166	0.0025	388.283	9.963	16.6	0.4
CHJ13_37	549	431	0.05055	0.00160	0.0182	0.0038	379.919	9.728	16.9	0.4
CHJ13_38	802	894	0.04797	0.00124	0.0171	0.0026	382.349	9.710	16.8	0.4
CHJ13_39	610	579	0.04836	0.00127	0.0175	0.0027	380.836	9.096	16.9	0.4
CHJ13_40	456	305	0.04903	0.00142	0.0175	0.0029	385.118	9.913	16.7	0.4
CHJ13_41	366	251	0.04897	0.00150	0.0176	0.0034	383.478	9.468	16.7	0.4
CHJ13_42	646	579	0.04797	0.00133	0.0168	0.0025	391.460	9.878	16.4	0.4
CHJ15_1	266	156	0.04968	0.00172	0.0185	0.0038	368.080	9.238	17.4	0.4
CHJ15_2	294	160	0.04932	0.00170	0.0183	0.0039	370.016	9.124	17.3	0.4
CHJ15_3	618	545	0.04784	0.00130	0.0171	0.0022	380.571	9.263	16.9	0.4
CHJ15_4	334	224	0.05142	0.00183	0.0191	0.0050	370.960	10.310	17.2	0.5
CHJ15_5	441	262	0.04865	0.00150	0.0179	0.0030	372.042	8.797	17.3	0.4
CHJ15_6	821	785	0.05022	0.00180	0.0184	0.0047	374.586	10.457	17.1	0.5

Supplemental File 3

CHJ15_7	397	240	0.04779	0.00145	0.0176	0.0031	372.192	9.298	17.3	0.4
CHJ15_8	462	371	0.04865	0.00145	0.0175	0.0032	380.944	9.630	16.9	0.4
CHJ15_9	429	216	0.04923	0.00146	0.0181	0.0034	372.479	9.832	17.2	0.5
CHJ15_10	405	402	0.07291	0.00265	0.0308	0.0151	325.801	11.899	19.1	0.7
CHJ15_11	201	109	0.05072	0.00217	0.0192	0.0068	362.105	14.217	17.7	0.7
CHJ15_12	330	196	0.04899	0.00150	0.0181	0.0033	369.512	9.757	17.4	0.5
CHJ15_13	728	521	0.04747	0.00125	0.0170	0.0026	381.875	10.076	16.8	0.4
CHJ15_14	452	315	0.04849	0.00143	0.0180	0.0035	372.831	10.019	17.2	0.5
CHJ15_15	1056	1621	0.04779	0.00120	0.0176	0.0026	373.724	9.885	17.2	0.5
CHJ15_16	278	162	0.04974	0.00172	0.0184	0.0042	372.685	9.999	17.2	0.5
CHJ15_17	342	213	0.04896	0.00152	0.0182	0.0035	373.081	9.519	17.2	0.4
CHJ15_18	528	368	0.05647	0.00169	0.0208	0.0048	372.945	9.824	17.0	0.5
CHJ15_19	388	213	0.04869	0.00156	0.0180	0.0038	371.800	9.954	17.3	0.5
CHJ15_20	346	195	0.04819	0.00141	0.0183	0.0030	363.128	9.381	17.7	0.5
CHJ15_21	344	228	0.04944	0.00159	0.0181	0.0036	375.429	9.643	17.1	0.4
CHJ15_22	423	306	0.05118	0.00183	0.0187	0.0046	374.950	10.264	17.1	0.5
CHJ15_23	330	174	0.04962	0.00169	0.0182	0.0037	374.057	9.648	17.1	0.4
CHJ15_24	397	244	0.04947	0.00142	0.0182	0.0032	375.936	9.872	17.1	0.4
CHJ15_25	567	362	0.04729	0.00130	0.0172	0.0027	378.942	9.930	17.0	0.4
CHJ15_26	419	259	0.04936	0.00145	0.0183	0.0038	371.943	10.195	17.2	0.5
CHJ15_27	438	213	0.04898	0.00146	0.0177	0.0034	381.508	9.914	16.8	0.4
CHJ15_28	447	236	0.04901	0.00151	0.0178	0.0032	378.624	9.994	16.9	0.4
CHJ15_29	316	173	0.04891	0.00155	0.0179	0.0036	375.363	10.126	17.1	0.5
CHJ15_30	342	209	0.05172	0.00179	0.0199	0.0046	357.995	9.296	17.9	0.5
CHJ15_31	168	91	0.05186	0.00237	0.0197	0.0060	362.335	10.173	17.6	0.5
CHJ15_32	378	223	0.04919	0.00137	0.0185	0.0032	367.645	9.199	17.4	0.4
CHJ15_33	180	88	0.05237	0.00231	0.0195	0.0059	369.957	10.579	17.3	0.5
CHJ15_34	259	147	0.05083	0.00182	0.0191	0.0046	369.474	9.133	17.3	0.4
CHJ15_35	434	321	0.04882	0.00141	0.0179	0.0030	378.319	9.328	17.0	0.4
CHJ15_36	688	447	0.04887	0.00130	0.0180	0.0027	377.090	9.474	17.0	0.4
CHJ15_37	262	147	0.04980	0.00198	0.0184	0.0055	374.831	11.393	17.1	0.5
CHJ15_38	355	219	0.04859	0.00150	0.0181	0.0038	373.490	10.804	17.2	0.5
CHJ15_39	290	183	0.05050	0.00194	0.0191	0.0046	362.776	10.159	17.7	0.5
CHJ15_40	237	124	0.05062	0.00184	0.0190	0.0048	371.867	10.493	17.2	0.5
CHJ15_41	757	727	0.04771	0.00119	0.0175	0.0024	375.973	9.338	17.1	0.4
CHJ15_42	482	275	0.04831	0.00139	0.0179	0.0032	374.043	10.169	17.2	0.5
CHJ16_1	401	238	0.04973	0.00154	0.0500	0.0099	139.333	3.559	45.9	1.2
CHJ16_2	530	410	0.04812	0.00137	0.0484	0.0079	137.754	3.549	46.6	1.2
CHJ16_3	868	870	0.04807	0.00122	0.0481	0.0081	139.264	3.685	46.1	1.2
CHJ16_4	652	453	0.04855	0.00133	0.0486	0.0082	137.959	3.552	46.5	1.2
CHJ16_5	786	760	0.04972	0.00129	0.0490	0.0075	140.941	3.647	45.4	1.2
CHJ16_6	172	62	0.05224	0.00212	0.0536	0.0161	135.568	3.679	47.1	1.3
CHJ16_7	89	79	0.05624	0.00279	0.0587	0.0232	134.338	3.565	47.2	1.3
CHJ16_8	75	63	0.05704	0.00328	0.0601	0.0259	133.697	3.928	47.4	1.4
CHJ16_9	206	109	0.05166	0.00189	0.0514	0.0129	137.565	3.510	46.4	1.2
CHJ16_10	307	222	0.05059	0.00158	0.0503	0.0113	137.704	3.715	46.4	1.3
CHJ16_11	350	183	0.05668	0.00225	0.0573	0.0187	136.741	3.950	46.4	1.3
CHJ16_12	183	67	0.08180	0.00439	0.0855	0.0521	130.536	3.588	47.0	1.3
CHJ16_13	798	534	0.04726	0.00127	0.0467	0.0073	139.609	3.652	46.0	1.2
CHJ16_14	648	599	0.04776	0.00135	0.0476	0.0087	137.714	3.544	46.6	1.2
CHJ16_15	957	1054	0.04677	0.00124	0.0465	0.0088	140.451	3.845	45.7	1.3
CHJ16_16	313	222	0.04914	0.00171	0.0486	0.0106	137.928	3.641	46.4	1.2
CHJ16_17	467	312	0.04868	0.00131	0.0482	0.0074	138.166	3.986	46.4	1.3

Supplemental File 3

CHJ16_18	647	437	0.04890	0.00137	0.0472	0.0069	141.600	3.672	45.3	1.2
CHJ16_19	237	163	0.04976	0.00174	0.0493	0.0126	138.835	3.739	46.1	1.2
CHJ16_20	529	425	0.04848	0.00146	0.0481	0.0092	140.551	3.851	45.6	1.2
CHJ16_21	336	194	0.04845	0.00158	0.0480	0.0100	140.020	3.864	45.8	1.3
CHJ16_22	436	281	0.04806	0.00144	0.0467	0.0089	140.426	3.855	45.7	1.3
CHJ16_23	900	939	0.04798	0.00122	0.0461	0.0069	142.030	3.893	45.2	1.2
CHJ16_24	1077	1033	0.04797	0.00115	0.0474	0.0070	138.507	3.669	46.3	1.2
CHJ16_25	386	219	0.04875	0.00150	0.0477	0.0096	138.545	3.956	46.3	1.3
CHJ16_26	458	262	0.05029	0.00147	0.0489	0.0104	140.302	4.024	45.6	1.3
CHJ16_27	701	467	0.04816	0.00128	0.0477	0.0079	139.078	3.685	46.1	1.2
CHJ16_28	401	233	0.04840	0.00145	0.0477	0.0099	139.550	3.937	45.9	1.3
CHJ16_29	1119	1782	0.06672	0.00206	0.0663	0.0198	137.748	3.832	45.5	1.3
CHJ16_30	699	611	0.04745	0.00122	0.0469	0.0071	138.748	3.717	46.3	1.2
CHJ16_31	463	303	0.04829	0.00154	0.0482	0.0099	137.612	3.800	46.6	1.3
CHJ16_32	785	695	0.04788	0.00125	0.0469	0.0081	140.765	3.862	45.6	1.2
CHJ16_33	610	541	0.04760	0.00132	0.0471	0.0091	137.282	3.906	46.7	1.3
CHJ16_34	562	295	0.04823	0.00133	0.0478	0.0087	138.725	3.852	46.2	1.3
CHJ16_35	236	117	0.04926	0.00192	0.0489	0.0142	139.670	4.102	45.9	1.3
CHJ16.1_1	322	378	0.05094	0.00258	0.0216	0.0068	327.342	7.973	19.6	0.5
CHJ16.1_2	272	251	0.05286	0.00237	0.0219	0.0068	329.400	8.242	19.4	0.5
CHJ16.1_3	312	249	0.05618	0.00233	0.0251	0.0073	312.972	7.233	20.3	0.5
CHJ16.1_4	244	185	0.05265	0.00245	0.0218	0.0066	326.589	7.716	19.6	0.5
CHJ16.1_5	2903	4987	0.04699	0.00113	0.0200	0.0023	324.162	7.450	19.8	0.5
CHJ16.1_6	310	255	0.05138	0.00227	0.0216	0.0064	331.756	7.829	19.3	0.5
CHJ16.1_7	449	320	0.05214	0.00219	0.0227	0.0064	316.908	7.756	20.2	0.5
CHJ16.1_8	329	218	0.05060	0.00252	0.0215	0.0071	328.639	7.487	19.5	0.4
CHJ16.1_9	310	203	0.05061	0.00217	0.0213	0.0058	327.170	8.031	19.6	0.5
CHJ16.1_10	288	277	0.05147	0.00254	0.0216	0.0070	330.925	8.221	19.3	0.5
CHJ16.1_11	263	199	0.05221	0.00251	0.0218	0.0070	332.825	8.392	19.2	0.5
CHJ16.1_12	202	148	0.07794	0.00446	0.0345	0.0203	315.030	7.622	19.6	0.5
CHJ16.1_13	158	101	0.05590	0.00315	0.0238	0.0096	323.405	8.264	19.7	0.5
CHJ16.1_14	239	153	0.06375	0.00434	0.0275	0.0162	316.310	7.856	19.9	0.5
CHJ16.1_15	441	251	0.04830	0.00194	0.0202	0.0046	322.967	7.452	19.9	0.5
CHJ16.1_16	306	155	0.05102	0.00240	0.0215	0.0062	328.069	7.934	19.5	0.5
CHJ16.1_17	456	377	0.05355	0.00207	0.0228	0.0066	322.431	7.928	19.8	0.5
CHJ16.1_18	278	175	0.04908	0.00212	0.0212	0.0054	329.678	7.928	19.5	0.5
CHJ16.1_19	141	94	0.05432	0.00579	0.0229	0.0167	324.479	12.424	19.6	0.8
CHJ16.1_20	430	273	0.05225	0.00222	0.0219	0.0062	327.486	7.828	19.5	0.5
CHJ16.1_21	499	367	0.04716	0.00190	0.0193	0.0046	333.267	8.400	19.3	0.5
CHJ16.1_22	749	677	0.04778	0.00167	0.0200	0.0039	330.757	7.905	19.4	0.5
CHJ16.1_23	1341	1309	0.04737	0.00134	0.0200	0.0033	326.517	8.071	19.7	0.5
CHJ16.1_24	347	263	0.05055	0.00229	0.0210	0.0063	332.550	8.212	19.3	0.5
CHJ16.1_25	269	209	0.05161	0.00249	0.0213	0.0070	331.238	8.518	19.3	0.5
CHJ16.1_26	611	482	0.04870	0.00154	0.0199	0.0035	333.451	8.239	19.2	0.5
CHJ16.1_27	171	134	0.06135	0.00345	0.0259	0.0110	319.282	7.924	19.8	0.5
CHJ16.1_28	832	659	0.04792	0.00152	0.0201	0.0038	327.159	7.997	19.6	0.5
CHJ16.1_29	239	138	0.05144	0.00283	0.0213	0.0080	333.425	8.379	19.2	0.5
CHJ16.1_30	274	140	0.04766	0.00237	0.0200	0.0056	324.559	8.221	19.8	0.5
CHJ16.1_31	257	176	0.05199	0.00231	0.0230	0.0064	312.396	8.247	20.5	0.5
CHJ16.1_32	326	232	0.05090	0.00231	0.0213	0.0063	318.716	8.781	20.1	0.6
CHJ16.1_33	217	131	0.05592	0.00388	0.0244	0.0135	312.910	7.537	20.3	0.5
CHJ16.1_34	581	372	0.04970	0.00175	0.0204	0.0042	330.226	8.066	19.4	0.5
CHJ16.1_35	433	264	0.05048	0.00213	0.0213	0.0053	320.486	7.546	20.0	0.5

Supplemental File 3

CHJ24_1	410	370	0.04994	0.00165	0.0395	0.0081	174.030	4.295	36.8	0.9
CHJ24_2	236	125	0.05129	0.00199	0.0404	0.0109	175.566	4.552	36.4	0.9
CHJ24_3	105	33	0.05468	0.00289	0.0444	0.0167	171.476	4.659	37.1	1.0
CHJ24_4	322	155	0.04918	0.00185	0.0386	0.0085	175.589	4.592	36.5	1.0
CHJ24_5	116	45	0.05673	0.00275	0.0446	0.0172	174.185	4.600	36.4	1.0
CHJ24_6	207	136	0.05076	0.00242	0.0395	0.0122	175.612	3.709	36.4	0.8
CHJ24_7	146	63	0.05210	0.00268	0.0414	0.0137	175.480	3.757	36.4	0.8
CHJ24_8	302	314	0.04693	0.00171	0.0365	0.0087	177.013	4.497	36.3	0.9
CHJ24_9	48	22	0.05961	0.00492	0.0475	0.0301	169.759	4.227	37.2	1.0
CHJ24_10	116	43	0.05349	0.00257	0.0419	0.0130	175.252	3.847	36.4	0.8
CHJ24_11	252	189	0.04770	0.00209	0.0382	0.0094	173.389	3.707	37.0	0.8
CHJ24_12	308	120	0.04797	0.00177	0.0373	0.0074	176.304	3.677	36.4	0.8
CHJ24_13	194	93	0.05110	0.00214	0.0405	0.0106	171.848	4.309	37.2	0.9
CHJ24_14	304	249	0.04798	0.00180	0.0372	0.0093	178.446	5.155	36.0	1.0
CHJ24_15	334	187	0.04801	0.00155	0.0385	0.0084	173.637	4.662	37.0	1.0
CHJ24_16	326	190	0.04778	0.00178	0.0376	0.0086	175.491	4.216	36.6	0.9
CHJ24_17	196	106	0.05080	0.00236	0.0402	0.0122	174.569	4.671	36.6	1.0
CHJ24_18	159	100	0.05189	0.00255	0.0404	0.0126	175.476	4.599	36.4	1.0
CHJ24_19	236	194	0.04930	0.00200	0.0384	0.0093	177.358	4.427	36.1	0.9
CHJ24_20	811	818	0.04725	0.00131	0.0367	0.0055	174.130	5.035	36.9	1.1
CHJ24_21	68	24	0.05750	0.00796	0.0459	0.0497	168.993	7.737	37.5	1.8
CHJ24_22	368	375	0.04844	0.00183	0.0411	0.0097	162.363	4.668	39.5	1.1
CHJ24_23	877	779	0.04733	0.00126	0.0378	0.0058	171.579	4.345	37.4	0.9
CHJ24_24	107	56	0.05205	0.00297	0.0426	0.0173	168.794	4.511	37.8	1.0
CHJ24_25	218	153	0.04902	0.00218	0.0392	0.0109	172.997	4.679	37.0	1.0
CHJ24_26	99	49	0.05556	0.00336	0.0467	0.0224	164.761	5.185	38.6	1.2
CHJ24_27	206	145	0.05189	0.00205	0.0423	0.0114	172.888	4.591	36.9	1.0
CHJ24_28	292	170	0.04860	0.00191	0.0388	0.0099	174.183	4.928	36.8	1.0
CHJ24_29	233	110	0.04962	0.00209	0.0401	0.0101	170.677	4.782	37.5	1.1
CHJ24_30	376	228	0.04982	0.00165	0.0402	0.0087	170.375	4.688	37.6	1.0
CHJ24_31	290	234	0.04877	0.00185	0.0401	0.0101	166.016	4.901	38.6	1.1
CHJ24_32	186	79	0.05385	0.00236	0.0427	0.0135	173.210	5.239	36.8	1.1
CHJ24_33	263	170	0.05108	0.00180	0.0402	0.0112	177.669	5.655	36.0	1.1
CHJ24_34	307	266	0.05481	0.00195	0.0463	0.0125	165.414	4.946	38.5	1.2
CHJ24_35	1013	2048	0.04780	0.00122	0.0379	0.0072	173.740	5.362	36.9	1.1
CHJ27_1	229	134	0.04909	0.00150	0.0757	0.0143	89.526	2.174	71.5	1.7
CHJ27_2	237	127	0.04987	0.00148	0.0776	0.0132	88.478	2.199	72.2	1.8
CHJ27_3	520	487	0.04842	0.00128	0.0775	0.0120	85.205	2.034	75.1	1.8
CHJ27_4	654	426	0.04729	0.00129	0.0724	0.0109	88.534	2.146	72.4	1.8
CHJ27_5	410	210	0.04750	0.00130	0.0746	0.0124	88.069	2.228	72.8	1.8
CHJ27_6	436	411	0.04739	0.00128	0.0716	0.0120	91.228	2.276	70.3	1.8
CHJ27_7	317	204	0.04878	0.00136	0.0752	0.0142	89.839	2.343	71.2	1.9
CHJ27_8	483	334	0.04735	0.00130	0.0718	0.0104	89.822	2.217	71.4	1.8
CHJ27_9	518	405	0.04757	0.00124	0.0742	0.0099	88.102	2.258	72.7	1.9
CHJ27_10	595	446	0.04797	0.00118	0.0744	0.0096	88.792	2.158	72.1	1.8
CHJ27_11	368	208	0.04857	0.00140	0.0764	0.0121	87.387	2.312	73.2	1.9
CHJ27_12	355	239	0.04763	0.00136	0.0732	0.0122	88.738	2.210	72.2	1.8
CHJ27_13	314	207	0.04925	0.00144	0.0773	0.0146	87.272	2.176	73.3	1.8
CHJ27_14	496	402	0.04870	0.00130	0.0754	0.0111	88.529	2.275	72.3	1.9
CHJ27_15	603	481	0.04700	0.00122	0.0756	0.0110	86.398	2.108	74.2	1.8
CHJ27_16	689	564	0.04792	0.00120	0.0734	0.0104	88.728	2.189	72.2	1.8
CHJ27_17	508	290	0.05054	0.00132	0.0797	0.0127	86.998	2.207	73.4	1.9

Supplemental File 3

CHJ27_18	287	211	0.04898	0.00147	0.0755	0.0137	89.475	2.262	71.5	1.8
CHJ27_19	376	209	0.04855	0.00139	0.0748	0.0128	89.603	2.206	71.4	1.8
CHJ27_20	281	206	0.04802	0.00151	0.0730	0.0125	90.412	2.316	70.9	1.8
CHJ27_21	439	265	0.04933	0.00136	0.0756	0.0112	89.201	2.143	71.7	1.7
CHJ27_22	256	145	0.04950	0.00163	0.0769	0.0163	89.152	2.170	71.7	1.7
CHJ27_23	449	273	0.04917	0.00132	0.0757	0.0126	89.253	2.257	71.7	1.8
CHJ27_24	347	192	0.04914	0.00145	0.0771	0.0163	87.466	2.368	73.1	2.0
CHJ27_25	324	188	0.04955	0.00140	0.0775	0.0141	88.394	2.232	72.3	1.8
CHJ27_26	633	414	0.04758	0.00121	0.0749	0.0110	87.776	2.245	73.0	1.9
CHJ27_27	489	336	0.04913	0.00127	0.0765	0.0117	88.354	2.248	72.4	1.8
CHJ27_28	657	477	0.04893	0.00121	0.0770	0.0123	88.205	2.319	72.5	1.9
CHJ27_29	387	280	0.04955	0.00140	0.0788	0.0139	87.536	2.258	73.0	1.9
CHJ27_30	366	245	0.04908	0.00147	0.0770	0.0138	88.587	2.245	72.2	1.8
CHJ27_31	226	151	0.04962	0.00150	0.0771	0.0134	88.424	2.293	72.3	1.9
CHJ27_32	350	179	0.04994	0.00136	0.0800	0.0144	87.901	2.123	72.7	1.8
CHJ27_33	548	375	0.04915	0.00122	0.0782	0.0114	86.897	2.179	73.6	1.8
CHJ27_34	347	160	0.04918	0.00147	0.0794	0.0140	87.066	2.237	73.5	1.9
CHJ27_35	807	762	0.04796	0.00113	0.0759	0.0103	88.396	2.260	72.5	1.8
CHJ33_1	167	115	0.04777	0.00116	0.0953	0.0147	68.872	1.955	92.9	2.6
CHJ33_2	376	180	0.04754	0.00109	0.0756	0.0100	86.170	2.261	74.4	1.9
CHJ33_3	795	844	0.04774	0.00102	0.0753	0.0093	86.950	2.307	73.7	2.0
CHJ33_4	1472	1375	0.04908	0.00107	0.0771	0.0111	87.624	2.408	73.0	2.0
CHJ33_5	528	657	0.04796	0.00106	0.0765	0.0099	86.230	2.222	74.3	1.9
CHJ33_6	481	341	0.04745	0.00105	0.0755	0.0108	86.248	2.350	74.3	2.0
CHJ33_7	368	211	0.04716	0.00110	0.0750	0.0099	86.102	2.270	74.5	2.0
CHJ33_8	584	357	0.04766	0.00105	0.0758	0.0099	85.938	2.242	74.6	1.9
CHJ33_9	419	230	0.04804	0.00109	0.0741	0.0101	87.900	2.342	72.9	1.9
CHJ33_10	246	124	0.04787	0.00117	0.0751	0.0099	86.985	2.192	73.7	1.9
CHJ33_11	704	956	0.04780	0.00102	0.0739	0.0097	88.292	2.393	72.6	2.0
CHJ33_12	456	323	0.04767	0.00106	0.0761	0.0102	85.393	2.382	75.0	2.1
CHJ33_13	542	439	0.04779	0.00105	0.0746	0.0092	87.314	2.238	73.4	1.9
CHJ33_14	642	596	0.04780	0.00104	0.0748	0.0100	86.878	2.351	73.7	2.0
CHJ33_15	218	150	0.05605	0.00131	0.1047	0.0157	72.826	1.870	87.0	2.2
CHJ33_16	478	354	0.04778	0.00109	0.0758	0.0094	85.876	2.122	74.6	1.8
CHJ33_17	136	80	0.04874	0.00134	0.0781	0.0139	85.195	2.384	75.1	2.1
CHJ33_18	363	210	0.04802	0.00110	0.0756	0.0098	86.607	2.225	74.0	1.9
CHJ33_19	429	286	0.04840	0.00108	0.0765	0.0108	86.414	2.432	74.1	2.1
CHJ33_20	691	395	0.04789	0.00105	0.0767	0.0085	85.303	2.187	75.1	1.9
CHJ33_21	324	210	0.04808	0.00115	0.0779	0.0112	84.589	2.236	75.7	2.0
CHJ33_22	916	1164	0.04738	0.00101	0.0748	0.0070	86.991	2.121	73.7	1.8
CHJ33_23	347	145	0.04762	0.00109	0.0743	0.0095	87.713	2.319	73.1	1.9
CHJ33_24	463	312	0.04825	0.00109	0.0749	0.0107	88.224	2.385	72.6	2.0
CHJ33_25	309	174	0.04709	0.00111	0.0758	0.0107	85.297	2.255	75.2	2.0
CHJ33_26	380	325	0.04862	0.00113	0.0746	0.0110	89.422	2.464	71.6	2.0
CHJ33_27	254	149	0.04793	0.00116	0.0772	0.0107	85.430	2.218	75.0	1.9
CHJ33_28	328	249	0.04778	0.00115	0.0738	0.0119	89.276	2.449	71.8	2.0
CHJ33_29	309	174	0.04776	0.00110	0.0740	0.0098	89.038	2.266	72.0	1.8
CHJ33_30	564	453	0.04760	0.00104	0.0744	0.0095	88.197	2.309	72.7	1.9
CHJ33_31	263	131	0.04781	0.00112	0.0765	0.0097	86.334	2.149	74.2	1.8
CHJ33_32	567	399	0.04794	0.00105	0.0750	0.0105	88.145	2.432	72.7	2.0
CHJ33_33	458	307	0.04748	0.00103	0.0761	0.0095	86.167	2.260	74.4	1.9
CHJ33_34	235	134	0.04782	0.00115	0.0772	0.0122	85.779	2.306	74.7	2.0
CHJ33_35	462	263	0.04842	0.00107	0.0750	0.0081	89.004	2.219	71.9	1.8

Supplemental File 3

CHJ33_36	1053	1501	0.04759	0.00101	0.0764	0.0100	86.096	2.280	74.4	2.0
CHJ33_37	527	312	0.04769	0.00104	0.0761	0.0099	86.581	2.269	74.0	1.9
CHJ33_38	278	179	0.04771	0.00111	0.0758	0.0102	86.821	2.277	73.8	1.9
CHJ33_39	306	159	0.04801	0.00112	0.0761	0.0101	87.487	2.186	73.2	1.8
CHJ33_40	410	311	0.04767	0.00108	0.0758	0.0101	87.032	2.243	73.6	1.9
CHJ33_41	258	127	0.04833	0.00118	0.0774	0.0120	86.377	2.351	74.1	2.0
CHJ33_42	368	172	0.04813	0.00109	0.0765	0.0100	87.317	2.203	73.3	1.8
CHJ_34_1	518	286	0.04926	0.00068	0.0765	0.0118	88.311	1.442	72.4	1.2
CHJ_34_2	323	170	0.04850	0.00116	0.0715	0.0145	93.932	1.469	68.2	1.1
CHJ_34_3	336	182	0.05010	0.00095	0.0739	0.0123	93.413	1.372	68.4	1.0
CHJ_34_4	203	139	0.04994	0.00104	0.1201	0.0206	57.434	0.897	111.0	1.7
CHJ_34_5	287	148	0.05049	0.00121	0.0750	0.0144	93.507	1.284	68.3	0.9
CHJ_34_6	480	370	0.04831	0.00074	0.0710	0.0115	94.493	1.460	67.8	1.0
CHJ_34_7	283	170	0.04857	0.00107	0.0700	0.0133	97.100	1.432	65.9	1.0
CHJ_34_8	258	123	0.04960	0.00133	0.0751	0.0177	92.362	1.639	69.2	1.2
CHJ_34_9	456	316	0.04751	0.00077	0.0717	0.0108	92.355	1.436	69.4	1.1
CHJ_34_10	179	110	0.04969	0.00108	0.1377	0.0253	49.976	0.835	127.5	2.1
CHJ_34_11	262	135	0.04871	0.00128	0.0719	0.0148	93.174	1.290	68.7	1.0
CHJ_34_12	298	176	0.04989	0.00104	0.0750	0.0142	93.277	1.537	68.5	1.1
CHJ_34_13	341	226	0.04880	0.00082	0.0711	0.0111	94.576	1.512	67.7	1.1
CHJ_34_14	267	183	0.04947	0.00112	0.0725	0.0140	94.017	1.318	68.0	1.0
CHJ_34_15	358	215	0.04846	0.00103	0.0716	0.0135	94.155	1.544	68.0	1.1
CHJ_34_16	447	440	0.04810	0.00091	0.0690	0.0115	95.679	1.628	67.0	1.1
CHJ_34_17	132	74	0.04856	0.00159	0.0794	0.0208	85.049	1.546	75.3	1.4
CHJ_34_18	287	164	0.05203	0.00109	0.0766	0.0146	93.946	1.606	67.9	1.2
CHJ_34_19	247	112	0.04984	0.00103	0.0715	0.0145	94.755	1.640	67.5	1.2
CHJ_34_20	252	153	0.04918	0.00106	0.0717	0.0143	94.658	1.671	67.6	1.2
CHJ_34_21	640	527	0.04794	0.00080	0.0682	0.0120	97.691	1.913	65.6	1.3
CHJ_34_22	416	302	0.04772	0.00094	0.0708	0.0126	93.581	1.681	68.5	1.2
CHJ_34_23	605	620	0.04738	0.00085	0.0684	0.0095	95.110	1.731	67.4	1.2
CHJ_34_24	282	212	0.05284	0.00138	0.0807	0.0170	90.972	1.488	70.0	1.1
CHJ_34_25	1406	935	0.04655	0.00048	0.0701	0.0088	92.476	1.490	69.4	1.1
CHJ_34_26	290	171	0.04932	0.00129	0.0736	0.0162	93.916	1.461	68.1	1.1
CHJ_34_27	549	414	0.04810	0.00087	0.0684	0.0099	96.838	1.502	66.2	1.0
CHJ_34_28	435	478	0.04869	0.00085	0.0734	0.0118	91.180	1.343	70.2	1.0
CHJ_34_29	438	345	0.04855	0.00102	0.0694	0.0130	95.535	1.841	67.0	1.3
CHJ_34_30	293	153	0.04872	0.00127	0.0721	0.0154	94.235	1.515	67.9	1.1
CHJ_34_31	424	300	0.04916	0.00097	0.0705	0.0113	97.517	1.463	65.6	1.0
CHJ_34_32	191	146	0.05063	0.00140	0.0766	0.0183	91.570	1.791	69.7	1.4
CHJ_34_33	689	509	0.04829	0.00076	0.0701	0.0099	94.554	1.474	67.7	1.1
CHJ_34_34	237	117	0.04814	0.00125	0.0716	0.0158	92.891	1.649	69.0	1.2
CHJ_34_35	222	105	0.04941	0.00146	0.0727	0.0178	93.831	1.805	68.2	1.3
CHJ36_1	783	694	0.04833	0.00110	0.0736	0.0098	91.034	2.405	70.3	1.9
CHJ36_2	532	366	0.04828	0.00120	0.0772	0.0116	87.347	2.323	73.3	1.9
CHJ36_3	374	279	0.04825	0.00136	0.0753	0.0127	89.535	2.381	71.5	1.9
CHJ36_4	632	477	0.04732	0.00111	0.0739	0.0098	89.017	2.302	72.0	1.9
CHJ36_5	350	251	0.05652	0.00191	0.0896	0.0223	86.992	2.312	72.8	1.9
CHJ36_6	595	384	0.04807	0.00130	0.0758	0.0118	88.568	2.404	72.3	2.0
CHJ36_7	330	138	0.04837	0.00140	0.0766	0.0144	88.651	2.261	72.2	1.8
CHJ36_8	527	458	0.04812	0.00125	0.0744	0.0136	88.644	2.435	72.3	2.0
CHJ36_9	352	198	0.04742	0.00131	0.0747	0.0128	89.067	2.432	72.0	2.0
CHJ36_10	419	217	0.04790	0.00127	0.0739	0.0121	89.822	2.302	71.3	1.8

Supplemental File 3

CHJ36_11	383	157	0.04913	0.00138	0.0764	0.0141	88.254	2.350	72.5	1.9
CHJ36_12	744	666	0.04739	0.00113	0.0730	0.0103	89.663	2.285	71.5	1.8
CHJ36_13	430	284	0.04720	0.00130	0.0731	0.0120	88.778	2.449	72.2	2.0
CHJ36_14	319	154	0.06428	0.00228	0.1028	0.0321	86.976	2.297	72.1	1.9
CHJ36_15	558	318	0.04728	0.00115	0.0764	0.0113	86.380	2.245	74.2	1.9
CHJ36_16	408	317	0.05006	0.00131	0.0783	0.0126	87.908	2.343	72.7	1.9
CHJ36_17	320	239	0.04717	0.00130	0.0745	0.0118	89.168	2.198	71.9	1.8
CHJ36_18	427	247	0.04917	0.00121	0.0778	0.0121	86.767	2.247	73.7	1.9
CHJ36_19	328	407	0.04821	0.00147	0.0729	0.0146	91.182	2.518	70.2	1.9
CHJ36_20	278	155	0.04789	0.00150	0.0761	0.0154	87.129	2.307	73.5	1.9
CHJ36_21	412	265	0.04836	0.00124	0.0737	0.0113	89.725	2.394	71.4	1.9
CHJ36_22	996	989	0.04728	0.00108	0.0741	0.0091	87.601	2.318	73.2	1.9
CHJ36_23	645	497	0.04786	0.00122	0.0750	0.0101	88.699	2.300	72.2	1.9
CHJ36_24	324	229	0.04914	0.00146	0.0755	0.0145	89.401	2.282	71.6	1.8
CHJ36_25	330	200	0.04757	0.00155	0.0733	0.0157	88.897	2.436	72.1	2.0
CHJ36_26	439	282	0.04854	0.00129	0.0735	0.0107	89.659	2.326	71.4	1.8
CHJ36_27	244	105	0.04849	0.00157	0.0784	0.0148	84.760	2.210	75.5	2.0
CHJ36_28	696	678	0.04790	0.00117	0.0742	0.0101	88.739	2.229	72.2	1.8
CHJ36_29	709	500	0.04708	0.00111	0.0741	0.0100	87.482	2.136	73.3	1.8
CHJ36_30	407	238	0.04862	0.00145	0.0749	0.0140	88.638	2.234	72.2	1.8
CHJ36_31	614	447	0.04834	0.00119	0.0745	0.0116	88.844	2.347	72.1	1.9
CHJ36_32	508	261	0.04854	0.00152	0.0795	0.0197	84.973	2.279	75.3	2.0
CHJ36_33	407	394	0.04777	0.00131	0.0737	0.0123	87.870	2.272	72.9	1.9
CHJ36_34	286	258	0.04907	0.00147	0.0757	0.0129	88.489	2.285	72.3	1.9
CHJ36_35	379	279	0.04801	0.00127	0.0757	0.0129	86.869	2.248	73.7	1.9
CHJ41_1	701	809	0.04776	0.00133	0.0482	0.0072	138.329	3.375	46.4	1.1
CHJ41_2	890	846	0.04790	0.00119	0.0475	0.0069	139.264	3.534	46.1	1.2
CHJ41_3	455	331	0.05332	0.00158	0.0552	0.0112	132.762	3.457	48.0	1.3
CHJ41_4	830	814	0.04736	0.00125	0.0482	0.0077	136.342	3.453	47.1	1.2
CHJ41_5	1088	1072	0.04708	0.00121	0.0473	0.0068	138.266	3.423	46.4	1.1
CHJ41_6	1253	1363	0.04837	0.00121	0.0481	0.0075	138.506	3.779	46.3	1.3
CHJ41_7	5313	14678	0.04680	0.00099	0.0475	0.0062	136.864	3.676	46.9	1.3
CHJ41_8	1244	1341	0.04708	0.00115	0.0479	0.0070	135.905	3.635	47.3	1.3
CHJ41_9	832	902	0.04727	0.00120	0.0488	0.0074	134.604	3.453	47.7	1.2
CHJ41_10	302	211	0.05039	0.00186	0.0519	0.0121	131.990	3.616	48.4	1.3
CHJ41_11	1103	946	0.04732	0.00121	0.0491	0.0079	134.182	3.690	47.8	1.3
CHJ41_12	595	378	0.04930	0.00132	0.0504	0.0084	134.913	3.603	47.5	1.3
CHJ41_13	409	330	0.04836	0.00151	0.0488	0.0098	137.546	3.776	46.6	1.3
CHJ41_14	675	546	0.04757	0.00121	0.0474	0.0073	138.274	3.601	46.4	1.2
CHJ41_15	946	647	0.04696	0.00116	0.0478	0.0066	136.647	3.459	47.0	1.2
CHJ41_16	459	337	0.04871	0.00143	0.0487	0.0092	137.736	3.532	46.5	1.2
CHJ41_17	534	378	0.04777	0.00137	0.0488	0.0088	136.225	3.538	47.1	1.2
CHJ41_18	907	756	0.04729	0.00120	0.0472	0.0075	138.667	3.557	46.3	1.2
CHJ41_19	1485	2110	0.04709	0.00109	0.0467	0.0065	138.604	3.689	46.3	1.2
CHJ41_20	604	435	0.04755	0.00133	0.0466	0.0085	139.566	3.603	46.0	1.2
CHJ41_21	548	629	0.04815	0.00132	0.0493	0.0089	135.956	3.547	47.2	1.2
CHJ41_22	859	793	0.04705	0.00125	0.0480	0.0071	136.424	3.365	47.1	1.2
CHJ41_23	1248	1834	0.04737	0.00111	0.0473	0.0064	139.377	3.858	46.1	1.3
CHJ41_24	794	693	0.04717	0.00123	0.0473	0.0064	136.139	3.483	47.2	1.2
CHJ41_25	865	723	0.04809	0.00127	0.0491	0.0077	135.054	3.424	47.5	1.2
CHJ41_26	773	737	0.04941	0.00127	0.0482	0.0082	141.221	3.733	45.3	1.2
CHJ41_27	514	327	0.04721	0.00126	0.0485	0.0080	136.414	3.533	47.1	1.2
CHJ41_28	715	856	0.04936	0.00135	0.0489	0.0077	139.067	3.682	46.0	1.2

Supplemental File 3

CHJ41_29	684	593	0.04790	0.00134	0.0476	0.0081	138.671	3.418	46.3	1.1
CHJ41_30	774	548	0.04728	0.00128	0.0475	0.0078	138.511	3.779	46.4	1.3
CHJ41_31	465	319	0.04602	0.00143	0.0473	0.0088	136.418	3.607	47.1	1.2
CHJ41_32	263	123	0.04840	0.00159	0.0754	0.0156	88.570	2.383	72.3	1.9
CHJ41_33	734	904	0.04805	0.00134	0.0479	0.0082	138.763	3.808	46.2	1.3
CHJ41_34	679	844	0.04856	0.00132	0.0480	0.0078	138.825	3.716	46.2	1.2
CHJ41_35	440	335	0.04944	0.00154	0.0519	0.0098	131.868	3.413	48.5	1.3
J378_1	731	201	0.05518	0.00280	0.0129	0.0051	592.113	18.208	10.8	0.3
J378_2	586	758	0.05343	0.00312	0.0126	0.0056	581.598	19.256	11.0	0.4
J378_3	217	168	0.06961	0.00640	0.0169	0.0141	562.447	19.248	11.1	0.4
J378_4	1971	459	0.04979	0.00177	0.0121	0.0035	576.020	17.886	11.1	0.3
J378_5	374	308	0.05822	0.00418	0.0140	0.0087	569.247	18.616	11.1	0.4
J378_6	515	361	0.05675	0.00298	0.0137	0.0058	568.300	17.531	11.2	0.3
J378_7	410	115	0.05791	0.00399	0.0141	0.0076	566.960	19.364	11.2	0.4
J378_8	316	660	0.05164	0.00407	0.0126	0.0071	566.365	19.496	11.3	0.4
J378_9	867	290	0.04828	0.00215	0.0118	0.0037	568.320	18.676	11.3	0.4
J378_10	914	390	0.05023	0.00200	0.0123	0.0038	563.275	18.404	11.4	0.4
J378_11	424	223	0.04937	0.00356	0.0121	0.0058	562.698	19.629	11.4	0.4
J378_12	320	91	0.06055	0.00443	0.0150	0.0089	554.482	19.075	11.4	0.4
J378_13	2530	502	0.04824	0.00139	0.0119	0.0026	562.805	17.053	11.4	0.3
J378_14	502	469	0.04582	0.00269	0.0112	0.0039	564.073	17.088	11.4	0.3
J378_15	219	82	0.05411	0.00596	0.0135	0.0110	557.302	18.432	11.4	0.4
J378_16	231	105	0.04762	0.00550	0.0118	0.0090	560.818	17.810	11.5	0.4
J378_17	884	196	0.05229	0.00211	0.0129	0.0039	557.272	17.731	11.5	0.4
J378_18	2610	812	0.04854	0.00130	0.0121	0.0026	553.036	18.084	11.6	0.4
J378_19	62	15	0.09426	0.01556	0.0255	0.0567	518.790	20.127	11.7	0.5
J378_20	317	183	0.06086	0.00436	0.0155	0.0094	542.130	18.708	11.7	0.4
J378_21	221	145	0.06436	0.00595	0.0162	0.0121	538.886	20.152	11.7	0.4
J378_22	166	107	0.06903	0.00682	0.0181	0.0177	535.501	18.265	11.7	0.4
J378_23	646	458	0.04802	0.00278	0.0122	0.0050	548.938	18.313	11.7	0.4
J378_24	661	747	0.05117	0.00257	0.0129	0.0047	545.746	19.359	11.7	0.4
J378_25	363	532	0.05721	0.00350	0.0148	0.0074	539.528	17.276	11.8	0.4
J378_26	386	172	0.05363	0.00350	0.0137	0.0067	541.758	18.566	11.8	0.4
J378_27	790	900	0.05731	0.00257	0.0147	0.0047	538.249	16.720	11.8	0.4
J378_28	367	126	0.05080	0.00329	0.0132	0.0064	542.511	16.454	11.8	0.4
J378_29	539	778	0.05357	0.00263	0.0138	0.0053	539.175	16.948	11.8	0.4
J378_30	858	243	0.06784	0.00448	0.0179	0.0123	526.581	16.432	11.9	0.4
J378_31	736	280	0.04843	0.00196	0.0125	0.0039	535.442	18.548	12.0	0.4
J378_32	947	297	0.05065	0.00180	0.0133	0.0037	530.078	16.388	12.1	0.4
J378_33	482	199	0.05161	0.00275	0.0136	0.0054	525.458	17.760	12.2	0.4
J378_34	194	114	0.04831	0.00557	0.0131	0.0101	508.326	16.586	12.6	0.4
J378_35	409	345	0.05222	0.00352	0.0144	0.0069	498.492	16.714	12.8	0.4
J378_36	242	66	0.05108	0.00457	0.0140	0.0087	497.091	18.236	12.9	0.5
J378_37	78	38	0.15303	0.01216	0.0539	0.0884	385.215	14.102	14.5	0.6
J378_38	881	95	0.05266	0.00109	0.3950	0.0797	18.405	0.610	341.3	11.1
J378_39	1229	166	0.05239	0.00108	0.3933	0.0773	18.373	0.593	342.0	10.9
J378_40	914	101	0.05270	0.00109	0.4006	0.0952	18.152	0.670	346.0	12.6
J378_41	316	12	0.05990	0.00126	0.8116	0.1822	10.175	0.339	604.4	19.7
J378_42	319	13	0.05933	0.00124	0.8102	0.1991	10.121	0.349	608.0	20.4
J378_43	314	13	0.05961	0.00126	0.8111	0.1930	10.081	0.359	610.1	21.2
J417_1	191	163	0.05645	0.00260	0.0256	0.0086	303.122	8.065	21.0	0.6
J417_2	99	47	0.06482	0.00538	0.0290	0.0212	307.899	8.120	20.4	0.6

Supplemental File 3

J417_3	71	54	0.06841	0.00697	0.0306	0.0296	307.859	8.828	20.3	0.6
J417_4	87	52	0.06163	0.00581	0.0278	0.0219	306.047	8.456	20.6	0.6
J417_5	203	141	0.05563	0.00327	0.0255	0.0108	298.663	7.945	21.3	0.6
J417_6	1475	979	0.04753	0.00121	0.0202	0.0027	322.376	7.835	19.9	0.5
J417_7	237	228	0.05249	0.00243	0.0230	0.0068	313.153	8.459	20.4	0.6
J417_8	92	89	0.06692	0.00557	0.0302	0.0218	299.754	9.173	20.9	0.7
J417_9	240	135	0.05350	0.00298	0.0258	0.0106	284.222	8.106	22.4	0.6
J417_10	472	450	0.05156	0.00199	0.0222	0.0059	320.069	8.212	20.0	0.5
J417_11	1021	1032	0.04769	0.00142	0.0207	0.0038	317.105	8.386	20.3	0.5
J417_12	375	328	0.04917	0.00195	0.0210	0.0057	323.352	8.410	19.8	0.5
J417_13	3034	427	0.04728	0.00108	0.0215	0.0027	301.536	7.466	21.3	0.5
J417_14	64	28	0.07376	0.00720	0.0340	0.0330	298.218	8.958	20.8	0.7
J417_15	490	594	0.04954	0.00162	0.0220	0.0048	307.457	8.121	20.9	0.6
J417_16	119	72	0.06971	0.00514	0.0305	0.0228	321.065	9.508	19.5	0.6
J417_17	1555	1287	0.04830	0.00116	0.0214	0.0029	309.932	8.201	20.7	0.5
J417_18	116	92	0.06805	0.00470	0.0301	0.0207	315.777	8.928	19.8	0.6
J417_19	180	41	0.06392	0.00534	0.0286	0.0213	305.194	13.481	20.6	0.9
J417_20	197	157	0.05905	0.00315	0.0261	0.0102	307.768	8.901	20.6	0.6
J417_21	88	70	0.07442	0.00521	0.0331	0.0243	312.217	9.363	19.9	0.6
J417_22	81	56	0.07694	0.00632	0.0338	0.0290	311.112	8.428	19.9	0.6
J417_23	288	142	0.05355	0.00238	0.0231	0.0071	318.722	8.574	20.0	0.5
J417_24	85	54	0.07232	0.00595	0.0316	0.0252	314.871	9.415	19.8	0.6
J417_25	89	70	0.07361	0.00590	0.0339	0.0271	297.861	8.644	20.9	0.6
J417_26	86	53	0.07320	0.00584	0.0327	0.0260	306.794	8.921	20.3	0.6
J417_27	158	146	0.06313	0.00421	0.0273	0.0154	318.421	9.322	19.8	0.6
J417_28	278	197	0.05702	0.00261	0.0245	0.0077	320.188	8.670	19.8	0.5
J417_29	129	87	0.06710	0.00360	0.0306	0.0153	302.229	8.530	20.7	0.6
J417_30	397	395	0.05888	0.00232	0.0255	0.0078	317.758	8.156	19.9	0.5
J417_31	61	41	0.08376	0.00826	0.0373	0.0399	304.319	9.494	20.1	0.7
J417_32	669	302	0.04938	0.00150	0.0232	0.0049	292.786	9.597	21.9	0.7
J417_33	260	104	0.05625	0.00269	0.0245	0.0089	315.970	8.589	20.1	0.6
J417_34	173	74	0.06176	0.00284	0.0295	0.0121	291.290	8.483	21.7	0.6
J417_35	90	54	0.07500	0.00529	0.0330	0.0253	315.829	9.022	19.6	0.6
J417_36	111	91	0.06586	0.00507	0.0290	0.0194	310.850	9.476	20.2	0.6
J417_37	116	81	0.07093	0.00500	0.0313	0.0223	314.810	8.795	19.8	0.6
J417_38	88	71	0.09549	0.00769	0.0458	0.0463	284.490	12.408	21.2	1.0
J417_39	300	448	0.05514	0.00199	0.0237	0.0059	319.345	9.094	19.9	0.6
J417_40	104	58	0.06832	0.00438	0.0307	0.0185	307.776	8.219	20.3	0.6
J417_41	473	52	0.05846	0.00122	0.4458	0.0858	18.086	0.559	344.7	10.5
J417_42	805	118	0.05307	0.00109	0.3997	0.0615	18.309	0.524	342.9	9.7
J417_43	819	120	0.05320	0.00109	0.4020	0.0724	18.242	0.578	344.1	10.7
J417_44	204	8	0.06040	0.00125	0.8201	0.1448	10.156	0.288	605.1	16.7
J417_45	205	8	0.06008	0.00126	0.8123	0.1327	10.161	0.293	605.1	17.0
J417_46	205	8	0.05985	0.00124	0.8141	0.1572	10.136	0.310	606.7	18.1
J473_1	318	12	0.05958	0.00124	0.8114	0.1741	10.160	0.323	605.5	18.8
J473_2	320	13	0.05922	0.00124	0.8026	0.1732	10.191	0.337	604.0	19.5
J473_3	146	95	0.05741	0.00508	0.0244	0.0169	324.443	10.033	19.6	0.6
J473_4	139	102	0.05838	0.00618	0.0243	0.0196	326.981	10.365	19.4	0.6
J473_5	722	1385	0.05690	0.00233	0.0244	0.0079	319.376	10.269	19.9	0.6
J473_6	156	118	0.06261	0.00575	0.0257	0.0194	332.590	11.549	19.0	0.7
J473_7	147	111	0.05857	0.00567	0.0244	0.0195	333.955	10.823	19.0	0.6
J473_8	116	59	0.05821	0.00682	0.0244	0.0224	328.248	10.771	19.3	0.7
J473_9	235	173	0.05320	0.00391	0.0223	0.0112	325.868	10.346	19.6	0.6

Supplemental File 3

J473_10	83	73	0.05745	0.00855	0.0252	0.0312	319.340	11.212	19.9	0.7
J473_11	291	241	0.05114	0.00287	0.0215	0.0088	330.833	9.942	19.3	0.6
J473_12	134	81	0.06109	0.00612	0.0256	0.0209	327.259	10.549	19.3	0.6
J473_13	254	169	0.04783	0.00325	0.0199	0.0082	328.727	9.905	19.5	0.6
J473_14	175	134	0.04368	0.00395	0.0183	0.0097	326.773	9.598	19.8	0.6
J473_15	361	390	0.04663	0.00280	0.0195	0.0078	329.975	9.944	19.5	0.6
J473_16	133	109	0.09162	0.00670	0.0408	0.0417	311.427	10.569	19.5	0.7
J473_17	165	124	0.05279	0.00431	0.0223	0.0128	324.405	9.888	19.7	0.6
J473_18	182	126	0.05256	0.00420	0.0223	0.0119	317.567	9.577	20.1	0.6
J473_19	134	89	0.06840	0.00608	0.0295	0.0254	318.945	10.875	19.6	0.7
J473_20	129	97	0.06878	0.00596	0.0289	0.0225	325.130	11.298	19.2	0.7
J473_21	86	55	0.06779	0.00769	0.0299	0.0332	315.459	11.205	19.9	0.7
J473_22	147	109	0.06587	0.00555	0.0281	0.0206	320.847	10.217	19.6	0.6
J473_23	187	129	0.06337	0.00433	0.0272	0.0155	318.216	11.325	19.8	0.7
J473_24	276	213	0.05574	0.00341	0.0240	0.0111	321.038	9.309	19.8	0.6
J473_25	196	139	0.06238	0.00481	0.0261	0.0168	328.383	10.180	19.2	0.6
J473_26	903	1745	0.05007	0.00173	0.0214	0.0053	321.232	9.777	19.9	0.6
J473_27	136	78	0.06162	0.00573	0.0266	0.0218	323.073	11.187	19.5	0.7
J473_28	230	129	0.05781	0.00370	0.0248	0.0131	320.475	12.237	19.8	0.8
J473_29	164	103	0.05721	0.00514	0.0244	0.0169	322.087	10.224	19.7	0.6
J473_30	143	88	0.08397	0.00889	0.0374	0.0490	308.118	10.676	19.9	0.7
J473_31	94	43	0.06955	0.01231	0.0322	0.0610	304.951	17.747	20.5	1.2
J473_32	195	216	0.05534	0.00422	0.0239	0.0127	314.714	10.433	20.2	0.7
J473_33	216	167	0.05607	0.00356	0.0247	0.0120	313.510	10.026	20.3	0.7
J473_34	41	19	0.09094	0.01812	0.0416	0.1039	304.429	12.724	20.0	1.0
J473_35	187	152	0.05813	0.00462	0.0251	0.0180	325.833	9.904	19.5	0.6
J473_36	576	1027	0.04703	0.00195	0.0196	0.0052	332.139	9.699	19.4	0.6
J473_37	96	81	0.13796	0.01276	0.0696	0.1251	272.890	10.134	20.8	0.9
J473_38	197	139	0.04695	0.00369	0.0197	0.0105	329.469	9.783	19.5	0.6
J473_39	134	100	0.04419	0.00486	0.0199	0.0130	305.431	10.811	21.1	0.8
J473_40	129	94	0.04733	0.00603	0.0202	0.0155	315.830	10.996	20.4	0.7
J473_41	223	177	0.04489	0.00368	0.0196	0.0096	315.302	9.418	20.5	0.6
J473_42	136	89	0.04320	0.00650	0.0182	0.0158	328.569	11.546	19.7	0.7
J473_43	164	136	0.05010	0.00475	0.0208	0.0146	329.146	11.071	19.5	0.7
J473_44	151	99	0.04487	0.00436	0.0191	0.0115	321.940	10.528	20.0	0.7
J473_45	217	163	0.04553	0.00342	0.0192	0.0096	327.478	11.437	19.7	0.7
J473_46	208	163	0.04436	0.00382	0.0183	0.0091	333.065	11.012	19.4	0.6
J473_47	268	180	0.04596	0.00321	0.0192	0.0085	332.070	11.191	19.4	0.7
J473_48	183	160	0.04782	0.00393	0.0198	0.0104	333.598	9.644	19.3	0.6
J473_49	201	189	0.04397	0.00423	0.0184	0.0103	327.462	10.127	19.7	0.6
J473_50	154	76	0.04684	0.00507	0.0195	0.0131	332.572	11.231	19.3	0.7
J473_51	264	282	0.04687	0.00340	0.0197	0.0091	328.333	10.189	19.6	0.6
J473_52	206	150	0.04855	0.00339	0.0206	0.0095	326.058	10.855	19.7	0.7
J473_53	319	13	0.06036	0.00126	0.8260	0.2239	10.102	0.377	608.3	22.1
J473_54	318	13	0.05978	0.00126	0.8231	0.1995	10.041	0.346	612.4	20.6
Standards										
GJ1_1	300	10	0.06033	0.00023	0.7899	0.0082	10.497	0.100	586.0	5.5
GJ1_2	4	1	0.06105	0.07191	0.8238	0.0092	10.146	0.108	605.2	55.1
GJ1_3	304	11	0.06042	0.00022	0.8031	0.0101	10.455	0.130	588.3	7.1
GJ1_4	296	10	0.06066	0.00035	0.8313	0.0111	10.168	0.124	604.2	7.2
GJ1_5	293	10	0.06025	0.00038	0.8259	0.0132	10.147	0.149	605.8	8.7
GJ1_6	294	11	0.06028	0.00021	0.8126	0.0145	10.316	0.181	596.1	10.2
GJ1_7	295	10	0.06037	0.00038	0.8225	0.0137	10.139	0.165	606.1	9.6

Supplemental File 3

GJ1_8	292	10	0.06052	0.00042	0.8347	0.0158	10.190	0.177	603.1	10.2
GJ1_9	287	10	0.06000	0.00039	0.8112	0.0125	10.171	0.137	604.6	7.9
GJ1_10	298	10	0.06020	0.00022	0.7969	0.0129	10.405	0.166	591.2	9.2
GJ1_11	300	10	0.06004	0.00037	0.8240	0.0128	10.031	0.156	612.7	9.3
GJ1_12	293	10	0.06021	0.00041	0.8166	0.0153	10.104	0.170	608.3	10.0
GJ1_13	297	10	0.05987	0.00039	0.8081	0.0134	10.278	0.177	598.5	10.1
GJ1_14	285	10	0.06001	0.00039	0.8102	0.0114	10.124	0.122	607.3	7.2
GJ1_15	301	10	0.06020	0.00024	0.7977	0.0134	10.408	0.166	591.0	9.2
GJ1_16	294	10	0.06008	0.00036	0.8201	0.0149	10.137	0.158	606.5	9.2
GJ1_17	292	10	0.06104	0.00039	0.8348	0.0130	10.151	0.133	604.9	7.7
GJ1_18	298	10	0.05991	0.00039	0.8119	0.0158	10.228	0.176	601.4	10.1
GJ1_19	279	10	0.06003	0.00033	0.8225	0.0128	10.043	0.157	612.1	9.3
GJ1_20	303	10	0.05998	0.00022	0.7925	0.0114	10.487	0.141	586.8	7.7
GJ1_21	282	10	0.06001	0.00045	0.8206	0.0141	10.125	0.166	607.3	9.7
GJ1_22	279	9	0.06065	0.00034	0.8323	0.0150	10.209	0.176	601.9	10.1
GJ1_23	290	10	0.06048	0.00039	0.8298	0.0145	10.168	0.154	604.4	8.9
GJ1_24	299	11	0.06006	0.00024	0.8059	0.0146	10.325	0.184	595.7	10.3
GJ1_25	301	11	0.05998	0.00024	0.8005	0.0123	10.403	0.157	591.4	8.7
GJ1_26	337	12	0.05974	0.00023	0.7874	0.0099	10.579	0.117	582.0	6.3
GJ1_27	5	1	0.05998	0.11402	0.7982	0.0082	10.324	0.100	595.8	85.6
GJ1_28	317	11	0.05996	0.00022	0.7944	0.0111	10.459	0.142	588.3	7.8
GJ1_29	294	10	0.06044	0.00040	0.8204	0.0121	10.199	0.156	602.6	9.0
GJ1_30	291	10	0.05979	0.00034	0.8181	0.0116	10.134	0.140	606.9	8.2
GJ1_31	296	11	0.05947	0.00022	0.7977	0.0142	10.314	0.182	596.8	10.3
GJ1_32	290	10	0.05992	0.00042	0.8053	0.0150	10.264	0.164	599.3	9.3
GJ1_33	288	10	0.05945	0.00041	0.8153	0.0145	10.194	0.167	603.7	9.6
GJ1_34	296	10	0.05974	0.00021	0.7828	0.0129	10.584	0.169	581.7	9.1
GJ1_35	5	0	0.05921	-0.06307	0.7937	0.0098	10.334	0.106	595.9	47.6
GJ1_36	309	11	0.05950	0.00021	0.7894	0.0105	10.407	0.131	591.6	7.3
GJ1_37	292	10	0.05954	0.00038	0.8065	0.0138	10.254	0.178	600.2	10.2
GJ1_38	285	10	0.05926	0.00040	0.7977	0.0121	10.229	0.144	601.8	8.3
GJ1_39	288	10	0.05962	0.00024	0.7948	0.0170	10.267	0.210	599.4	12.0
GJ1_40	295	10	0.05968	0.00042	0.7984	0.0168	10.410	0.181	591.3	10.0
GJ1_41	288	10	0.05991	0.00035	0.8100	0.0135	10.220	0.164	601.8	9.4
GJ1_42	296	11	0.05984	0.00019	0.7940	0.0114	10.354	0.146	594.3	8.2
GJ1_43	5	0	0.05879	0.08193	0.7888	0.0087	10.304	0.101	597.9	61.7
GJ1_44	302	11	0.05963	0.00025	0.7947	0.0120	10.358	0.141	594.2	7.9
GJ1_45	296	10	0.05923	0.00047	0.8011	0.0130	10.237	0.150	601.4	8.6
GJ1_46	282	10	0.05942	0.00032	0.7932	0.0106	10.294	0.129	597.9	7.3
GJ1_47	289	10	0.06008	0.00022	0.7994	0.0149	10.257	0.191	599.6	10.9
GJ1_48	294	10	0.05911	0.00039	0.7890	0.0131	10.329	0.153	596.2	8.6
GJ1_49	288	10	0.05942	0.00045	0.7955	0.0131	10.281	0.161	598.7	9.1
GJ1_50	300	11	0.05980	0.00021	0.8086	0.0161	10.147	0.198	606.1	11.6
GJ1_51	5	1	0.06005	-0.02652	0.8085	0.0123	10.272	0.132	598.7	21.3
GJ1_52	311	11	0.05980	0.00020	0.7845	0.0119	10.480	0.158	587.3	8.6
GJ1_53	298	11	0.05959	0.00042	0.8044	0.0112	10.194	0.136	603.6	7.8
GJ1_54	291	10	0.05964	0.00041	0.8004	0.0129	10.311	0.153	596.8	8.6
GJ1_55	291	10	0.06000	0.00024	0.7975	0.0136	10.301	0.169	597.2	9.6
GJ1_56	295	10	0.05953	0.00039	0.7981	0.0153	10.253	0.195	600.2	11.1
GJ1_57	286	10	0.05915	0.00038	0.7962	0.0148	10.252	0.169	600.6	9.7
GJ1_58	304	11	0.06003	0.00018	0.8037	0.0123	10.309	0.153	596.7	8.6
GJ1_59	308	11	0.06001	0.00022	0.7909	0.0121	10.425	0.158	590.2	8.7
GJ1_60	294	10	0.05958	0.00040	0.7979	0.0134	10.205	0.148	602.9	8.5
GJ1_61	292	9	0.05998	0.00045	0.8103	0.0134	10.143	0.160	606.2	9.3

Supplemental File 3

GJ1_62	292	10	0.05988	0.00022	0.8024	0.0149	10.260	0.186	599.5	10.6
GJ1_63	292	10	0.05981	0.00040	0.8044	0.0152	10.261	0.178	599.6	10.2
GJ1_64	292	10	0.05984	0.00044	0.8019	0.0157	10.221	0.176	601.8	10.1
GJ1_65	296	11	0.06029	0.00024	0.8065	0.0135	10.336	0.166	594.9	9.3
GJ1_66	285	9	0.05961	0.00035	0.8060	0.0112	10.208	0.129	602.8	7.4
GJ1_67	302	11	0.06001	0.00021	0.7911	0.0119	10.399	0.153	591.7	8.5
GJ1_68	289	10	0.05946	0.00042	0.8023	0.0145	10.185	0.173	604.2	10.0
GJ1_69	284	9	0.05913	0.00046	0.7922	0.0123	10.273	0.145	599.4	8.3
GJ1_70	293	11	0.06016	0.00021	0.8125	0.0135	10.220	0.162	601.6	9.3
GJ1_71	284	10	0.05905	0.00040	0.7973	0.0145	10.217	0.161	602.6	9.3
GJ1_72	295	11	0.06001	0.00025	0.8075	0.0144	10.278	0.179	598.4	10.2
GJ1_73	286	9	0.05965	0.00040	0.8073	0.0117	10.295	0.131	597.8	7.4
GJ1_74	298	11	0.06006	0.00024	0.7954	0.0117	10.402	0.154	591.4	8.6
GJ1_75	303	10	0.05951	0.00038	0.8003	0.0121	10.183	0.146	604.2	8.5
GJ1_76	287	9	0.05918	0.00041	0.7943	0.0145	10.205	0.169	603.2	9.7
GJ1_77	297	11	0.06026	0.00023	0.8137	0.0124	10.249	0.156	599.9	8.9
GJ1_78	285	10	0.05937	0.00038	0.8099	0.0157	10.118	0.188	608.1	11.0
GJ1_79	291	10	0.05994	0.00033	0.8158	0.0111	10.140	0.118	606.4	6.9
GJ1_80	295	10	0.05987	0.00021	0.7918	0.0124	10.407	0.156	591.3	8.7
GJ1_81	297	10	0.05966	0.00036	0.8054	0.0124	10.210	0.144	602.6	8.3
GJ1_82	288	9	0.06014	0.00040	0.8166	0.0140	10.146	0.163	605.9	9.5
GJ1_83	296	11	0.06008	0.00022	0.8133	0.0139	10.231	0.171	601.0	9.8
GJ1_84	297	10	0.05995	0.00046	0.8029	0.0143	10.206	0.185	602.6	10.6
GJ1_85	5	0	0.06002	0.06852	0.8091	0.0119	10.239	0.135	600.6	52.3
Plesovice_1	741	68	0.05303	0.00017	0.3863	0.0038	18.929	0.175	331.9	3.0
Plesovice_2	13	1	0.05361	-0.05950	0.3980	0.0053	18.503	0.211	339.1	25.7
Plesovice_3	711	67	0.05329	0.00020	0.3969	0.0052	18.659	0.227	336.5	4.0
Plesovice_4	714	70	0.05379	0.00032	0.4046	0.0064	18.562	0.260	338.0	4.7
Plesovice_5	709	69	0.05289	0.00032	0.4018	0.0045	18.186	0.166	345.3	3.1
Plesovice_6	752	76	0.05303	0.00022	0.4003	0.0073	18.390	0.326	341.5	6.0
Plesovice_7	751	74	0.05331	0.00031	0.3990	0.0066	18.524	0.293	338.9	5.3
Plesovice_8	768	76	0.05303	0.00033	0.4058	0.0065	18.304	0.287	343.0	5.3
Plesovice_9	927	102	0.05322	0.00024	0.3996	0.0106	18.438	0.478	340.5	8.7
Plesovice_10	717	70	0.05269	0.00032	0.3967	0.0058	18.279	0.242	343.6	4.5
Plesovice_11	664	61	0.05324	0.00018	0.3976	0.0068	18.446	0.312	340.3	5.7
Plesovice_12	760	75	0.05295	0.00028	0.3975	0.0064	18.414	0.298	341.0	5.4
Plesovice_13	654	64	0.05298	0.00031	0.3948	0.0061	18.529	0.276	339.0	5.0
Plesovice_14	758	74	0.05271	0.00027	0.3944	0.0063	18.435	0.287	340.8	5.2
Plesovice_15	702	67	0.05269	0.00029	0.3946	0.0059	18.369	0.268	342.0	4.9
Plesovice_16	682	64	0.05335	0.00019	0.3990	0.0063	18.495	0.294	339.4	5.3
Plesovice_17	749	74	0.05282	0.00031	0.3976	0.0060	18.421	0.256	341.0	4.7
Plesovice_18	689	67	0.05330	0.00032	0.3990	0.0063	18.522	0.273	339.0	4.9
Plesovice_19	753	73	0.05285	0.00032	0.3983	0.0065	18.507	0.296	339.4	5.3
Plesovice_20	705	69	0.05235	0.00025	0.3919	0.0054	18.356	0.236	342.4	4.3
Plesovice_21	705	66	0.05324	0.00018	0.3978	0.0072	18.512	0.326	339.1	5.9
Plesovice_22	717	70	0.05285	0.00031	0.3985	0.0066	18.436	0.283	340.7	5.1
Plesovice_23	695	68	0.05356	0.00034	0.4069	0.0069	18.455	0.304	340.0	5.5
Plesovice_24	742	72	0.05310	0.00032	0.3963	0.0070	18.466	0.326	340.0	5.9
Plesovice_25	667	63	0.05329	0.00018	0.3979	0.0063	18.559	0.289	338.3	5.2
Plesovice_26	675	68	0.05319	0.00018	0.4007	0.0074	18.435	0.321	340.6	5.8
Plesovice_27	764	67	0.05281	0.00019	0.3873	0.0037	19.041	0.175	330.1	3.0
Plesovice_28	13	1	0.05251	0.01206	0.3877	0.0050	18.691	0.221	336.3	6.4
Plesovice_29	707	67	0.05282	0.00017	0.3937	0.0053	18.581	0.243	338.1	4.4

Supplemental File 3

Plesovice_30	700	68	0.05283	0.00032	0.3977	0.0054	18.444	0.243	340.6	4.4
Plesovice_31	693	67	0.05251	0.00032	0.3911	0.0057	18.553	0.253	338.7	4.5
Plesovice_32	761	78	0.05274	0.00017	0.3979	0.0071	18.313	0.314	343.0	5.8
Plesovice_33	752	77	0.05569	0.00032	0.4175	0.0084	18.451	0.332	339.2	6.0
Plesovice_34	768	77	0.05261	0.00026	0.3967	0.0076	18.435	0.331	340.8	6.0
Plesovice_35	668	66	0.05281	0.00030	0.4010	0.0107	18.224	0.491	344.6	9.1
Plesovice_36	649	61	0.05290	0.00018	0.3900	0.0063	18.801	0.292	334.2	5.1
Plesovice_37	12	1	0.05230	-0.01118	0.3878	0.0045	18.603	0.194	337.9	5.9
Plesovice_38	673	63	0.05294	0.00021	0.3922	0.0053	18.629	0.238	337.2	4.2
Plesovice_39	698	69	0.05236	0.00032	0.3911	0.0057	18.456	0.267	340.5	4.9
Plesovice_40	668	65	0.05234	0.00035	0.3858	0.0056	18.681	0.231	336.5	4.1
Plesovice_41	750	77	0.05298	0.00021	0.3948	0.0065	18.348	0.297	342.3	5.4
Plesovice_42	747	74	0.05351	0.00031	0.4002	0.0069	18.511	0.325	339.0	5.9
Plesovice_43	766	76	0.05223	0.00028	0.3919	0.0070	18.340	0.312	342.7	5.7
Plesovice_44	535	49	0.05324	0.00038	0.3978	0.0122	18.500	0.547	339.4	9.9
Plesovice_45	681	66	0.05320	0.00019	0.3962	0.0070	18.442	0.310	340.4	5.6
Plesovice_46	12	1	0.05219	-0.06409	0.3859	0.0056	18.772	0.236	335.0	27.3
Plesovice_47	661	63	0.05275	0.00018	0.3921	0.0055	18.530	0.249	339.0	4.5
Plesovice_48	725	71	0.05250	0.00035	0.3899	0.0062	18.509	0.269	339.5	4.9
Plesovice_49	674	64	0.05271	0.00032	0.3904	0.0060	18.648	0.261	336.9	4.6
Plesovice_50	726	72	0.05320	0.00019	0.3973	0.0061	18.286	0.280	343.3	5.2
Plesovice_51	756	75	0.05206	0.00032	0.3898	0.0067	18.507	0.310	339.7	5.6
Plesovice_52	751	75	0.05212	0.00032	0.3872	0.0063	18.569	0.287	338.6	5.2
Plesovice_53	530	48	0.05328	0.00034	0.4008	0.0117	18.369	0.534	341.7	9.8
Plesovice_54	694	67	0.05339	0.00017	0.4031	0.0065	18.185	0.284	345.1	5.3
Plesovice_55	17	2	0.05245	-0.09346	0.3892	0.0058	18.653	0.235	337.0	39.8
Plesovice_56	713	68	0.05304	0.00019	0.3905	0.0067	18.696	0.311	336.0	5.5
Plesovice_57	731	73	0.05284	0.00030	0.3936	0.0058	18.424	0.285	340.9	5.2
Plesovice_58	682	66	0.05265	0.00031	0.3904	0.0059	18.497	0.255	339.7	4.6
Plesovice_59	703	70	0.05340	0.00019	0.4000	0.0072	18.217	0.336	344.5	6.3
Plesovice_60	731	72	0.05209	0.00034	0.3888	0.0068	18.625	0.297	337.6	5.3
Plesovice_61	752	76	0.05218	0.00030	0.3865	0.0074	18.440	0.327	340.9	5.9
Plesovice_62	661	62	0.05314	0.00018	0.4017	0.0067	18.257	0.306	343.8	5.7
Plesovice_63	12	1	0.05293	-0.04147	0.3979	0.0049	18.619	0.197	337.4	17.9
Plesovice_64	678	63	0.05326	0.00021	0.3922	0.0060	18.655	0.284	336.6	5.0
Plesovice_65	753	75	0.05241	0.00033	0.3920	0.0059	18.338	0.299	342.7	5.5
Plesovice_66	689	66	0.05266	0.00038	0.3927	0.0065	18.515	0.279	339.3	5.0
Plesovice_67	695	68	0.05306	0.00018	0.4005	0.0074	18.239	0.321	344.2	6.0
Plesovice_68	730	72	0.05251	0.00031	0.3940	0.0065	18.323	0.275	342.9	5.1
Plesovice_69	756	75	0.05252	0.00031	0.3900	0.0071	18.506	0.314	339.6	5.7
Plesovice_70	670	66	0.05350	0.00019	0.4005	0.0070	18.473	0.320	339.7	5.8
Plesovice_71	714	68	0.05252	0.00032	0.3914	0.0058	18.521	0.261	339.3	4.7
Plesovice_72	679	64	0.05306	0.00018	0.3937	0.0050	18.529	0.231	338.9	4.2
Plesovice_73	753	74	0.05218	0.00033	0.3907	0.0066	18.224	0.287	344.9	5.3
Plesovice_74	667	64	0.05240	0.00029	0.3880	0.0061	18.478	0.240	340.1	4.3
Plesovice_75	705	69	0.05313	0.00018	0.4005	0.0068	18.275	0.307	343.5	5.7
Plesovice_76	729	72	0.05236	0.00030	0.3900	0.0064	18.427	0.300	341.1	5.5
Plesovice_77	655	63	0.05362	0.00019	0.4053	0.0061	18.309	0.264	342.7	4.9
Plesovice_78	698	67	0.05272	0.00034	0.3953	0.0063	18.352	0.249	342.3	4.6
Plesovice_79	691	67	0.05321	0.00018	0.3949	0.0055	18.545	0.253	338.6	4.5
Plesovice_80	752	74	0.05270	0.00029	0.3928	0.0058	18.356	0.263	342.2	4.8
Plesovice_81	650	62	0.05264	0.00035	0.3920	0.0072	18.429	0.296	340.9	5.4
Plesovice_82	726	74	0.05339	0.00017	0.4067	0.0062	18.188	0.264	345.0	4.9
Plesovice_83	727	72	0.05421	0.00035	0.4074	0.0085	18.359	0.373	341.5	6.8

Plesovice_84	667	63	0.05267	0.00034	0.3976	0.0055	18.376	0.249	341.9	4.6
Plesovice_85	681	65	0.05337	0.00016	0.4012	0.0069	18.315	0.303	342.7	5.6
Plesovice_86	756	75	0.05265	0.00030	0.3957	0.0059	18.345	0.236	342.4	4.3
Plesovice_87	676	66	0.05269	0.00030	0.3944	0.0069	18.370	0.311	342.0	5.7
Plesovice_88	711	70	0.05391	0.00024	0.4126	0.0077	18.055	0.335	347.3	6.3
Plesovice_89	738	72	0.06709	0.00100	0.5143	0.0133	18.077	0.354	341.1	6.6
SL1_1	632	134	0.05870	0.00024	0.7465	0.0124	10.887	0.168	566.7	8.6
SL1_2	664	142	0.05827	0.00028	0.7465	0.0227	10.908	0.298	566.0	15.1
SL1_3	415	89	0.05902	0.00030	0.7493	0.0126	10.853	0.172	568.2	8.8
SL1_4	613	131	0.05834	0.00028	0.7353	0.0201	10.913	0.297	565.6	15.0
SL1_5	615	132	0.05869	0.00033	0.7530	0.0234	10.765	0.328	572.9	17.0
SL1_6	604	132	0.05815	0.00028	0.7440	0.0239	10.810	0.333	571.0	17.1
SL1_7	413	89	0.05868	0.00028	0.7444	0.0150	10.869	0.217	567.6	11.1
SL1_8	616	134	0.05843	0.00030	0.7344	0.0132	10.999	0.203	561.2	10.1
SL1_9	625	134	0.05799	0.00028	0.7407	0.0200	10.826	0.283	570.3	14.5
SL1_10	425	91	0.05910	0.00027	0.7447	0.0127	10.931	0.180	564.2	9.1
SL1_11	604	129	0.05806	0.00027	0.7265	0.0171	10.986	0.260	562.2	13.0
SL1_12	616	137	0.05839	0.00027	0.7308	0.0135	11.048	0.195	558.8	9.6
SL1_13	653	139	0.05794	0.00031	0.7371	0.0204	10.867	0.295	568.2	15.0
SL1_14	411	89	0.05908	0.00029	0.7431	0.0133	10.995	0.183	561.0	9.1
SL1_15	647	138	0.05813	0.00022	0.7311	0.0156	10.937	0.234	564.6	11.8
SL1_16	612	135	0.05812	0.00033	0.7326	0.0159	10.965	0.232	563.1	11.6
SL1_17	609	130	0.05790	0.00028	0.7293	0.0217	10.913	0.329	565.9	16.7
SL1_18	419	90	0.05886	0.00022	0.7358	0.0118	11.024	0.165	559.7	8.2
SL1_19	624	133	0.05821	0.00025	0.7419	0.0193	10.800	0.278	571.5	14.4
SL1_20	603	132	0.05812	0.00024	0.7405	0.0162	10.869	0.223	568.0	11.4
SL1_21	637	139	0.05804	0.00029	0.7362	0.0200	10.905	0.284	566.2	14.4
SL1_22	432	92	0.05892	0.00033	0.7399	0.0147	10.970	0.211	562.3	10.6
SL1_23	615	131	0.05825	0.00024	0.7392	0.0185	10.856	0.266	568.6	13.6
SL1_24	621	137	0.05822	0.00026	0.7442	0.0165	10.828	0.235	570.0	12.1
SL1_25	668	144	0.05818	0.00025	0.7505	0.0237	10.718	0.335	575.8	17.6
SL1_26	421	90	0.05902	0.00027	0.7383	0.0142	11.021	0.201	559.8	10.0
SL1_27	610	130	0.05795	0.00023	0.7380	0.0208	10.843	0.296	569.5	15.2
SL1_28	606	131	0.05829	0.00027	0.7474	0.0152	10.779	0.213	572.5	11.1
SL1_29	650	140	0.05818	0.00030	0.7473	0.0217	10.803	0.295	571.4	15.2
SL1_30	425	91	0.05902	0.00024	0.7393	0.0126	11.007	0.178	560.4	8.8
SL1_31	595	128	0.05811	0.00025	0.7340	0.0191	10.939	0.276	564.5	13.9
SL1_32	618	132	0.05846	0.00028	0.7528	0.0186	10.723	0.257	575.3	13.4
SL1_33	658	141	0.05829	0.00030	0.7479	0.0207	10.783	0.291	572.3	15.1
SL1_34	427	92	0.05939	0.00029	0.7502	0.0159	10.913	0.223	564.9	11.3
SL1_35	586	126	0.05823	0.00027	0.7393	0.0202	10.891	0.285	566.8	14.5
SL1_36	614	130	0.05873	0.00028	0.7450	0.0166	10.881	0.245	566.9	12.4
SL1_37	638	137	0.05841	0.00027	0.7390	0.0220	10.915	0.304	565.5	15.4
SL1_38	416	90	0.05918	0.00026	0.7470	0.0136	10.916	0.197	564.9	10.0
SL1_39	611	131	0.05831	0.00028	0.7405	0.0222	10.889	0.315	566.8	16.0

Note:[a]format is: sample name_spot number. *^{207}Pb-corrected values.

Supplemental File 3

CH-89 Tera-Wasserburg diagram for analyses >0.95 concordant.

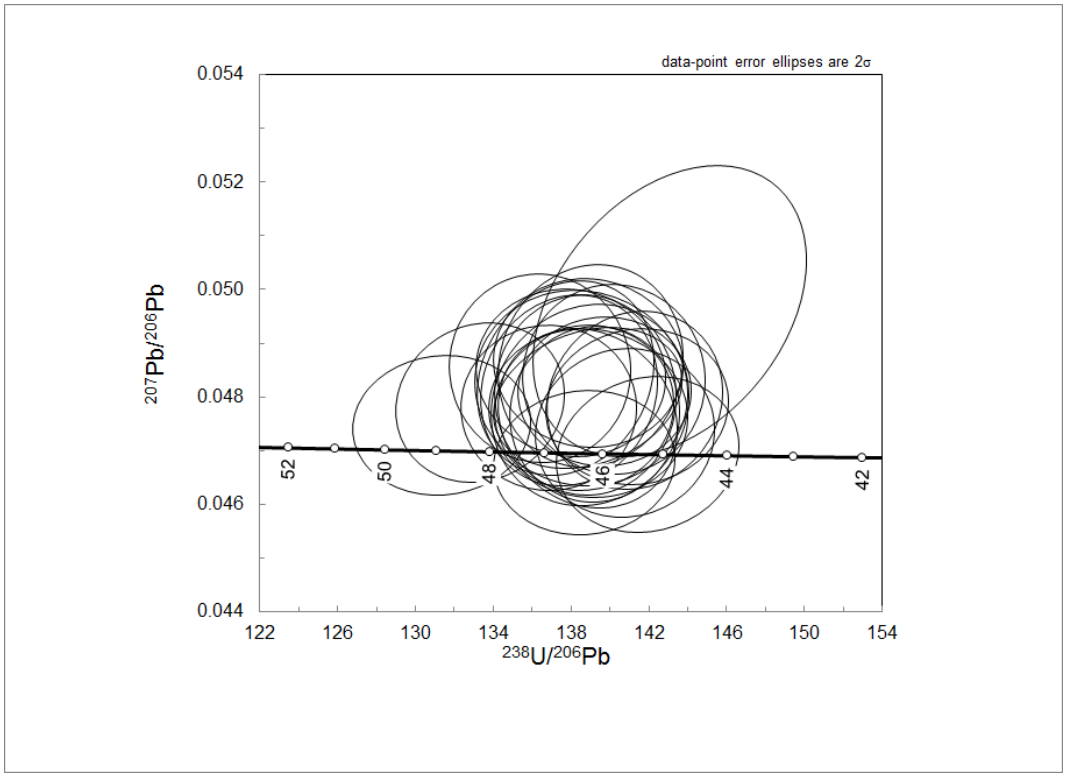

CH-89 Weighted mean for analyses >0.95 concordant.

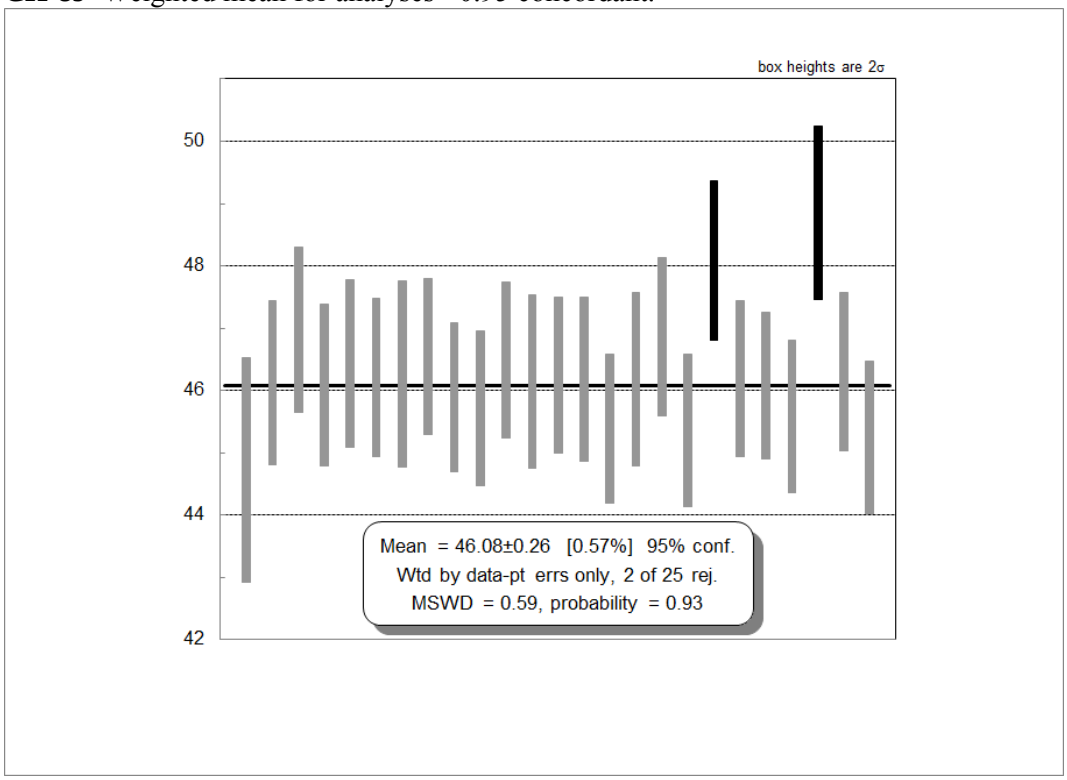

Supplemental File 3

CHJ-01 Tera-Wasserburg diagram of >50% concordant analyses.

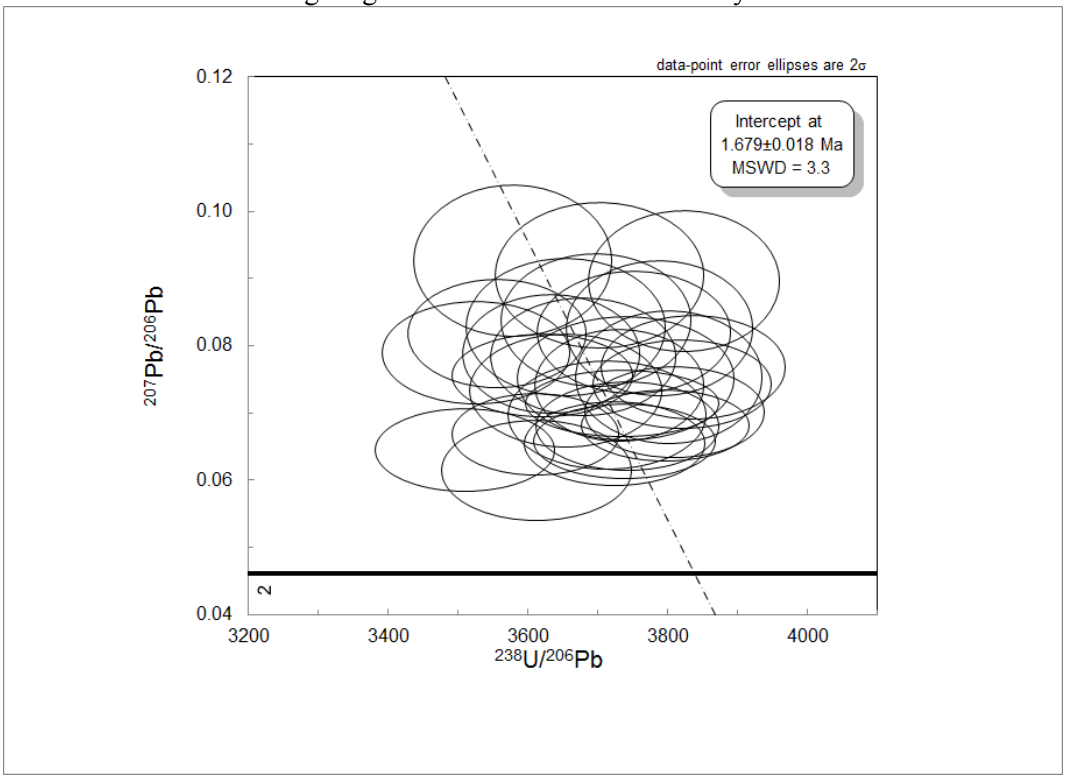

CHJ-01 Weighted mean of >50% concordant analyses.

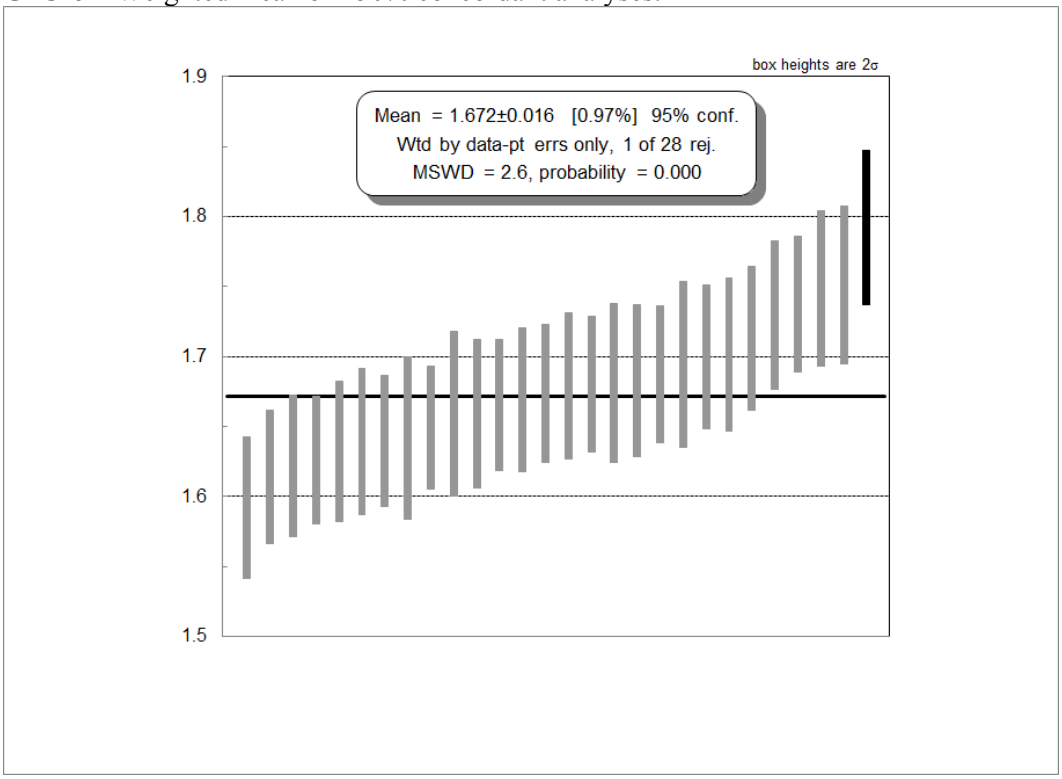

Supplemental File 3

CHJ-02 Tera-Wasserburg diagram for analyses >0.95 concordant.

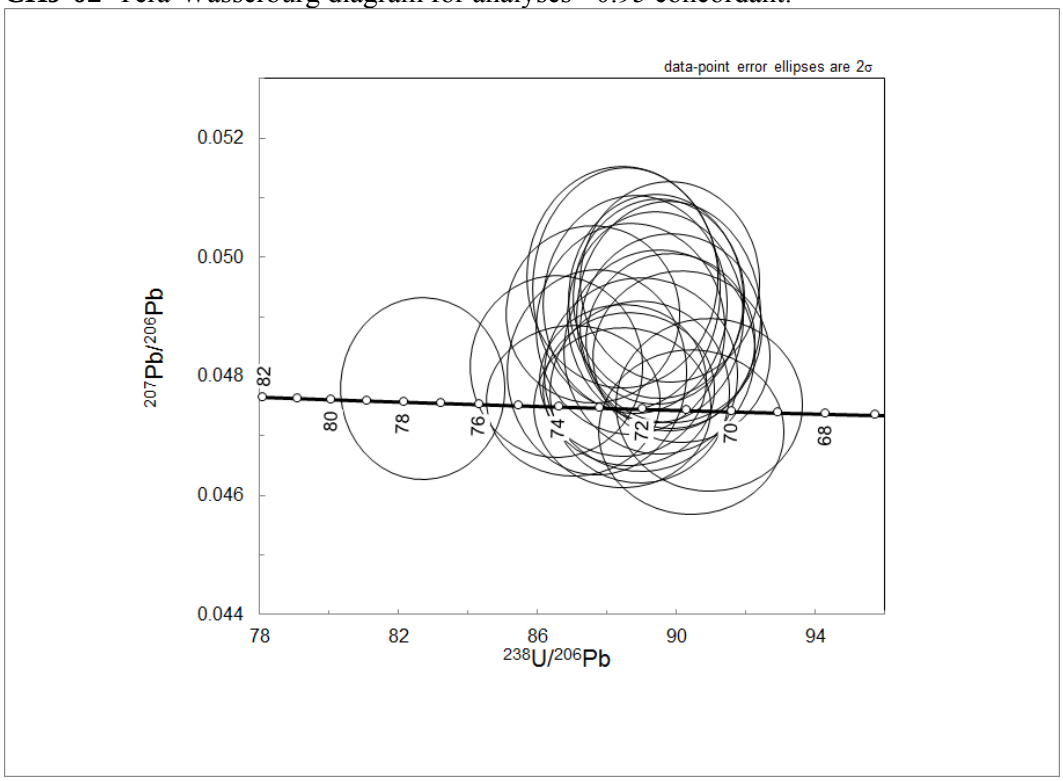

CHJ-02 Weighted mean for analyses >0.95 concordant

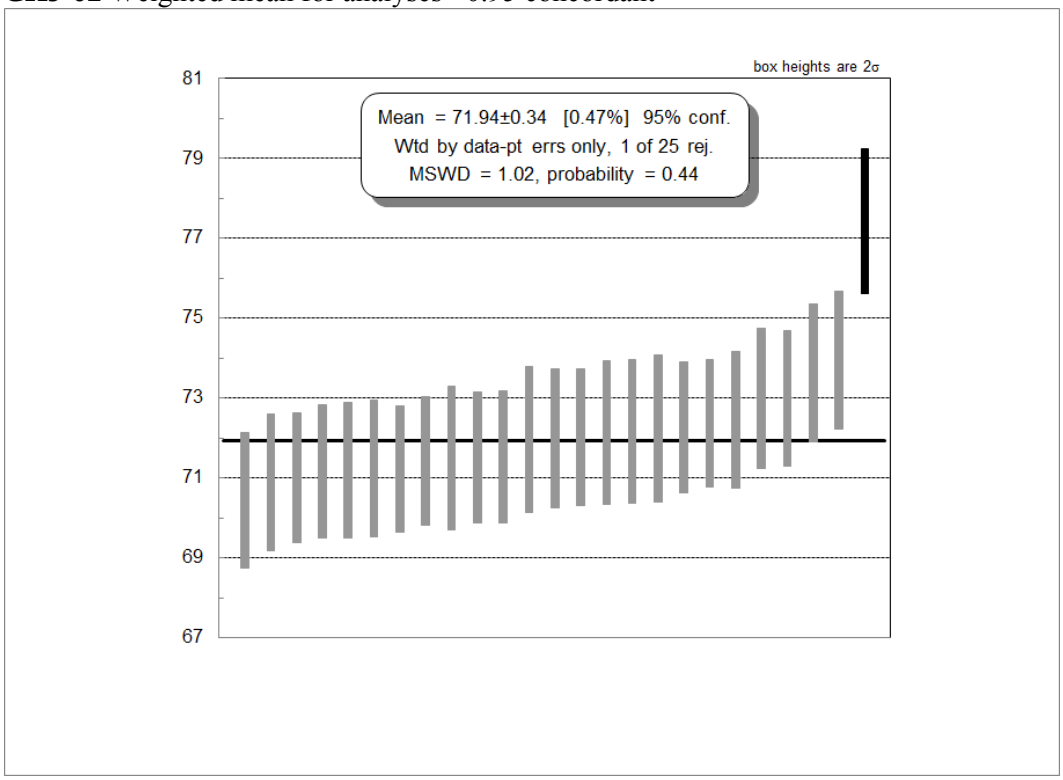

Supplemental File 3

CHJ-04 Tera-Wasserburg diagram for analyses >0.95 concordant.

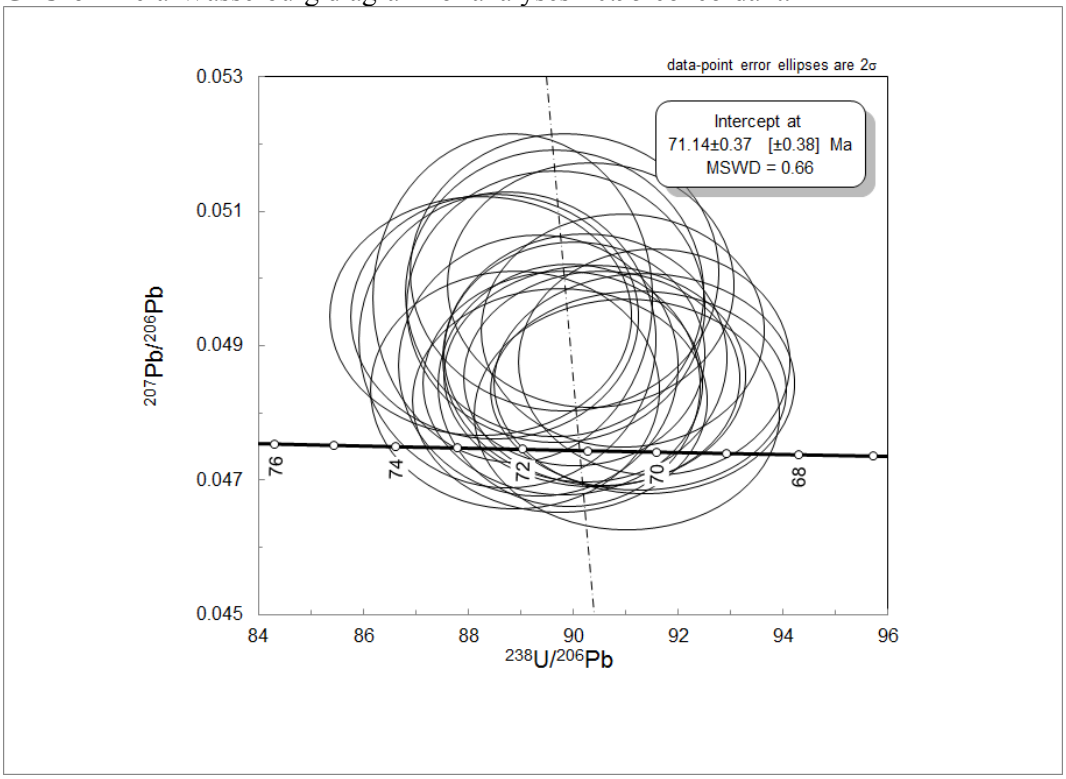

CHJ-04 Weighted mean plot for analyses >0.95 concordant.

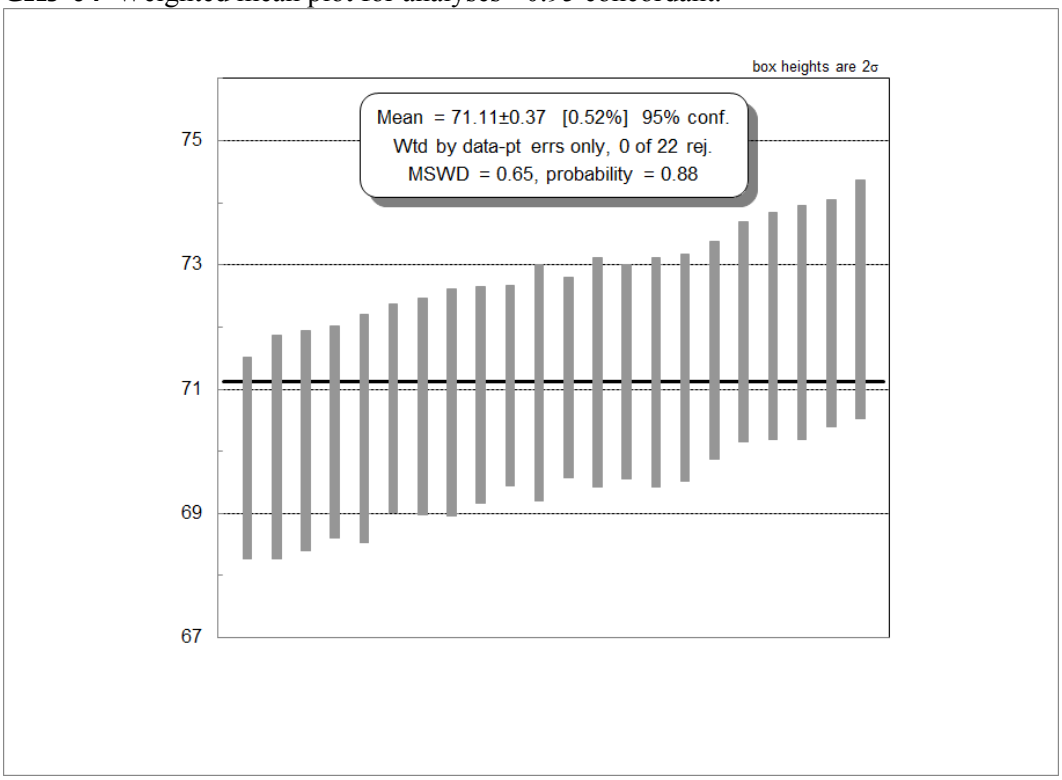

Supplemental File 3

CHJ-13 Tera-Wasserburg diagram for analyses >0.95 concordant.

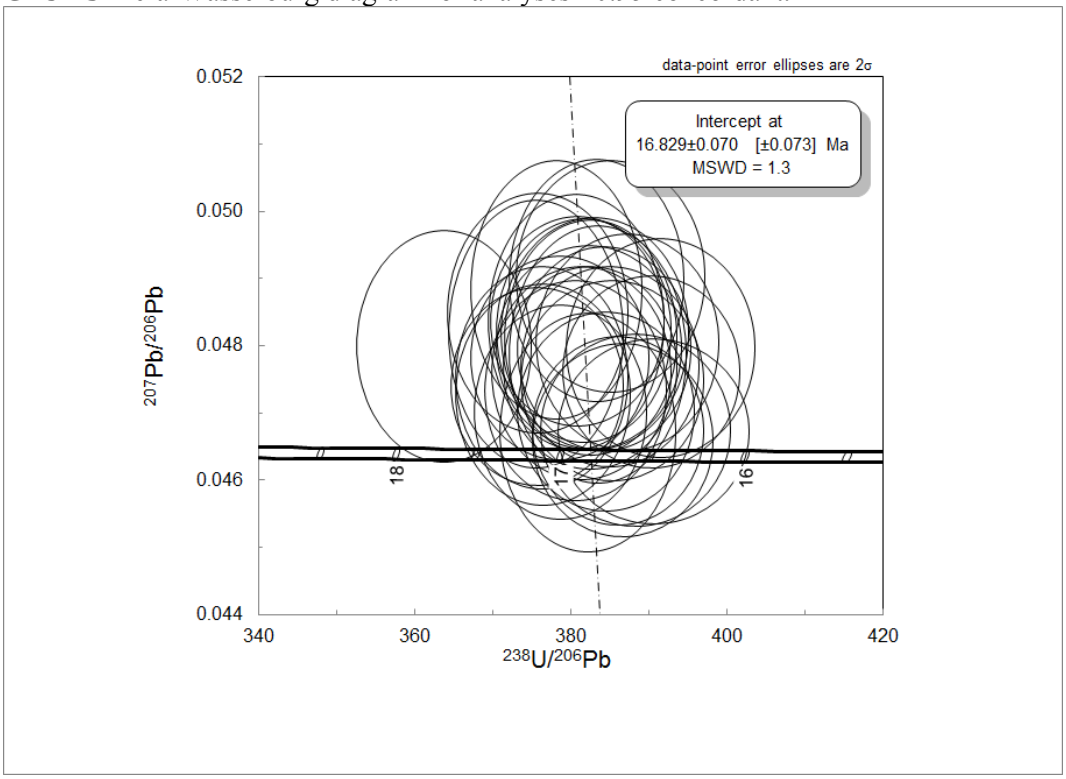

CHJ-13 Weighted mean for analyses >0.95 concordant.

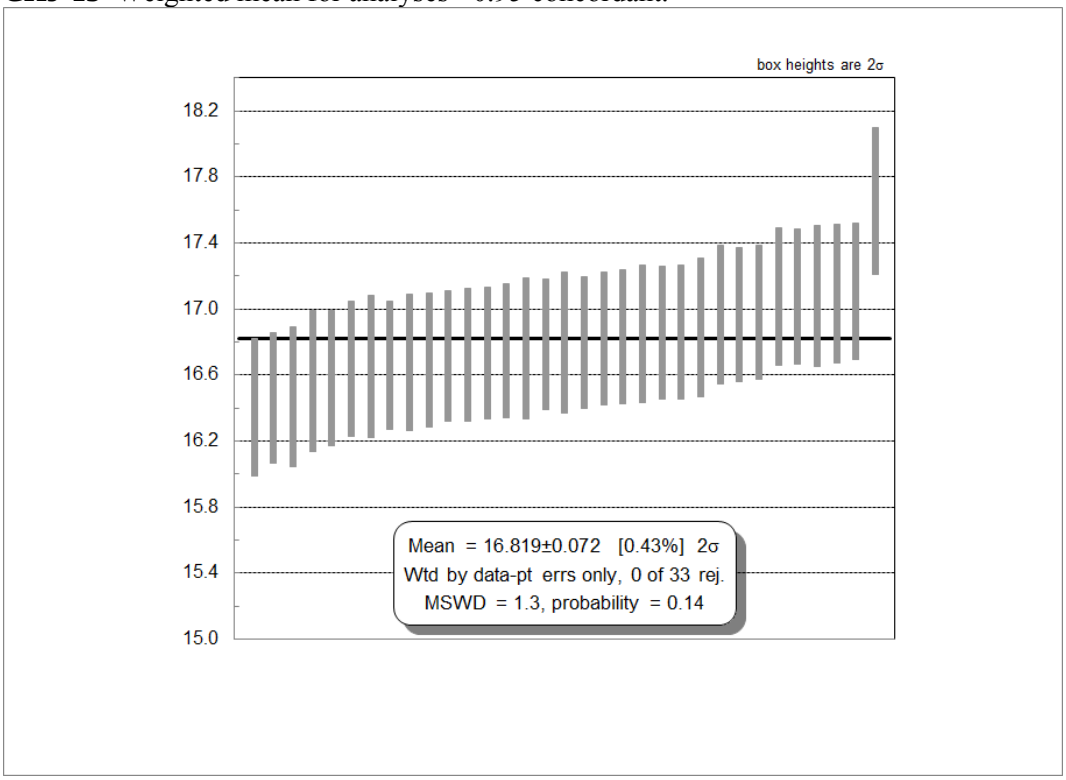

Supplemental File 3

CHJ-15 Tera-Wasserburg plot for analyses >0.90 concordant.

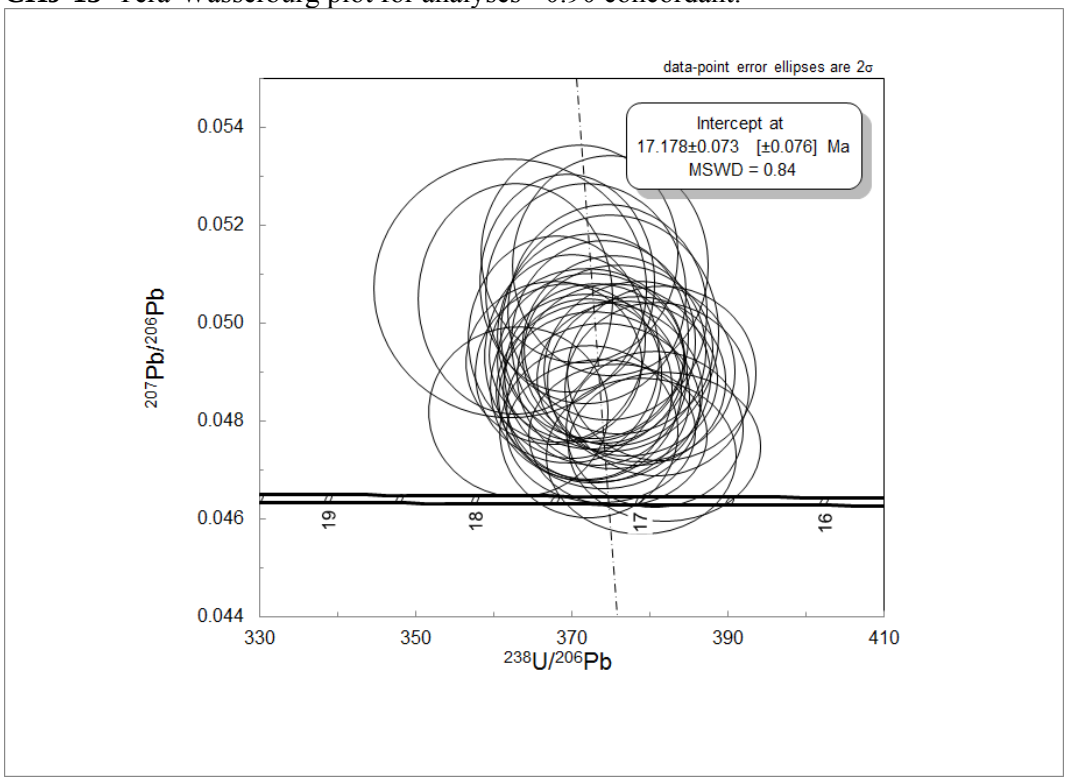

CHJ-15 Weighted mean for analyses >0.90 concordant

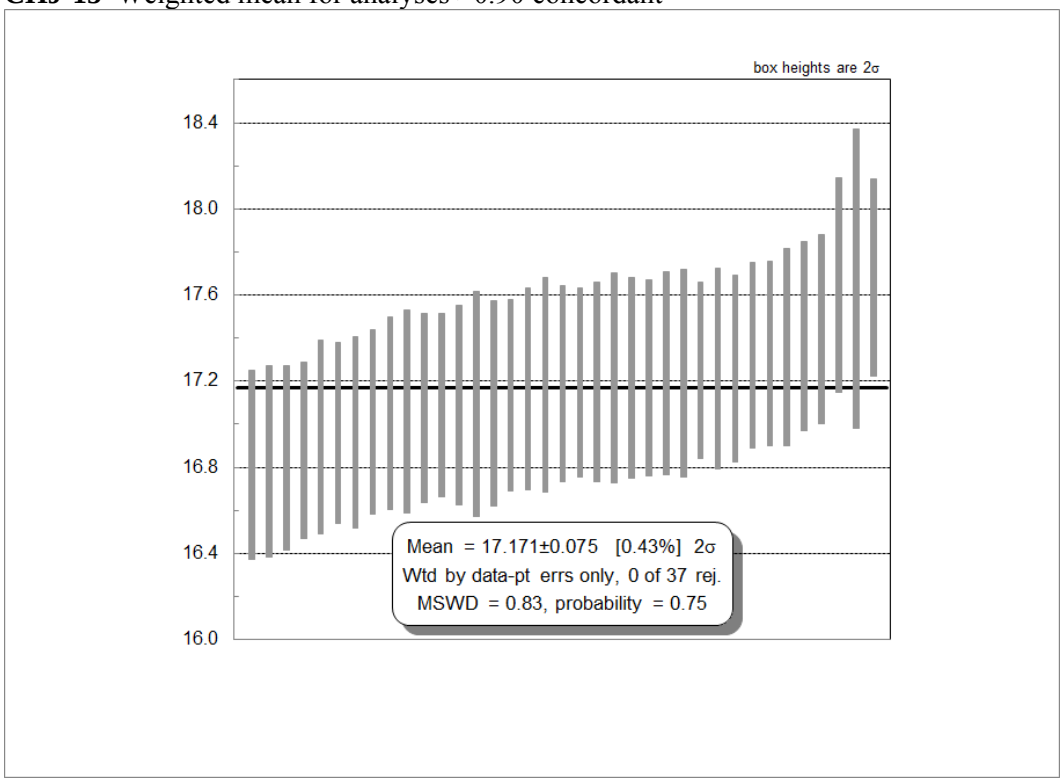

Supplemental File 3

CHJ-16 Tera-Wasserburg plot for analyses >0.95 concordant.

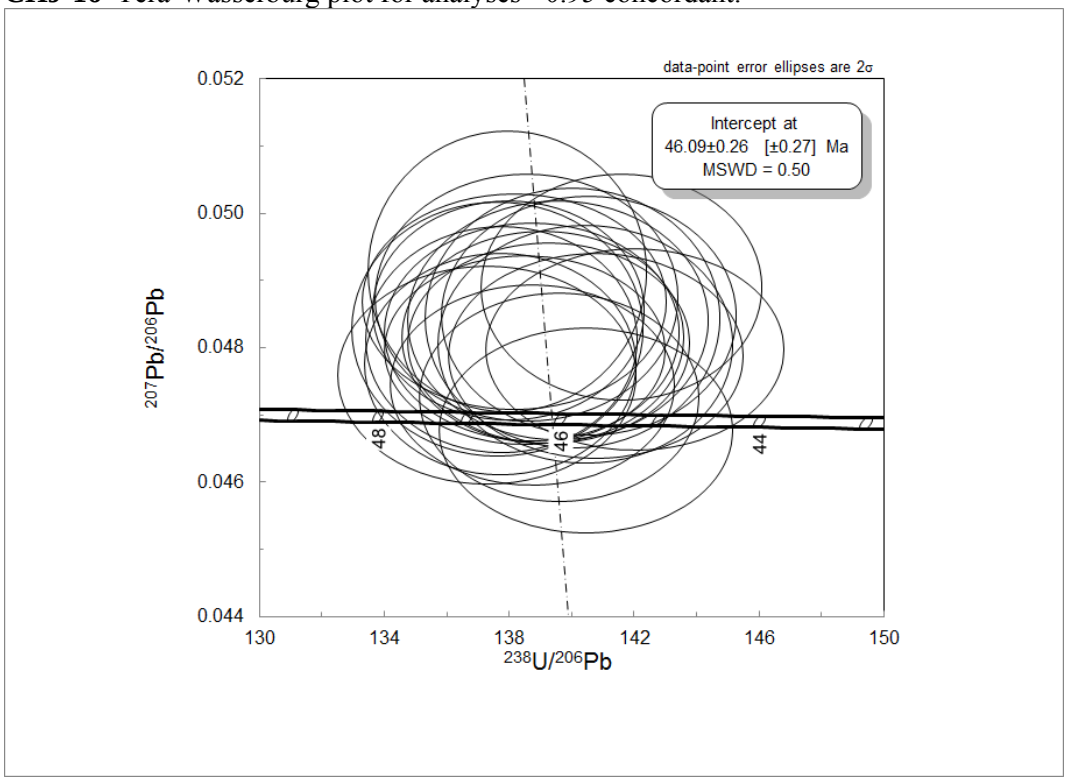

CHJ-16 Weighted mean for analyses >0.95 concordant.

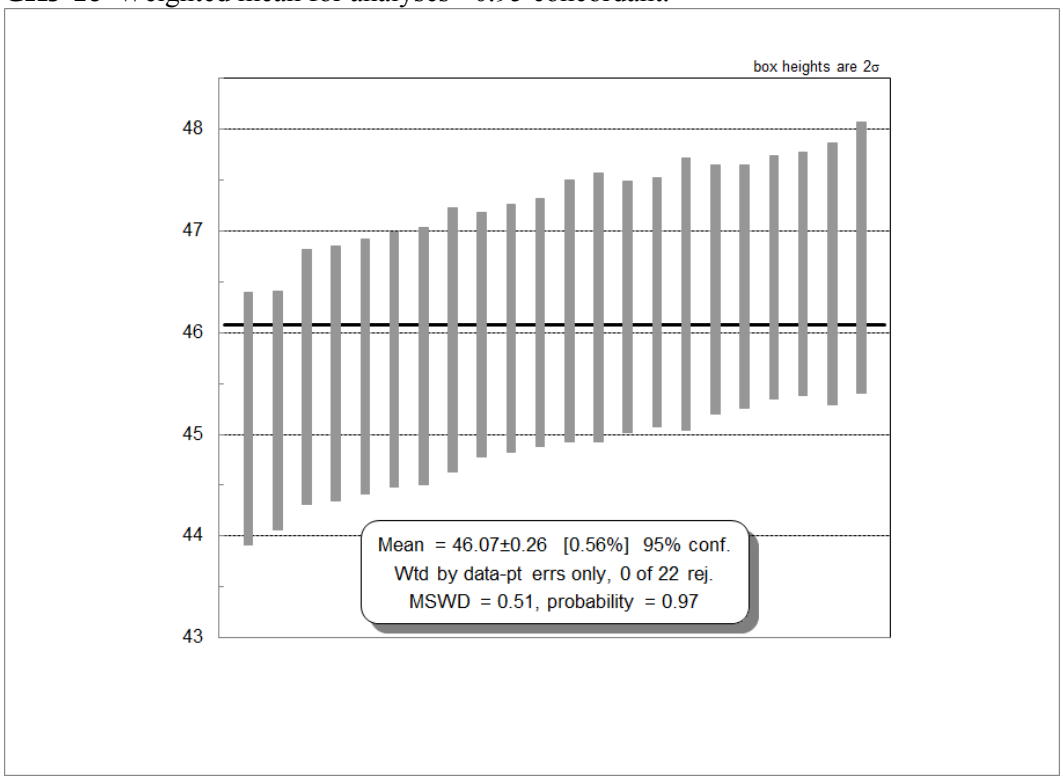

CHJ-16.1 Tera-Wasserburg plot for analyses >0.90 concordant.

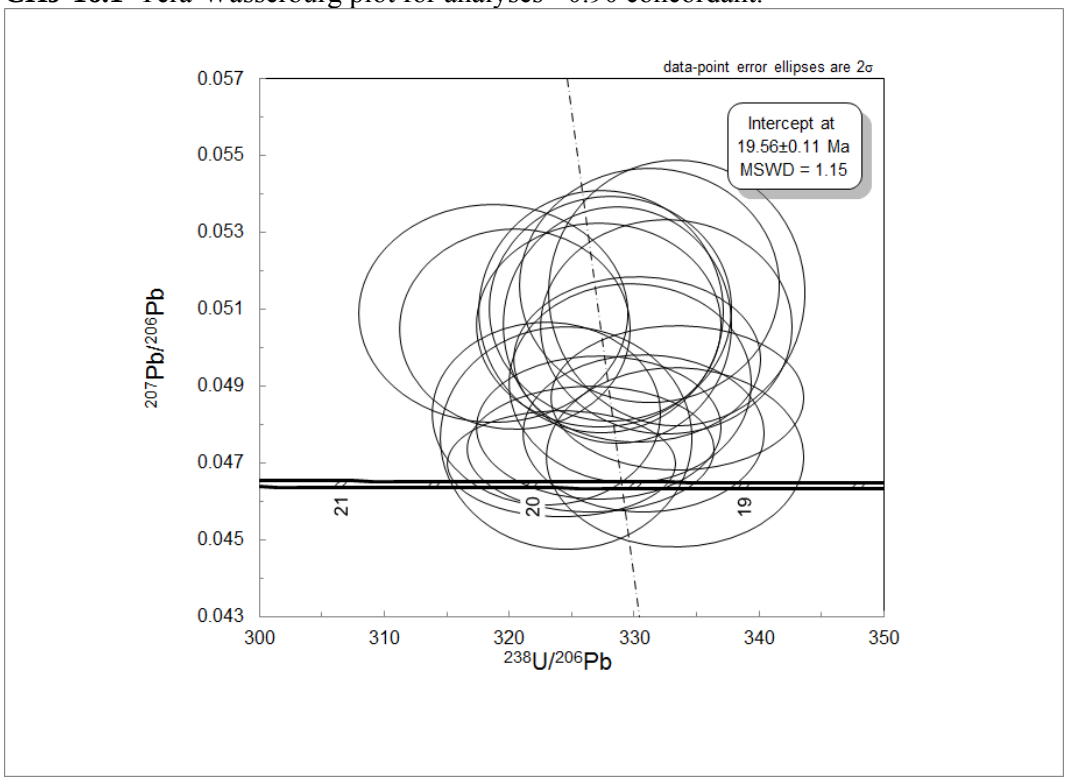

CHJ-16.1 Weighted mean for analyses >0.90 concordant.

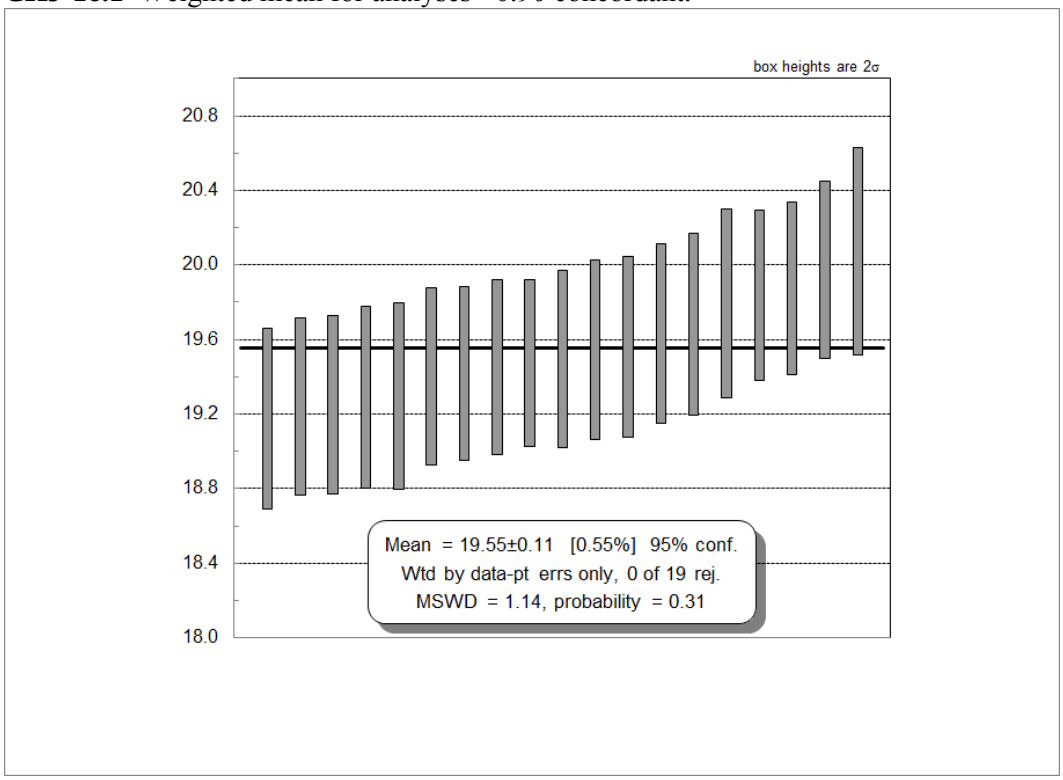

CHJ-24 Tera-Wasserburg plot for analyses >0.90 concordant.

Supplemental File 3

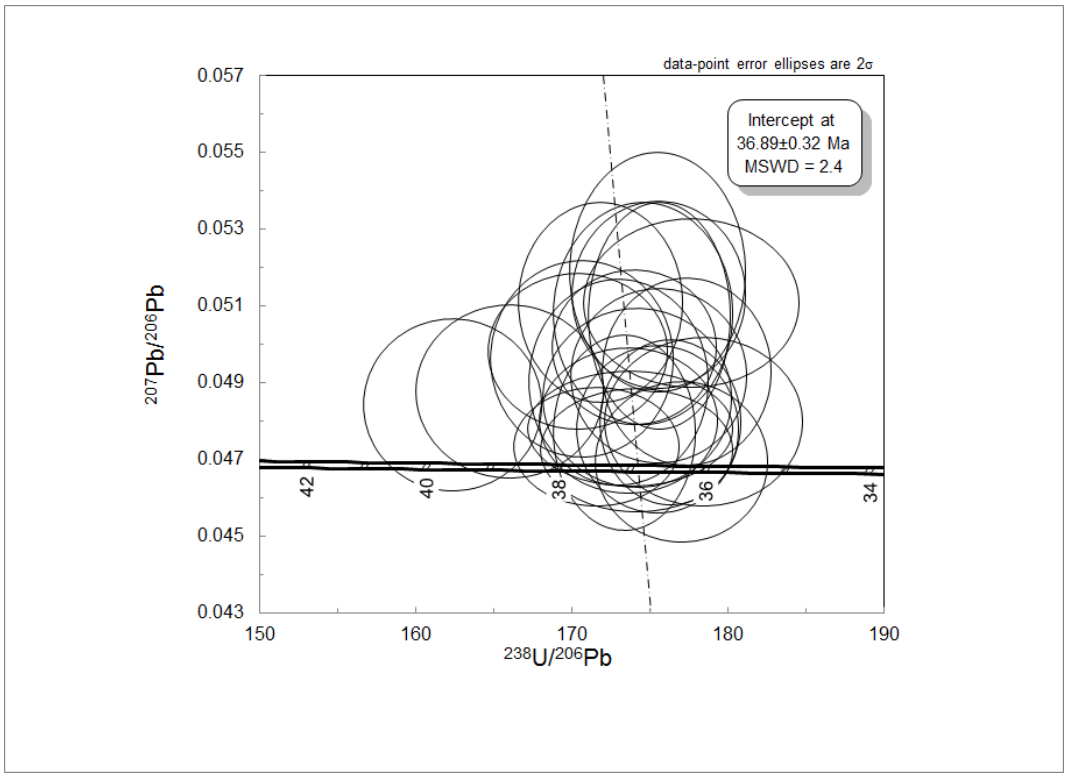

CHJ-24 Weighted mean for analyses >0.90 concordant.

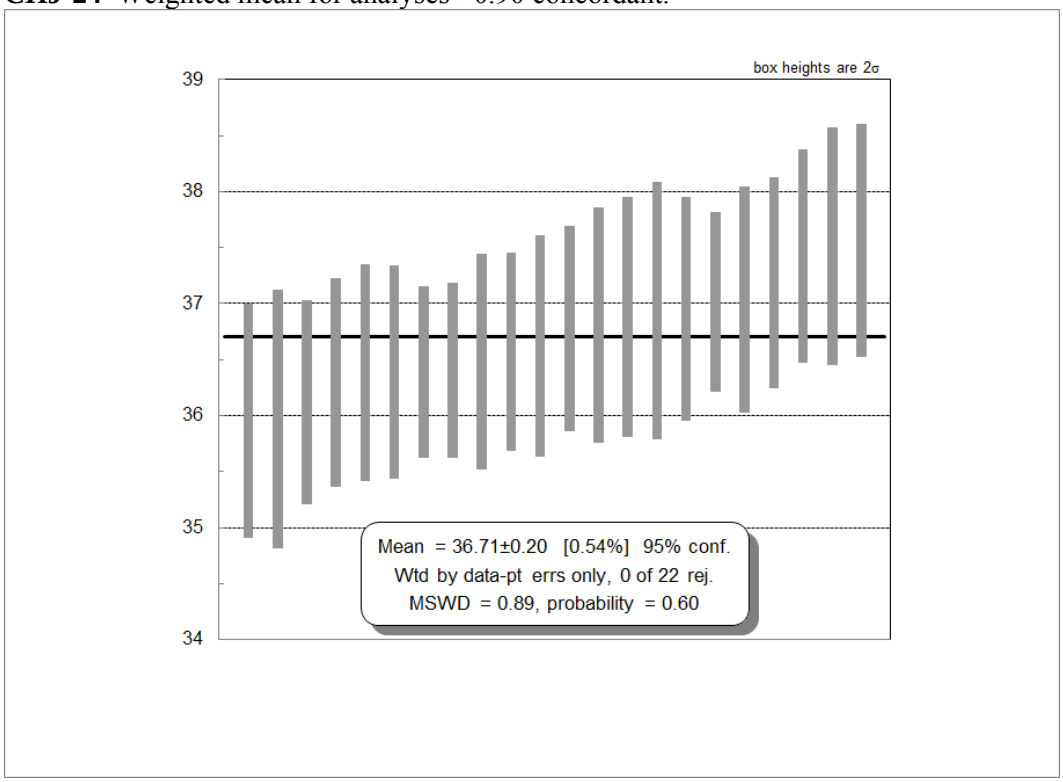

CHJ-27 Tera-Wasserburg plot for analyses >0.95 concordant.

Supplemental File 3

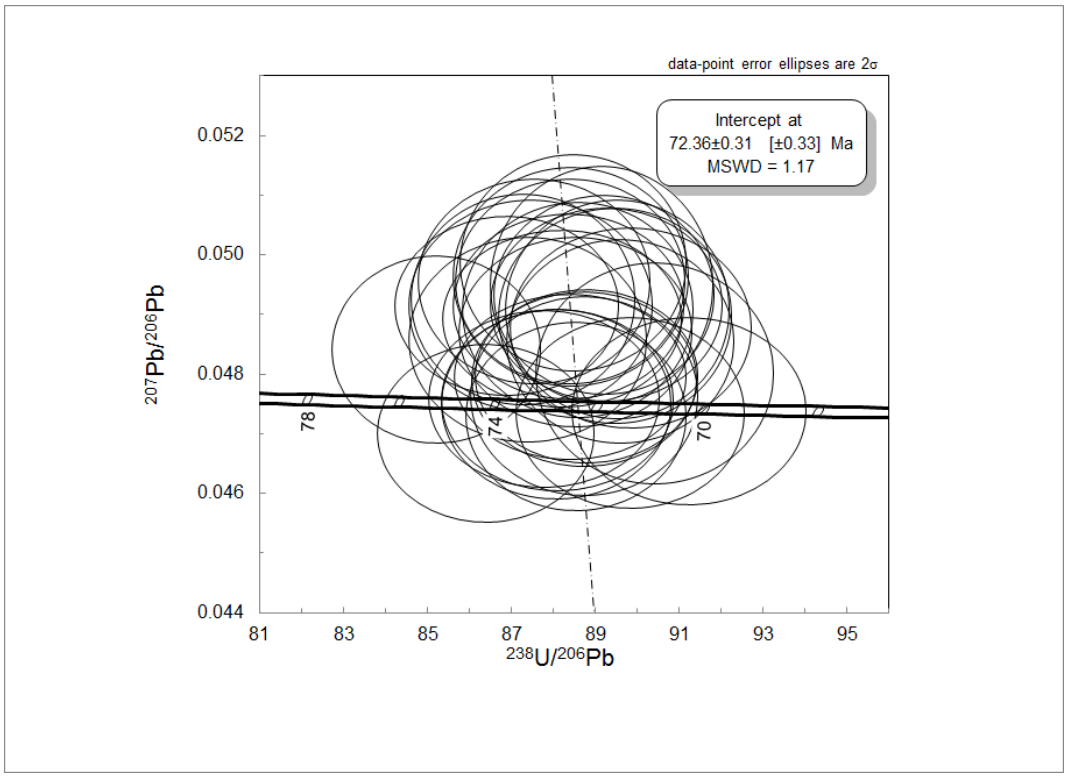

CHJ-27 Weighted mean for analyses >0.95 concordant.

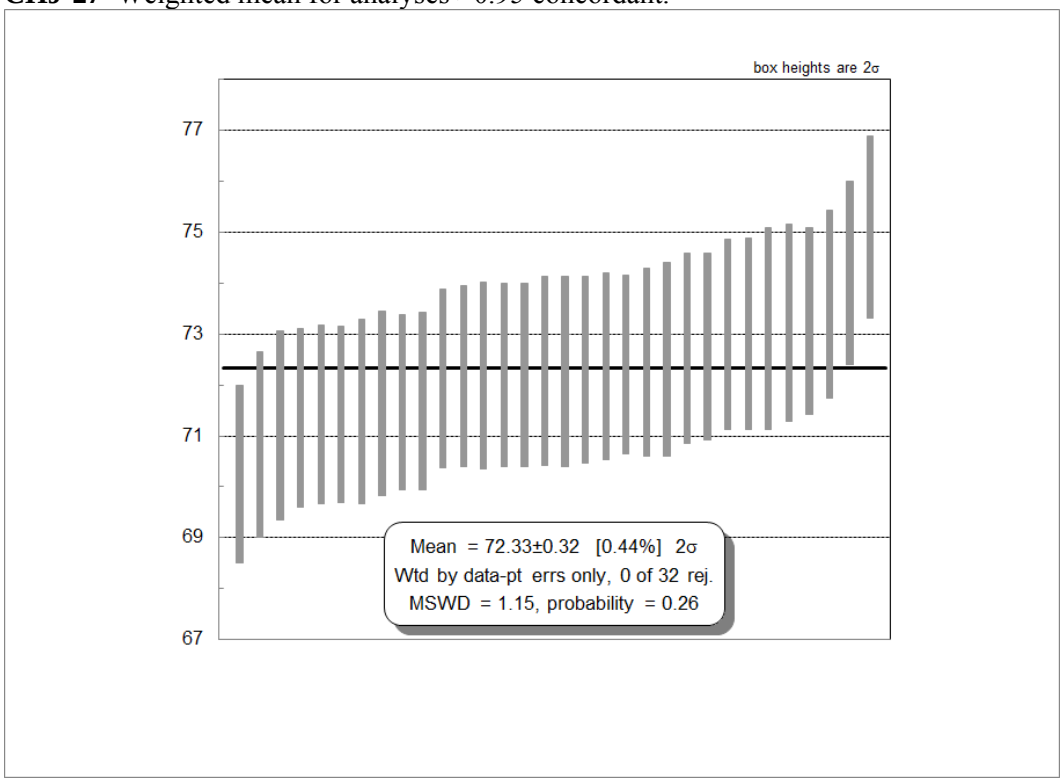

Supplemental File 3

CHJ-33 Tera-Wasserburg plot for analyses >0.95 concordant.

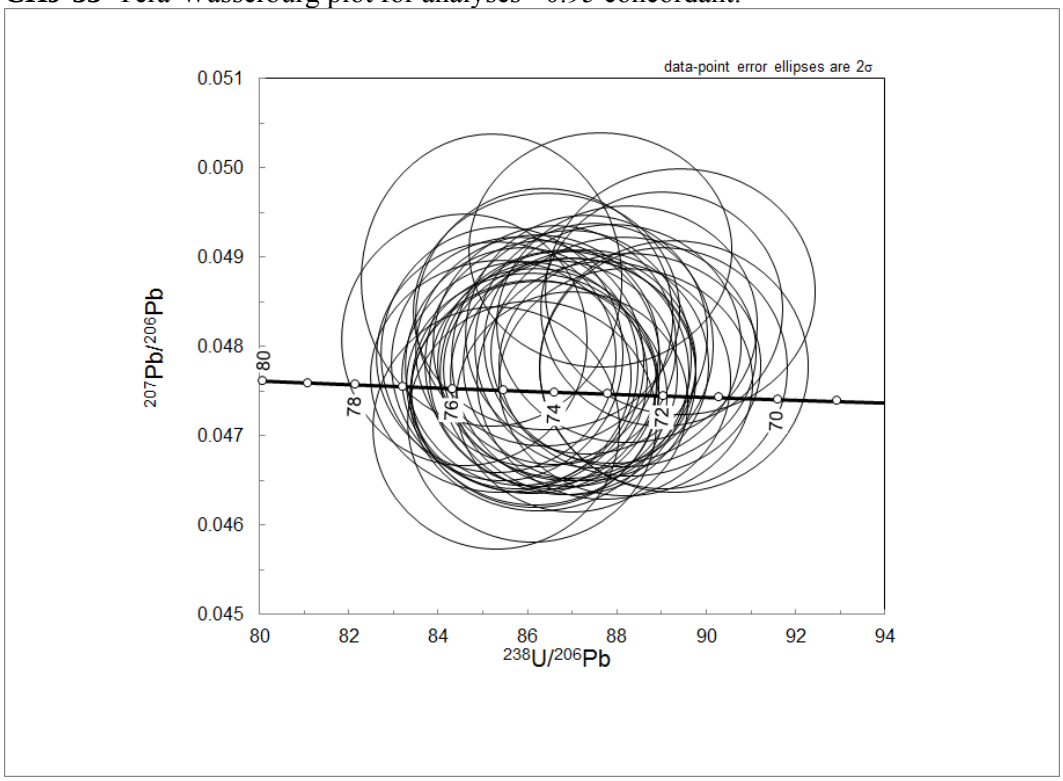

CHJ-33 Weighted mean for analyses >0.95 concordant.

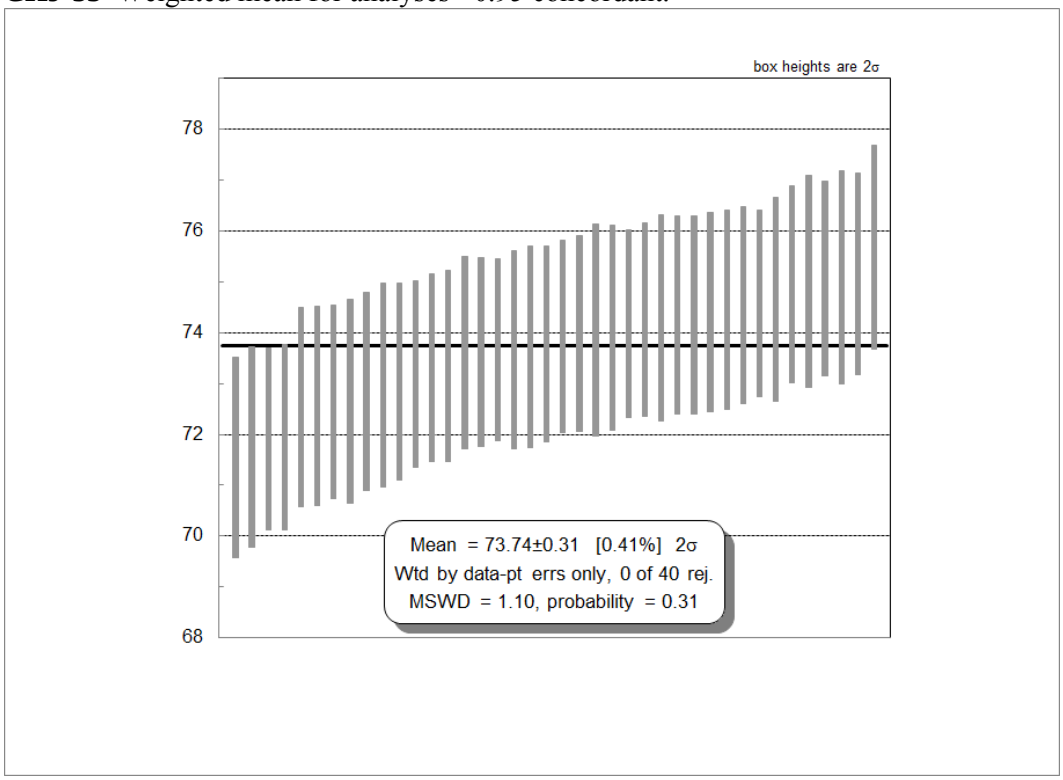

Supplemental File 3

CHJ-34 Tera-Wasserburg plot for analyses >0.95 concordant.

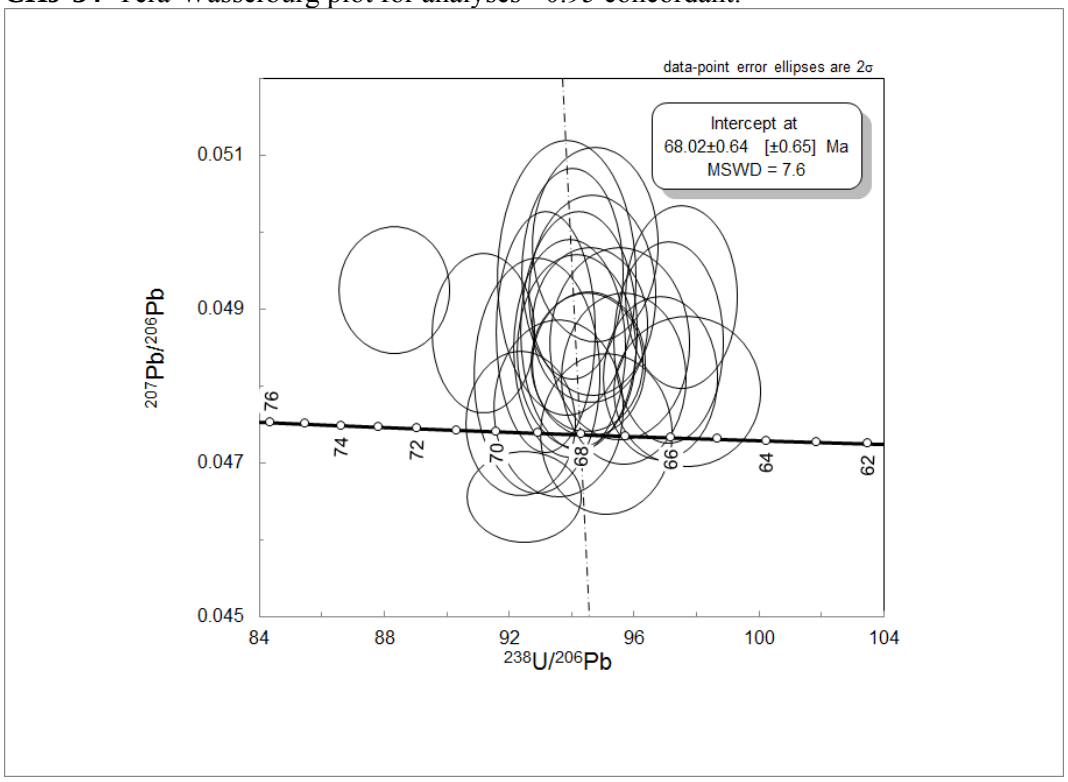

CHJ-34 Probability distribution for analyses >0.95 concordant.

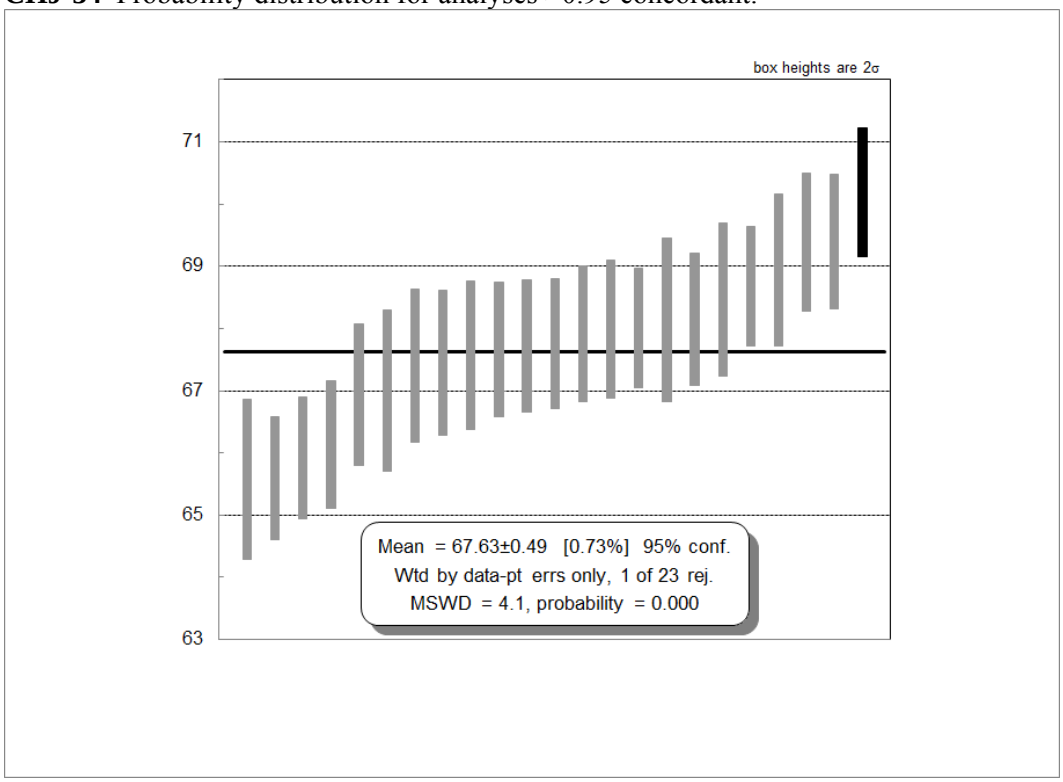

Supplemental File 3

CHJ-36 Tera-Wasserburg plot for analyses >0.95 concordant.

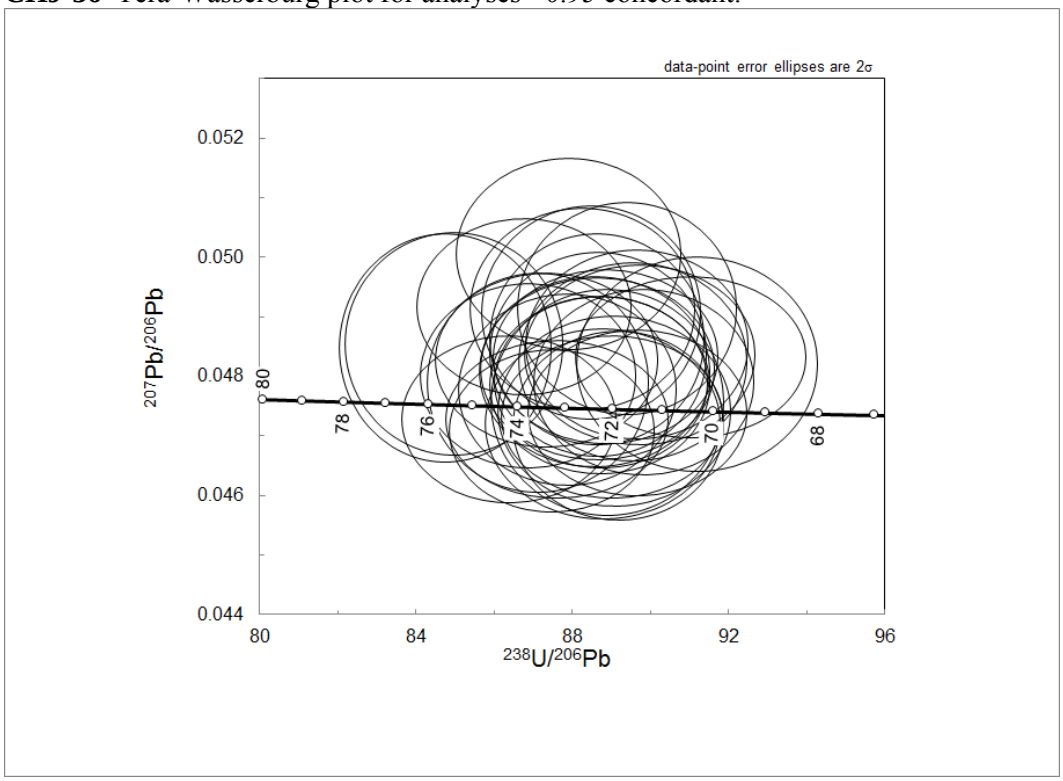

CHJ-36 Weighted mean for analyses >0.95 concordant.

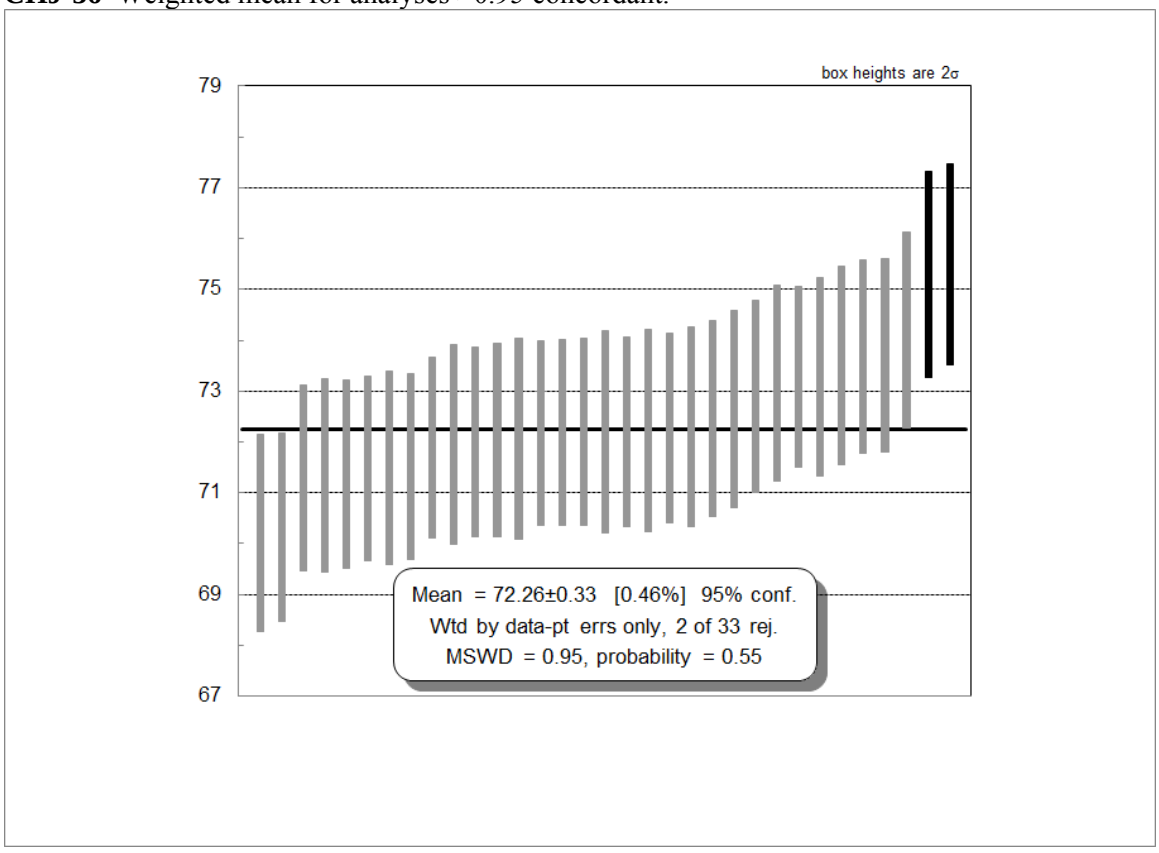

Supplemental File 3

CHJ-41 Tera-Wasserburg plot for analyses >0.95 concordant.

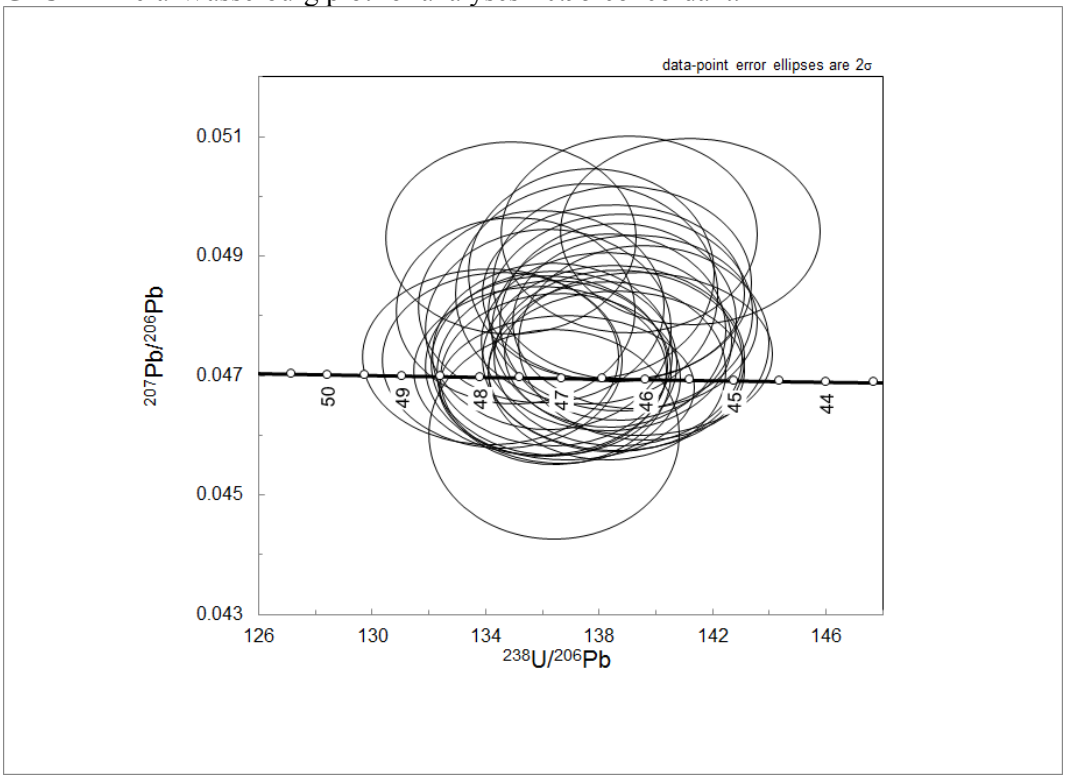

CHJ-41 Weighted mean for analyses >0.95 concordant.

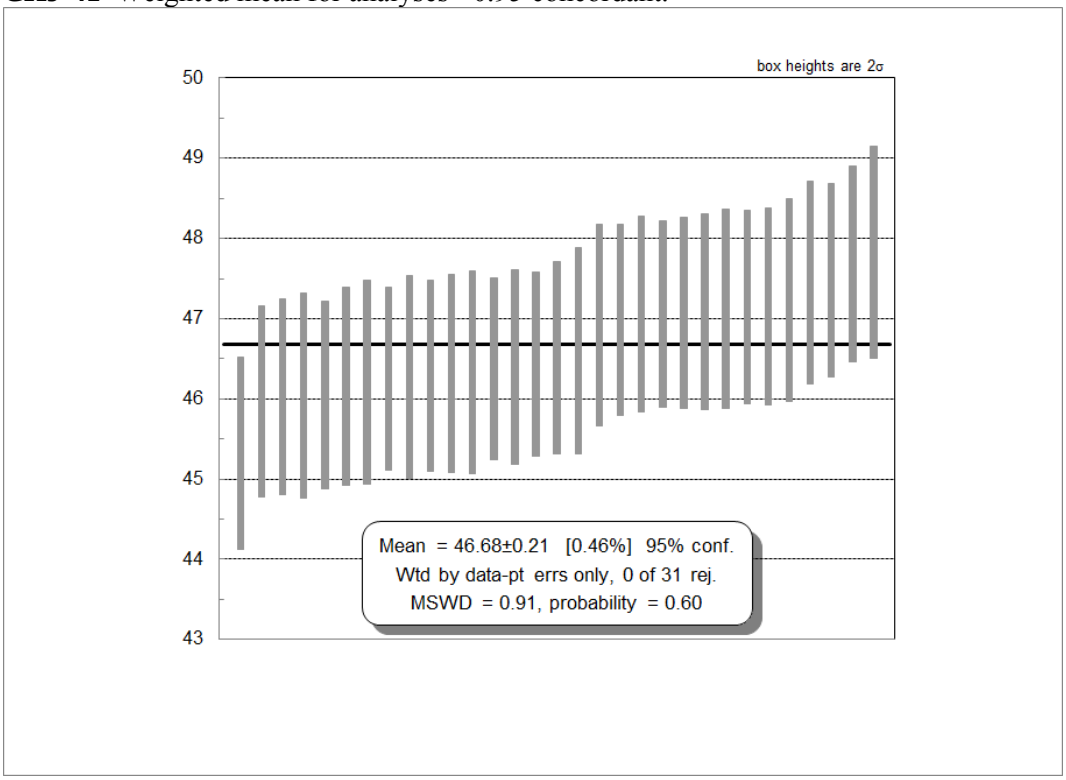

Supplemental File 3

J378 Tera-Wasserburg plot for analyses >0.80 concordant.

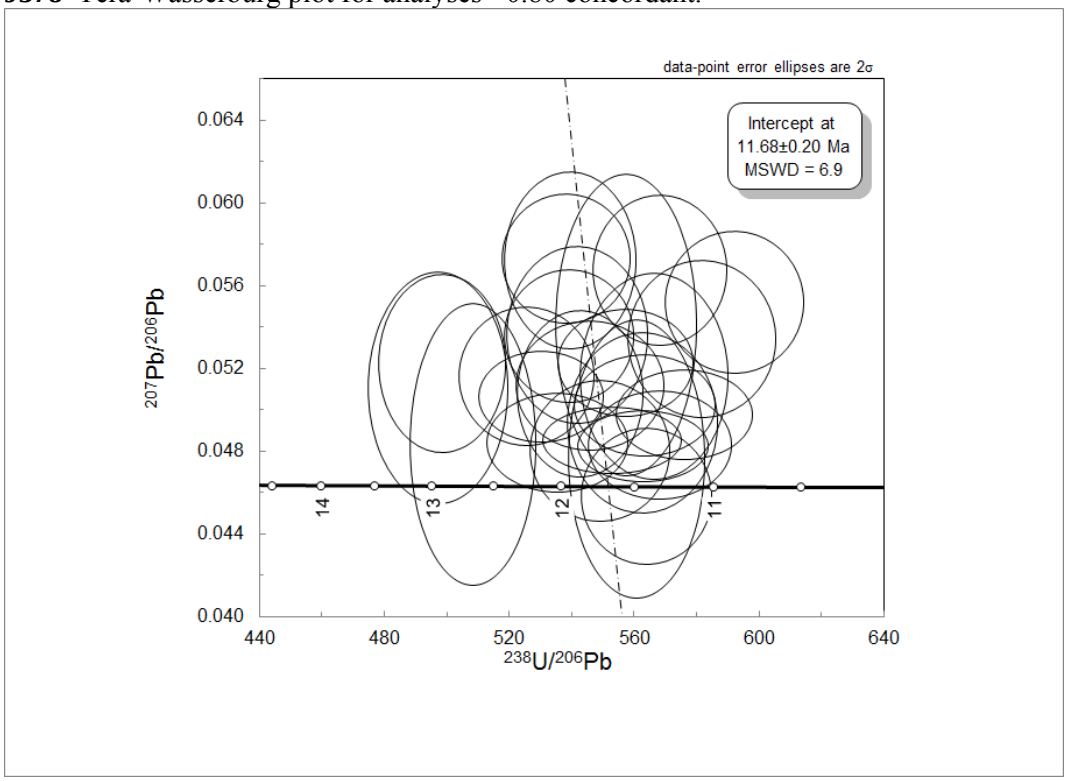

J378 Weighted mean for analyses >0.80 concordant.

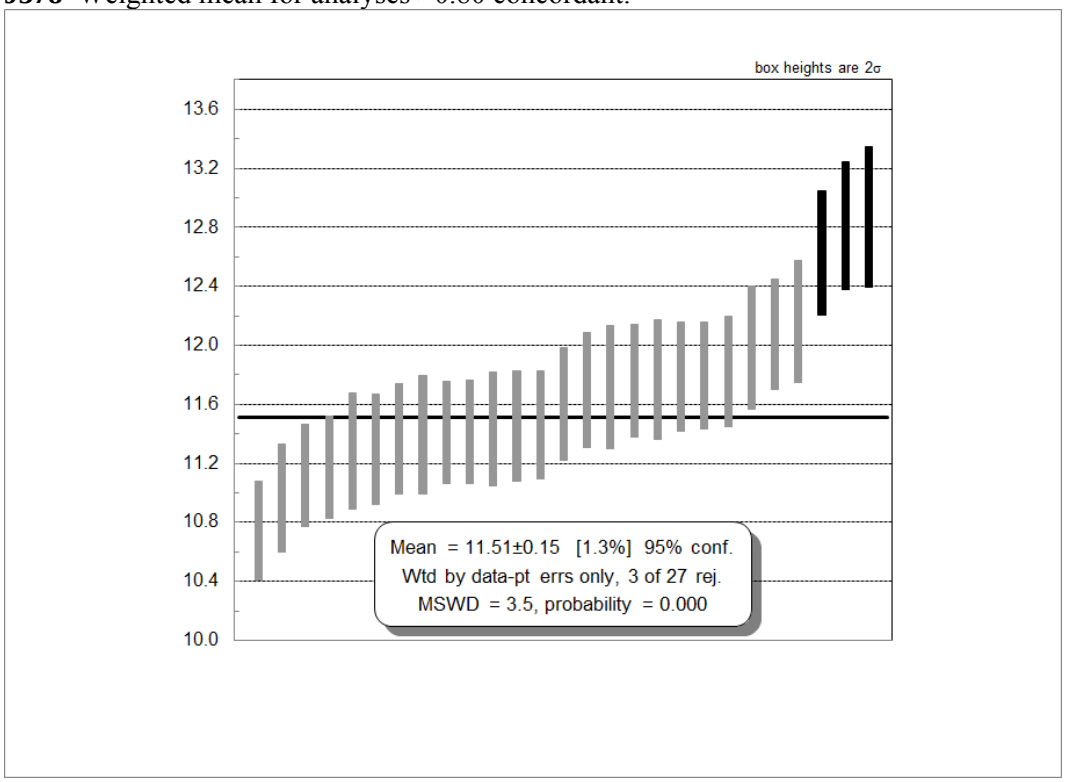

Supplemental File 3

J417 Tera-Wasserburg plot for analyses >0.70 concordant, <21 Ma.

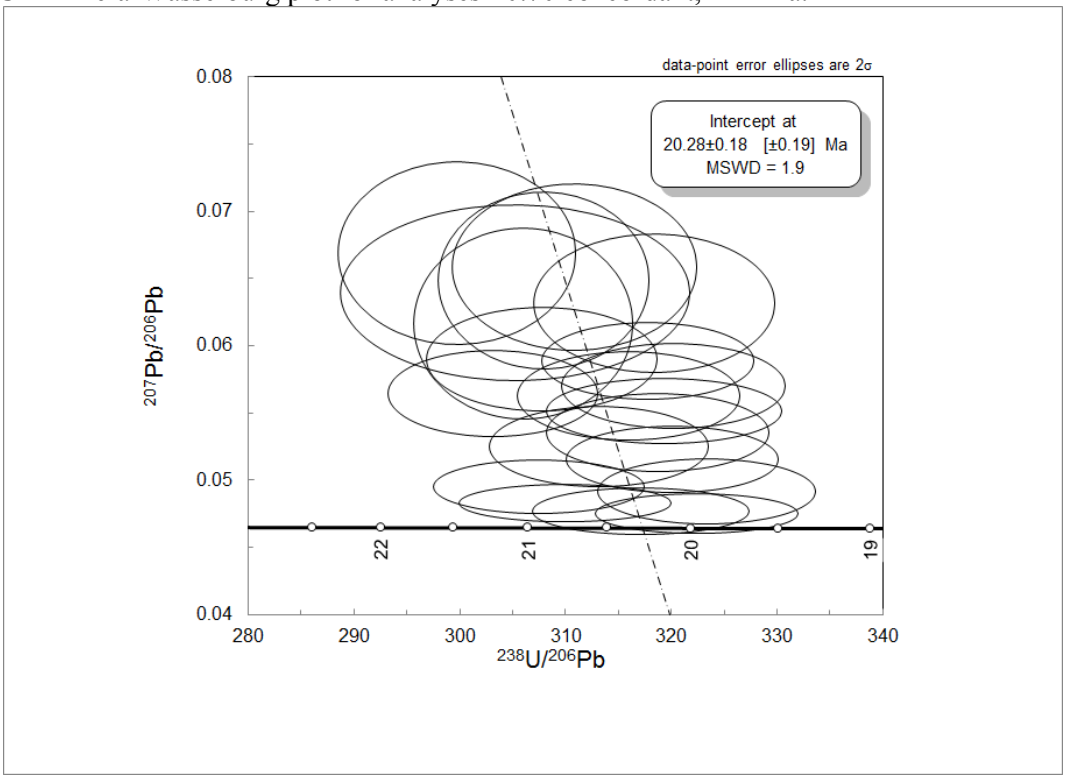

J417 Weighted mean for analyses >0.70 concordant, <21 Ma.

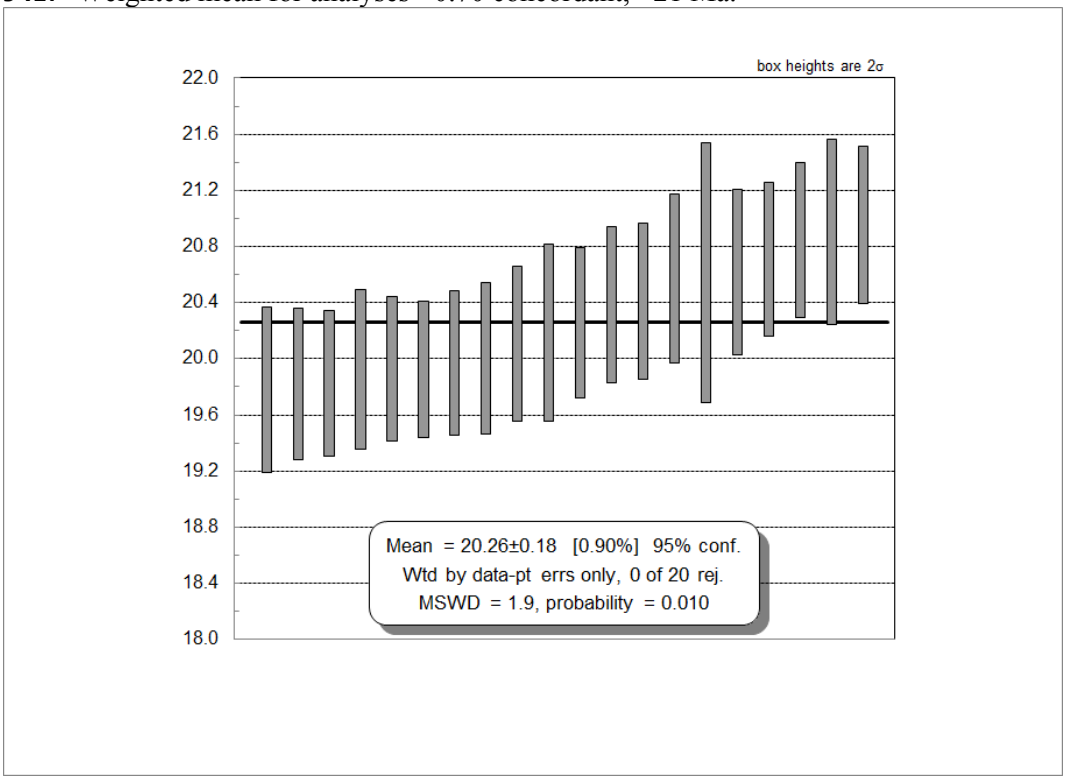

Supplemental File 3

J473 Tera-Wasserburg plot for analyses >0.80 concordant.

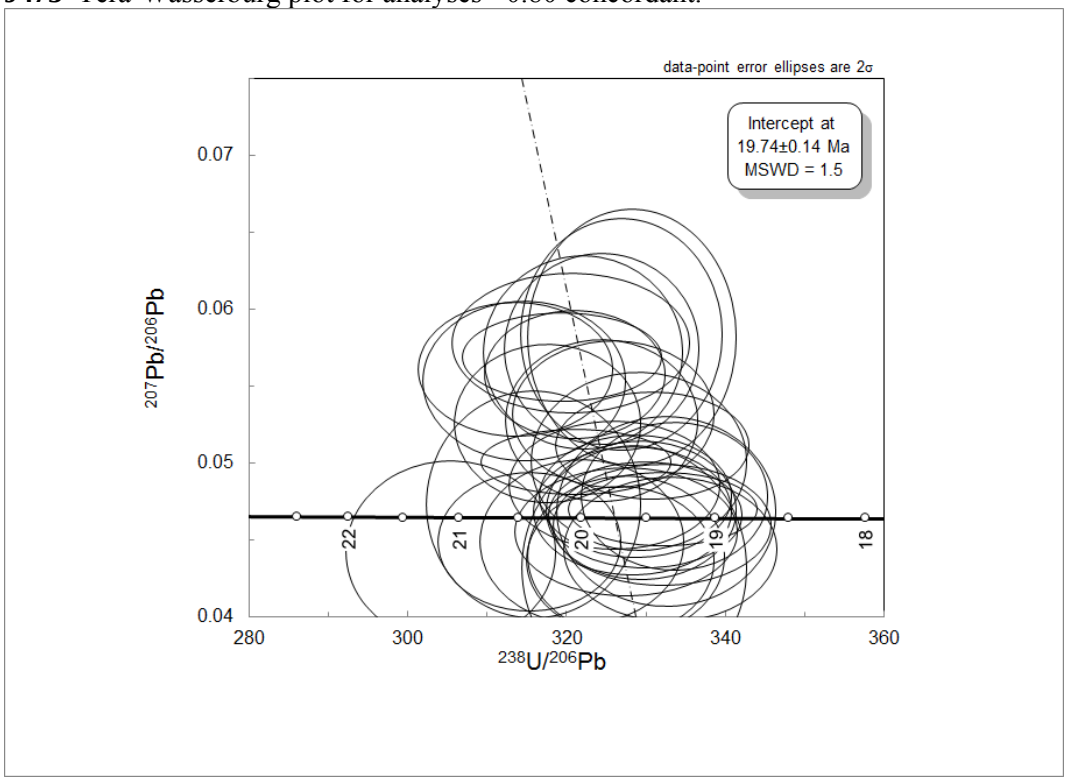

J473 Weighted mean for analyses >0.80 concordant.

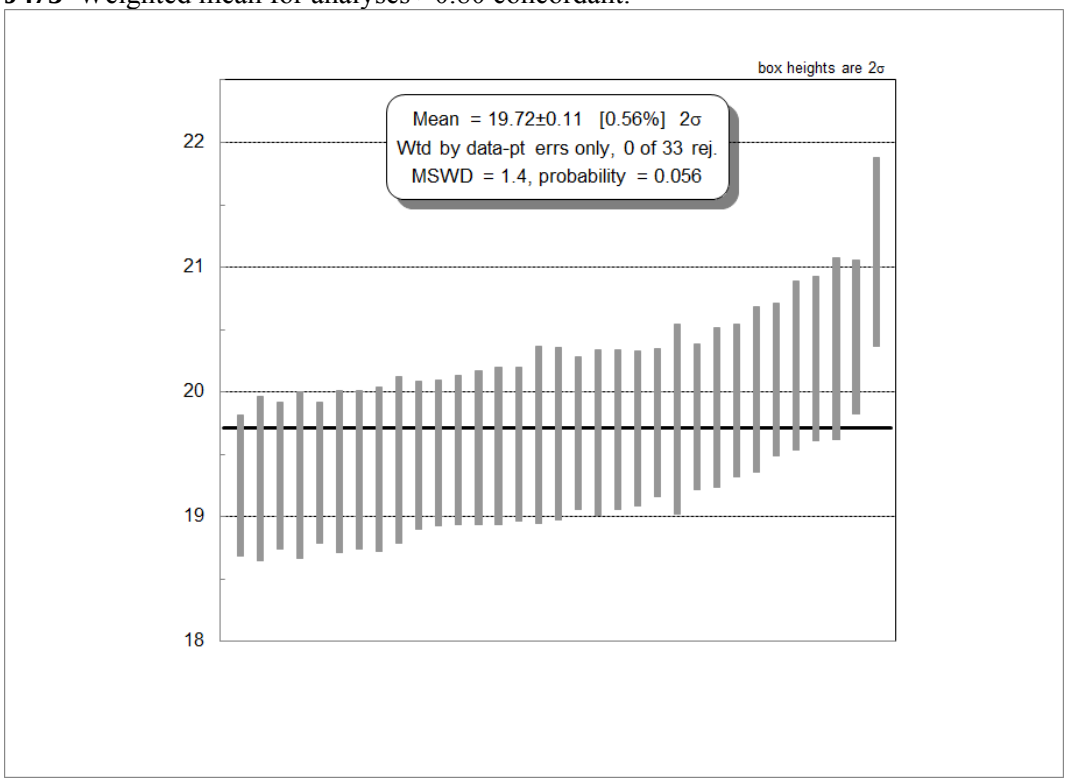

COMMON LITHOFACIES OBSERVED IN THE TINGUIRIRICA AREA

The Abanico Formation in the Río Tinguiririca area consists of complexly interdigitating volcanic, volcaniclastic and sedimentary strata, including primary volcanic, post-eruptive and inter-eruptive deposits, all of which are cut by hypabyssal intrusions of varying composition. These deposits commonly exhibit low grade metamorphism ranging from zeolite to lower greenschist facies (e.g., Levi et al., 1989).

Here, we describe the volcanic and sedimentary lithofacies that occur frequently in the Abanico Formation within the study area. These descriptions are derived from field observations and thin-section analysis of representative intervals of each lithofacies type. Lithofacies descriptions are sequenced in order of decreasing proximity to eruption centers and increasing temporal lag between eruptions and deposition inferred for these deposits. Tables S31 and S32 summarize the lithofacies described below and their inferred associations.

Volcanic deposits

Lithofacies Lb: Basaltic Lava Flows

Basaltic flows are generally 1–10 m thick, exhibit irregular-to-sheet-like geometries, and extend laterally for hundreds of meters, sometimes up to 3+ km. Individual flows are intercalated within volcaniclastic deposits or form multistoried stacks consisting of ~2–16 individual flows. Flows typically have dense, massive cores overlying highly irregular cinder rubble; vesiculated flow tops are rarely preserved. Basalt flows are occasionally seriate and microcrystalline in texture, but more commonly contain distinct phenocrysts of plagioclase, pyroxene, and olivine in

a microcrystalline groundmass. Phenocrysts constitute up to 5%–15% of the vesicle free volume, with ~0%–15% prismatic phenocrysts of plagioclase (1–2 mm) and 5%–10% subhedral to embayed olivine (1–2 mm) in a holocrystalline groundmass of randomly oriented, interlocking plagioclase laths with intergranular pyroxene and rare interstitial glass; the groundmass occasionally exhibits a trachytic texture. Phenocrysts of olivine are ubiquitously altered to iddingsite.

Basalt lava flows are interpreted to be subaerial, low viscosity lava flows flowing moderate-to-long distances from a vent, in some cases several kilometers (Cashman et al., 1998; Hulme, 1974; Walker, 1973). Brecciation, massive interiors, and vesiculated tops of flows are indicative of coherent flows that autobrecciated during flow advance (Cas and Wright, 1987; Walker, 1973). Flows were most likely associated with effusive eruptions from a central vent, parasitic cone, or fissures.

Lithofacies Lab: Basaltic-andesite and Andesite Lava Flows

Basaltic-andesite and andesitic flows are 2–20 m thick and typically exhibit irregular bedding geometries. They are commonly intercalated between volcaniclastic deposits or form multistory stacks of as many as ~40 flows. The flow cores are commonly massive and are encased by a thick, blocky carapace. They are typically porphyritic in texture and contain varying amounts of plagioclase, pyroxene, and occasional olivine phenocrysts. Phenocrysts constitute up to ~45% of the vesicle free volume, with ~10%–60% sub- to euhedral laths of plagioclase (1–5 mm), 2%–3% an- to subhedral ortho- and clinopyroxene (0.3–0.5 mm), 0%–3% sub- to eudhedral amphibole (<0.5 mm), and 0%–3% subhedral to embayed olivine (0.5–1 mm) in a groundmass of plagioclase laths with intergranular pyroxene and varying amounts of

interstitial glass that is commonly devitrified; the groundmass is commonly trachytic in texture. Olivine phenocrysts are commonly altered to iddingsite. Some flows contain glomeroporphyritic feldspar.

The volcanic basaltic-andesite and andesite lithofacies are interpreted as subaerial, slowly moving aa or block lava flows associated with effusive eruptions from a central vent or lava dome (Cashman et al., 1998; Hulme, 1974; Walker, 1973). Extensive brecciation and massive interiors indicate coherent lava flows in which autobrecciation processes were prevalent, forming scoriaceous rubble during flow advance (Cas and Wright, 1987; Walker, 1973).

Lithofacies Pml: Dacitic to Rhyolitic Massive Lapilli-ash Tuff

Massive dacitic to rhyolitic ash deposits are pumice rich, occurring either as single, ~1–30 m thick layers, or as multistory stacks exceeding 300 m in thickness. These deposits range from fine ash to coarse lapilli in grain size. Deposits are matrix supported and poorly sorted, consisting of subrounded pumice lapilli and subangular lithic clasts set in a poorly sorted crystal-ash matrix. Vesiculated pumice lapilli are commonly 2–4 cm in diameter, sometimes exceeding ~10 cm in pumice concentrated zones. Cognate and accidental lithic clasts of volcanic rock are commonly ~2–10 cm in diameter, with some lithic blocks up to 50 cm occurring locally within clast rich zones. The matrix is commonly a poorly sorted, fine-to-coarse crystal-ash consisting of bubble wall shards and varying percentages of free feldspar, quartz, biotite, occasional amphibole crystals, and rare pyroxene; free crystals, where present, are often fragmented and commonly embayed, while glassy components of the matrix are partially to fully devitrified to cryptocrystalline alteration minerals including clays, zeolites and/or quartz. Late phase vapor phase alteration is common in these deposits, giving outcrops a pocked appearance. Both welded

(ignimbrites) and non-welded tuffs occur in the Abanico Formation; welded deposits often contain diagnostic fiamme easily recognized in the field.

The massive lapilli-ash tuff lithofacies are interpreted as pyroclastic flow deposits stemming from eruptions of dacitic to rhyolitic magmas. Pyroclastic density currents formed during the collapse of eruption columns can flow tens to hundreds of kilometers from the vent (Sparks et al., 1997). Thick ash flow deposits containing concentrated zones of lithic blocks are interpreted as vent proximal deposits, whereas thinner ignimbrite sheets intercalated with volcaniclastic and epiclastic deposits are interpreted as having been emplaced at greater distances from the source vent.

Lithofacies Pt: Dacitic to Rhyolitic Stratified and Cross-stratified Pumiceous Tuff

Amalgamated beds of planar- and cross-stratified pumiceous tuff are 4+ meters thick. Internally discontinuous laminations are 2–10 cm thick and cross-bedded; wavy or lenticular bedforms are common. Deposits are moderately to poorly sorted, consisting of matrix supported pumice lapilli and minor lithic fragments set in a crystal-ash matrix. The matrix is predominantly a coarse crystal-ash, containing glass shards and varying amounts of free feldspar, quartz, biotite, and occasional amphibole crystals. Glassy components of the matrix are typically altered to cryptocrystalline alteration products. Stratified and cross-stratified pumiceous tuff intervals are commonly intercalated with massive lapilli-ash deposits (Lithofacies: Pml).

The Pt lithofacies are interpreted as subaerial pyroclastic surge deposits. Surge deposits are commonly associated with three turbulent eruption processes: phreatomagmatic and phreatic eruptions, pyroclastic flows, and pyroclastic falls (Cas and Wright, 1987). Distinguishing the surge type for ancient deposits is generally challenging. Here, cross-stratified pumiceous tuff

beds associated with ignimbrite deposits are interpreted as ground-surge deposits. Surge deposits are usually small in volume (< ~1 km^3), and rarely extend more than ~10 km from their source (Orton, 1996).

Lithofacies Pmb: Dacitic to Andesitic Massive Tuff Breccia

Massive tuff breccias occur as simple, ~1–4 m thick deposits, and as multistoried accumulations exceeding 100 m in thickness. Breccia beds commonly have planar or scoured lower contacts and flat tops, pinching out laterally over tens of meters. Tuff breccias are matrix to clast supported, consisting of poorly sorted, subangular to subrounded, fine lapilli to block (40+ cm) sized clasts of non-vesiculated andesite to dacite; clasts commonly bear alteration rims and weather a distinctive green. Pumice clasts are rare, constituting less than ~10% of the rock when present. The matrix is usually a poorly sorted, ash-to-fine lapilli, consisting of pyroclastic fragments including glass shards, lava particles, and free crystals that match the phenocryst phases in the clasts; glassy components of the matrix are commonly partially to fully devitrified to cryptocrystalline secondary minerals, including but not limited to clay, zeolites, and quartz.

The massive tuff breccia lithofacies are interpreted as subaerial block-and-ash flow deposits. Block-and-ash flows are small volume pyroclastic flows generated by sudden eruption or gravitational collapse of viscous lava flows, lava domes or coulees (Cas and Wright, 1987; Francis and Oppenheimer, 2004). Poorly-organized deposits represent channelized flows in proximal to medial volcanic environments, commonly traveling less than 10 km from the debris source (e.g., Boudon et al., 1993; Charbonnier and Gertisser, 2008; Fisher and Heiken, 1982). Although tuff breccia deposits in the study area have a primary volcanic character, it is unclear whether some of these deposits represent true block-and-ash flows, or debris flows of re-

mobilized volcanic detritus. We interpret monolithological tuff breccias with a crystal-ash dominated matrix as syn-eruptive block-and-ash flows, and polymictic breccias with epiclastic matrix as post-eruptive debris flows composed mainly of reworked volcanic debris (see Lithofacies Gml below).

Volcaniclastic deposits

Lithofacies Sml: Granule to Pebble Diamictite

Pebbly mudstone deposits commonly weather to a distinctive purple to red color, not infrequently containing terrestrial mammal fossils. Deposits consist of internally massive sheets generally ~1–4 m in thickness, but sometimes exceeding 150 m. Deposits are mono- or heterolithic, consisting of matrix supported, angular to subangular volcanic lithic fragments and pumice lapilli (2–4 cm) that together constitute up to ~30% of the rock; outsized cobble and boulder clasts occur locally. Lithic clasts and pumice lapilli are commonly set in a poorly sorted, fine-to-very coarse muddy sandstone matrix. Free crystals of prismatic feldspar (plagioclase) and anhedral quartz are common, constituting up to ~10% of the rock.

Pumiceous pebble diamictites are interpreted as the product of subaerial lahars (Smith, 1991). In the Tinguirirca area, these deposits are dominated by texturally immature volcaniclastic debris, indicative of a strict volcanic provenance. Lahars can be syn- or post-eruptive, forming either coincident with volcanism or decades to millions of years later, a difference in timing difficult to discriminate in ancient volcaniclastic accumulations (Vallance, 2000; Orton, 1996). “Vaporized” bone fragments, or clenched upper and lower tooth rows wholly entombed in matrix, without a trace of bone, indicate that some of these sediment flows were emplaced hot.

The preservation of delicate anatomy, including jaws and skulls, suggests minimal turbulence or violence in the interiors of these flows, or that they stopped flowing (perhaps at the flow's edge) shortly after entraining or burying mammalian remains. Lahars can travel tens of kilometers (e.g., Crandell, 1971; Janda et al., 1981), commonly delivering sediment to medial-to-distal locations in volcano ring-plain systems (Orton, 1996).

Lithofacies Gml: Cobble Diamictite

Pumiceous cobble diamictite beds are ~2–4 m thick, with amalgamated beds forming multistoried packages over six meters thick. These heterolithologic deposits are poorly sorted, consisting of matrix supported, subangular to subrounded clasts of andesite to dacite; clasts are commonly pebble to cobble in size–outsized boulder clasts reach up to ~2 m in diameter. Internally, beds are massive without grading patterns or recognizable stratification. The matrix typically weathers brown or red; it consists of poorly sorted, fine to very coarse muddy sandstone containing free crystals of feldspar, abundant lithic fragments, and rare pumice fragments (1–2 cm).

The pumiceous cobble diamictite lithofacies is considered the product of subaerial debris flows. These deposits are dominated by poorly sorted volcaniclastic debris, unequivocally linking them to a volcanic provenance. Debris flows were likely associated with lahars (Smith, 1991), which remobilized volcanic detritus near volcanoes (e.g., Smith, 1986; 1988). Volcanic debris flows are often far more voluminous than their non-volcanic counterparts, transporting as much as 10^7 m^3 of sediment over 100 km to distal volcanic environments (e.g., Janda et al., 1981; Naranjo et al., 1986; Rodolfo, 1989).

Epiclastic deposits

Lithofacies Gt: Cross-stratified Volcaniclastic Conglomerate

Cross-stratified conglomerate beds, ~0.1–2 m thick, occur as individual beds or as multistoried stacks, frequently interbedded with cross-stratified sandstone (Lithofacies: St). Individual bedforms are commonly lenticular, bounded by upper and lower scour surfaces. Deposits are moderately sorted, consisting of clast supported, subrounded to rounded, imbricated pebbles and cobbles of dacite to andesite, with subordinate clasts of pumice, sandstone and mudstone; deposits dominated by boulder-sized clasts (~0.2–1 m diameter) are rare. Matrix sediments are poorly sorted, fine to very coarse sand, consisting mainly of lithic fragments with subordinate free crystals of subrounded feldspar, quartz, and rare pyroxene.

The stratified and cross-stratified conglomerate lithofacies are interpreted as gravel bar deposits of braided river systems, or perhaps alluvial fans (Miall, 1977). Gravels were likely deposited by traction processes related to migrating gravel bars during periods of elevated stream flow (Miall, 1985), whereas the interstitial sand matrix infiltrated the framework during waning stream velocities. Heterolithologic volcanic detritus constituting the clast framework suggests a predominantly volcanic provenance, likely derived from an intra-arc (intermontane) setting. Gravel bedload deposits are commonly attributed to braided river systems in medial-to-distal volcanic environments (e.g., Hackett and Houghton, 1989; Smith, 1991; 1986).

Lithofacies St: Cross-stratified Volcaniclastic Sandstone and Grit

Cross-stratified sandstone and grit deposits commonly exhibit a buff weathering color and are frequently interbedded with coarse, cross-stratified gravel and thin mudstone intervals

(Lithofacies: Gt and Fl). Trough cross beds are the most prevalent sedimentary structure, but planar cross-beds and scour-fill bedforms are also common. Lenticular bedforms are bounded by scour surfaces with average bed thicknesses ranging from ~0.1–2 m. Individual beds are commonly stacked, forming multi-lateral and multistoried successions. Deposits vary widely in average grain size, ranging from well-sorted, fine-grained sandstone to moderately sorted grit. Sandstone and grit successions commonly fine upward, exhibiting amalgamated or sharp upper contacts with thin intervals of mud- or siltstone (Lithofacies: Fl); thin pebble train deposits are commonly associated with erosive basal contacts. Sandstone and grit deposits are texturally immature, consisting of subrounded lithic and pumice fragments, rounded glass shards and subangular to rounded crystals of feldspar and quartz intermingled with rare biotite and pyroxene.

The cross stratified tuffaceous sandstone and grit lithofacies is interpreted as channel fill in braided or meandering river systems (e.g., Miall, 1977); cross stratification, fining-upward successions and basal channel scours are all consistent with channel fill processes (Miall, 1977). Prevalent trough cross stratification represents infilling of channels by bedload processes associated with migrating dunes (Kataoka, 2005; Miall, 1977), whereas planar cross-beds were likely deposited by migrating straight-crested dunes in deeper portions of active stream channels, or by avalanching on the slipfaces of bars (Miall, 1985; 1996). Fining upward successions and thin mudstone drapes reflect periods of decreasing stream flow and channel abandonment; pebble trains are interpreted as lag deposits. Texturally immature volcaniclastic sandstones indicate a medial-to-distal volcanic provenance. Sediments, likely originating through the erosion of unconsolidated volcanic debris, were transported by braided and/or meandering river systems.

Lithofacies Sh: Planar-bedded Volcaniclastic Sandstone

Planar bedded volcaniclastic sandstone deposits are commonly interbedded with hyperconcentrated flow, debris flow, and primary pyroclastic deposits. They frequently make up multistoried successions consisting of ~0.1–0.3 m thick sheet-like bedforms that extend laterally for tens to hundreds of meters. Deposits commonly exhibit parallel or low-angle cross stratification; scour-fill channels are rare. Internally, deposits are normally graded and either massive or finely laminated. Subangular to subrounded, medium to coarse grains are moderately sorted and texturally immature, consisting of lithic fragments intermingled with free crystals of prismatic plagioclase, quartz, biotite, and rare amphibole; pumice lapilli (~1–4 cm) are rare. The interstitial matrix is commonly a very fine-grained, volcanic ash-mud mixture. Volcaniclastic sandstones commonly weather white to buff, their compositions closely matching those of primary pyroclastic deposits (e.g., Lithofacies Pml).

The planar-bedded volcaniclastic sandstone lithofacies are interpreted as subaerial sheet-flood deposits (Miall, 1985; 1977). Sheets of laminated sand are generally interpreted as the product of flash floods depositing sand under upper flow plane bed conditions (Tunbridge, 1981). Such deposits are texturally immature and closely resemble primary volcanics, suggesting that this volcanogenic sediment was rapidly stripped away from recently emplaced, unconsolidated pyroclastic deposits during floods, only to be redeposited at proximal-to-medial distances from the sediment source.

Lithofacies Fl: Siltstone and Mudstone

Siltstone and mudstone intervals, weathering gray to red, are frequently interbedded with cross-stratified sandstones and conglomerates (Lithofacies: St and Gt). Sheet-like or lenticular bedforms are commonly ~1–2 cm thick; accumulations over >1 m thick are rare. Basal contacts are gradational or sharp, exhibiting planar or undulatory geometries. Internally, these fine-grained deposits are massive or finely laminated. Dish and pillar structures, and rip up clasts are common; extensive pedogenic alteration, bioturbation, or calcareous nodules are minimal to non-existent.

Siltstone and mudstone beds are interpreted to represent overbank deposits associated with the flooding of braided river systems (Miall, 1977; 1996). Small, shallow, short-lived lakes commonly form on volcaniclastic aprons when drainages are impounded by lava flows, ignimbrites or landslides (Kuenzi et al., 1979). Thin intervals of overbank sediments were likely deposited through suspension fallout during stream avulsion and channel overtopping, whereas thicker muds and silts likely accumulated in small ponds or lakes formed during floods (Miall, 1985; Jones et al., 2001; Limarino et al., 2001; Mosolf et al., 2011).

LITHOFACIES ASSOCIATIONS

The lithofacies preserved in the Abanico Formation reflect deposition in a range of volcanic environments. The three lithofacies associations (Table S32)–proximal volcanic, medial volcaniclastic, and distal volcaniclastic–making up the bulk of the Abanico Formation in the Tinguiririca River region are briefly described below (following the terminology of Hackett and Houghton, 1989; Fisher and Schmincke, 1984). Complex stacking patterns, reflecting rapid

lateral and vertical facies transitions, record a prolonged but episodic eruptive history. In general, the lower stratigraphic levels of the Abanico Formation in the study region are dominated by proximal volcanic facies, with medial- and distal-volcaniclastic facies increasing up section in the mid- to upper-levels of the Abanico Formation. Each facies association is briefly discussed below.

Proximal volcanic facies association

The proximal volcanic facies association is dominated by lava flows, block-and-ash flows, pyroclastic tuff, and coarse debris flow deposits (Lithofacies: Lab, Lb, Pmb, Pml, Pt, and Gml), with subordinate intercalations of hyper-concentrated debris flow and sheet-flood deposits (Lithofacies: Sml and Sh). Proximal facies are repeated vertically throughout the Abanico Formation in the study region; however, proximal facies are most common lower in the section (e.g., Kll, Kga, and Kgz members).

The proximal lithofacies association is interpreted to have been deposited near volcanic vents. Volcanic deposits commonly consist of resistant, indurated rock such as lava flows, autoclastic and pyroclastic breccias, and intrusions (Smith and Landis, 1995). Unconsolidated volcanic and sedimentary deposits are quickly eroded from the steep flanks of volcanoes, thus resistant rocks, such as lava flows and welded tuffs, are disproportionally preserved and represented near the vent. Coarse debris flow deposits are sometimes preserved in proximal vent environments, however (Smith, 1991). Proximal facies are generally emplaced within ~0–10 km of the source vent (Orton, 1996) and are commonly hydrothermally altered.

Medial volcaniclastic facies association

The medial lithofacies association consists mainly of hyperconcentrated mass flow (lahars), subaerial debris flow and sheet-flood deposits (Lithofacies: Sml, Gml, and Sh), with minor intercalations of mafic lava flows, thin ignimbrite sheets, and fluvial sedimentary deposits (Lithofacies: Pb, Pml, St, and Gt). These facies are repeated throughout the Abanico Formation's stratigraphy but are most common in the mid- to upper-levels (e.g., Tt, Tg, and Tr members – see below).

This lithofacies association is interpreted to have formed at proximal- to medial-distances from eruptive centers, potentially in volcaniclastic aprons that encircled individual cones (ring plains), or as strings of coalescing prisms flanking the arc (Smith and Landis, 1995). Strata formed in volcaniclastic aprons are dominated by event deposits related to the stripping of loose pyroclastic debris from steep volcanic slopes during or shortly after eruption (Vessel and Davies, 1981; Smith, 1991). Thus, apron deposits are largely derived from hyperconcentrated mass flows (lahars), debris flows, and debris avalanches (e.g., Hackett and Houghton, 1989). Ignimbrite outflow sheets and low-viscosity lava flows are also common (Smith and Landis, 1995). Volcaniclastic aprons vary greatly, reflecting the size and steepness of a volcano, as well as its eruption frequency/volume. While lahars sometimes transport sediment greater than 100 km (Smith, 1991), volcaniclastic apron deposits are generally emplaced within ~5–35 km from their source (Smith and Landis, 1995).

Distal volcaniclastic facies association

The distal lithofacies association consists mainly of cross-bedded conglomerate and sandstone with intercalations of siltstone and mudstone (Lithofacies: Gt, St and Fl); subordinate lithofacies include thin debris flow and lahar deposits, thin ignimbrite sheets, and mafic lavas (Lithofacies: Gml, Sm, Sh, Pml, and Lb). The Los Ríos member (Tr) is the only map unit in which this facies association occurs abundantly.

This facies association is interpreted to represent sedimentation by braided- and meandering river systems, and perhaps braided fan environments and lacustrine systems distal from active eruptive centers, and/or sedimentation during periods of volcanic quiescence. It records volcaniclastic deposition in sites receiving little or no direct volcanic or sedimentary impact from eruptions themselves (Smith and Landis, 1995). Distal subaerial facies are thus composed primarily of fluvial and lacustrine sediments including volcanic and non-volcanic detritus (Smith and Landis, 1995). Primary volcanic products, such as far traveled mafic lavas or ignimbrite outflow sheets, are uncommon in distal volcanic environments and, when present, are relatively thin. Distal volcaniclastic depositional environments are generally considered to lie ~20–70 km from the source (Smith and Landis, 1995).

REFERENCES CITED

Boudon, G., Camus, G., Gourgaud, A., and Lajoie, J., 1993, The 1984 Nuee-Ardente deposits of Merapi Volcano, central Java, Indonesia - stratigraphy, textural characteristics, and transport mechanisms: Bulletin of Volcanology, v. 55, p. 327–342, https://doi.org/10.1007/BF00301144.

Cas, R.A.F., and Wright, J.V., 1987, Volcanic successions (modern and ancient): Allen and Unwin, London, Geology Journal, v. 23, 529 p, doi:https://doi.org/10.1007/978-94-009-3167-1.

Cashman, K., Pinkerton, H., and Stephenson, J., 1998, Introduction to special section: Long lava flows: Journal of Geophysical Research. Solid Earth, v. 103, p. 27281–27289, https://doi.org/10.1029/98JB01820.

Charbonnier, S.J., and Gertisser, R., 2008, Field observations and surface characteristics of pristine block-and-ash flow deposits from the 2006 eruption of Merapi Volcano, Java, Indonesia: Journal of Volcanology and Geothermal Research, v. 177, p. 971–982, doi:https://doi.org/10.1016/j.jvolgeores.2008.07.008.

Crandell, D.R., 1971, Postglacial lahars from Mount Rainier Volcano, Washington: US Geological Survey Professional Paper, v. 677, p. 75.

Fisher, R.V., and Heiken, G., 1982, Mt. Pelée, Martinique: May 8 and 20, 1902, pyroclastic flows and surges: Journal of Volcanology and Geothermal Research, v. 13, p. 339–371, https://doi.org/10.1016/0377-0273(82)90056-7.

Fisher, R.V., and Schmincke, H.-U., 1984, Pyroclastic rocks: Berlin, New York, 472 p, https://doi.org/10.1007/978-3-642-74864-6.

Francis, P., and Oppenheimer, C., 2004, Volcanoes: Oxford University Press.

Hackett, W., and Houghton, B., 1989, A facies model for a Quaternary andesitic composite volcano: Ruapehu, New Zealand: Bulletin of Volcanology, v. 51, p. 51–68, https://doi.org/10.1007/BF01086761.

Hulme, G., 1974, Interpretation of lava flow morphology: Geophysical Journal of the Royal Astronomical Society, v. 39, p. 361–383, https://doi.org/10.1111/j.1365-246X.1974.tb05460.x.

Janda, R.J., Scott, K.M., Nolan, K.M., and Martinson, H.A., 1981, Lahar movement, effect, and deposits, *in* Lipman, P.W., and Mullineaux, D.R., eds., The 1980 Eruptions of Mount St. Helens, Washington: U.S. Geological Survey Professional Paper, 1250: 461- 478.

Jones, S.J., Frostick, L.E., and Astin, T.R., 2001, Braided stream and flood plain architecture: the Rio Vero Formation, Spanish Pyrenees: Sedimentary Geology, v. 139, p. 229–260, https://doi.org/10.1016/S0037-0738(00)00165-2.

Kataoka, K., 2005, Distal fluvio-lacustrine volcaniclastic resedimentation in response to an explosive silicic eruption: the Pliocene Mushono tephra bed, central Japan: Geological Society of America Bulletin, v. 117, p. 3–17, doi:https://doi.org/10.1130/B25379.1.

Kuenzi, W.D., Horst, O.H., and McGehee, R.V., 1979, Effect of volcanic activity on fluvial-deltaic sedimentation in a modern arc-trench gap, southwestern Guatemala: Geological Society of America Bulletin, v. 90, p. 827–838, https://doi.org/10.1130/0016-7606(1979)90<827:EOVAOF>2.0.CO;2.

Levi, B., Aguirre, L., Nystrom, J.O., Padilla, H., and Vergara, M., 1989, Low-grade regional metamorphism in the Mesozoic-Cenozoic volcanic Sequences of the Central Andes: Journal

of Metamorphic Geology, v. 7, p. 487–495, https://doi.org/10.1111/j.1525-1314.1989.tb00611.x.

Limarino, C., Tripaldi, A., Marenssi, S., Net, L., Re, G., and Caselli, A., 2001, Tectonic control on the evolution of the fluvial systems of the Vinchina Formation (Miocene), northwestern Argentina: Journal of South American Earth Sciences, v. 14, p. 751–762, https://doi.org/10.1016/S0895-9811(01)00067-0.

Miall, A.D., 1985, Architectural-element analysis - a new method of facies analysis applied to fluvial deposits: Earth-Science Reviews, v. 22, p. 261–308, https://doi.org/10.1016/0012-8252(85)90001-7.

Miall, A.D., 1977, Review of braided-river depositional environment: Earth-Science Reviews, v. 13, p. 1–62, https://doi.org/10.1016/0012-8252(77)90055-1.

Miall, A.D., 1996, The Geology of Fluvial Deposits: New York, Springer, 582 p.

Mosolf, J., Horton, B., and Heizler, M., 2011, Unroofing the core of the central Andean fold-thrust belt during focused late Miocene exhumation: evidence from the Tipuani-Mapiri wedge-top basin, Bolivia: Basin Research, v. 23, p. 346–360, https://doi.org/10.1111/j.1365-2117.2010.00491.x.

Naranjo, J.L., Sigurdsson, H., Carey, S.N., and Fritz, W., 1986, Eruption of the Nevado-Del-Ruiz Volcano, Colombia, on 13 November 1985 - tephra fall and lahars: Science, v. 233, p. 961–963, https://doi.org/10.1126/science.233.4767.961.

Orton, G.J., 1996, Volcanic Environments, *in* Reading, H.G. ed., Sedimentary Environments: Processes, Facies and Stratigraphy: Oxford, Blackwell Science, p. 485–567.

Rodolfo, K.S., 1989, Origin and early evolution of lahar channel at Mabinit, Mayon Volcano, Philippines: Geological Society of America Bulletin, v. 101, p. 414–426, https://doi.org/10.1130/0016-7606(1989)101<0414:OAEEOL>2.3.CO;2.

Smith, G.A., 1986, Coarse-grained nonmarine volcaniclastic sediment - terminology and depositional Process: Geological Society of America Bulletin, v. 97, p. 1–10, https://doi.org/10.1130/0016-7606(1986)97<1:CNVSTA>2.0.CO;2.

Smith, G.A., 1988, Sedimentology of proximal to distal volcaniclastics dispersed across an active foldbelt - Ellensburg Formation (Late Miocene): Central Washington: Sedimentology, v. 35, p. 953–977.

Smith, G.A., 1991, Facies sequences and geometries in continental volcaniclastic sediments: Special Publication - Society of Economic Paleontologists and Mineralogists, v. 45, p. 109–121.

Smith, G.A., and Landis, C.A., 1995, *in* Busby C. J., Ingersoll R. V., eds., Intra-arc basins: Blackwell Science, Oxford.

Sparks, R., Bursik, M., Carey, S.N., Gilbert, J., Glaze, L., Sigurdsson, H., and Woods, A., 1997, Volcanic plumes: Chichester, Wiley, 574 p.

Tunbridge, I.P., 1981, Sandy high-energy flood sedimentation - some criteria for recognition, with an example from the Devonian of SW England: Sedimentary Geology, v. 28, p. 79–95, https://doi.org/10.1016/0037-0738(81)90058-0.

Vallance, J., 2000, Lahars, *in* Sigurdsson, H., Houghton, B.F., McNutt, S., Rymer, H., and Stix, J., eds., Encyclopedia of Volcanoes: London, Academic Press, p. 601–616.

Vessel, R.D., and Davies, D.K., 1981, Nonmarine sedimentation in an active fore arc basin, in Ethridge, *in* F.G. and Flores, R.M. eds., Nonmarine Depositional Enivornments: Models for Exploration: SEPM (Society for Sedimentary Geology) Special Publication, p. 34–45.

Walker, G., 1973, Lengths of Lava Flows: Philosophical Transactions of the Royal Society of London Series a-Mathematical Physical and Engineering Sciences, v. 274, p. 107–118.